DEPARTMENT OF PHYSICS
UNIVERSITY OF JYVÄSKYLÄ
RESEARCH REPORT No. 4/2001

# ANALYSIS OF THE TUNNELLING-CHARGING HAMILTONIAN OF A COOPER PAIR PUMP

BY
**MATIAS AUNOLA**

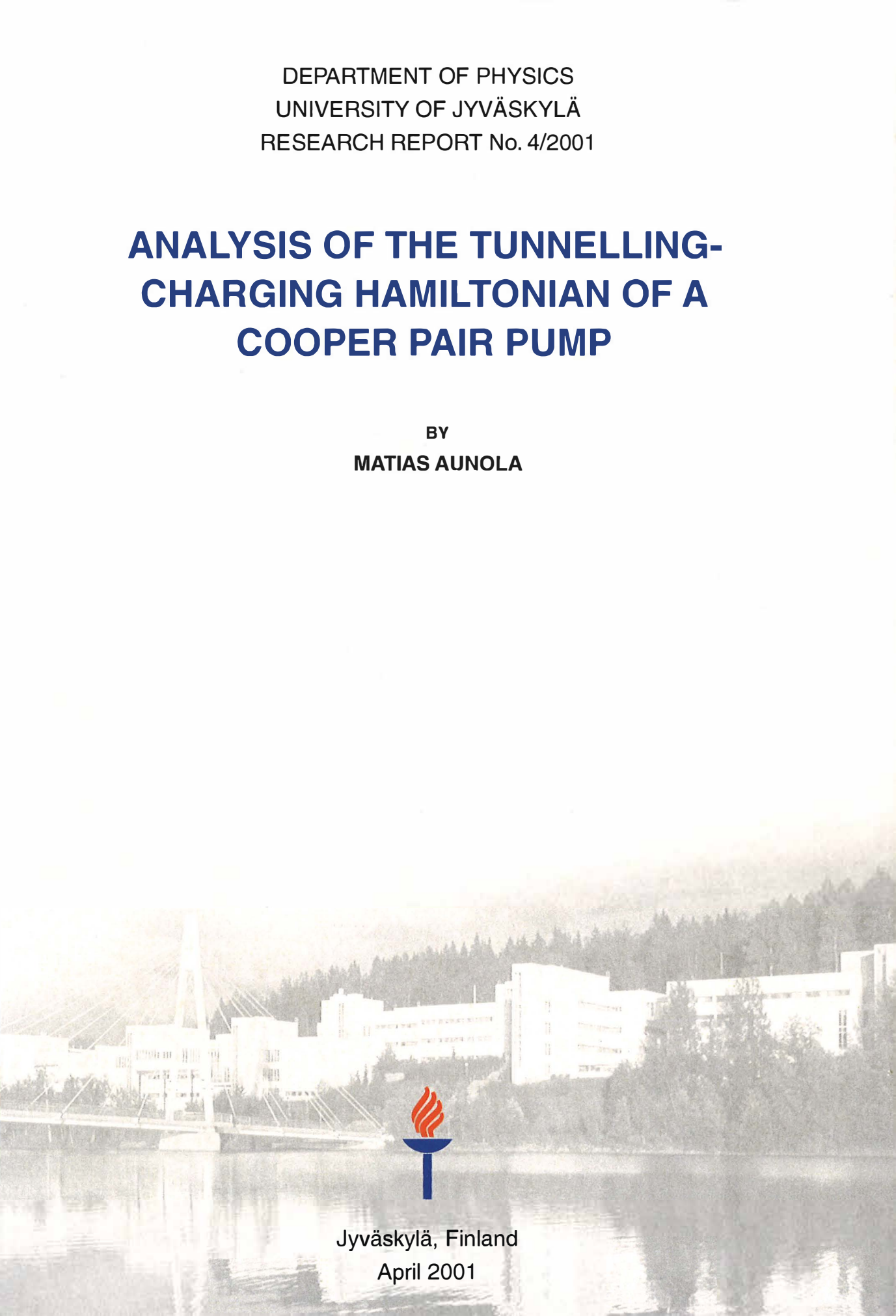

Jyväskylä, Finland
April 2001

DEPARTMENT OF PHYSICS, UNIVERSITY OF JYVÄSKYLÄ
RESEARCH REPORT No. 4/2001

# Analysis of the Tunnelling-Charging Hamiltonian of a Cooper pair pump

BY

**MATIAS AUNOLA**

Academic Dissertation
for the Degree of
Doctor of Philosophy

*To be presented, by permission of the*
*Faculty of Mathematics and Science*
*of the University of Jyväskylä,*
*for public Examination in Auditorium FYS-1 of the*
*University of Jyväskylä on April 20, 2001,*
*at 12 o'clock noon*

Jyväskylä, Finland
April 2001

URN:ISBN:978-951-39-9440-2
ISBN 978-951-39-9440-2 (PDF)
ISSN 0075-465X

Jyväskylän yliopisto, 2022

ISBN 951-39-0935-2
ISSN 0075-465X

**PREFACE**

The work reviewed in this thesis has been carried out during years 1999–2001 at the Department of Physics in the University of the Jyväskylä.

I must begin with apologies to my supervisor Prof. Jouni Suhonen for all the trouble related to this work. It has been an outright obsession to me, and it has delayed many of his research projects. I thank the other supervisor, Academy Prof. Jukka Pekola for introducing me to the field of superconductivity and fruitful collaboration.

Prof. Jouni Suhonen and Prof. (Emeritus) Pertti Lipas are warmly thanked for guiding me into the world of quantum mechanics which still continues to fascinate and amaze me. Dr Morten Hjorth–Jensen deserves a special mention for an instructive course on renormalisation methods.

I am grateful for collaboration, co-operation and help of Dr Jussi Toivanen, Dr Tuomas Hjelt, Dr Teemu Siiskonen, Mr Jussi Toppari and Dr Kimmo Tuominen. A warm thank you for friendship is extended to Mr Mika Latva-Kokko, Mr Juhani Hämäläinen, Mr Veli Maaranen, Mr Vesa Kolhinen, Dr Juha Merikoski, Dr Anniina Rytkönen and Dr Antti Koponen, as well as all those whom I have forgotten to mention. A general thank you goes to the staff and students of the Department of Physics for providing an inspiring atmosphere.

The financial support from the Graduate School of Particle and Nuclear Physics and the University of Jyväskylä is gratefully acknowledged.

This work is dedicated to Suvi and Sini for their love and support. Finally, my parents are thanked for encouraging me to study physics.

Jyväskylä, April 2001

Matias Aunola

**ABSTRACT**

This thesis consists of an introductory part and three research papers. The main body of the work can be summarised as the development of a model describing gated arrays of superconducting Josephson junctions or Cooper pair pumps.

The pumping of single electrons in gated arrays of normal-state tunnelling junctions has reached an accuracy that can be considered for metrological applications. The aim of the present study is to investigate whether the quantum mechanical nature of superconductivity restricts the accuracy of Cooper pair pumps. The answer is affirmative, at least if the impedance of the environment is assumed to be vanishingly small and the phase difference over the array $\phi$ is fixed.

By using the canonical Hamiltonian for $N$ independent Josephson junctions and neglecting any coupling to the environment as well as quasiparticle degrees of freedom, the problem becomes tractable. Both the direct supercurrent through the array and the adiabatically pumped charge are examined in detail. The leading order pumped charge for the most feasible pumping cycle is found to behave as $I \approx -2ef[1 - a_N(E_\mathrm{J}/E_\mathrm{C})^{N-2}\cos\phi]$, where $-2e$ is the charge of a Cooper pair, $f$ is the gating frequency, $a_N$ is a constant which only depends on $N$, $E_\mathrm{J}$ is the Josephson coupling energy, and $E_\mathrm{C}$ is the charging energy. The deviation is rather large for short arrays, and provided the other sources of inaccuracy can be suppressed, the adiabatic pumping can be tested experimentally when the direct supercurrent vanishes at $\phi = 0$. The measurents also probe the coherence of the system, especially the effects due to the dephasing, in other words the fluctuations in value of $\phi$.

The adopted renormalisation approach is then used for obtaining quantitative predictions of the pumping inaccuracy when the array is inhomogeneous or the gating sequence is not ideal. The predictions have been confirmed numerically and they can be related to experimentally measurable quantities. The small size of these corrections means that they may be masked by other effects in experiments. Further studies using more realistic and sophisticated models should be performed, also.

Finally, the symmetries of the model are examined in detail and the systematics of the pumped charge with respect to all of the model parameters are obtained, although not rigorously proven. This is done by using an efficient block-diagonalisation scheme combined with a Fourier expansion of the eigenstates.

## LIST OF PUBLICATIONS

The main results of this thesis have been published in the following articles:

[**P1**] *Adiabatic transport of Cooper pairs in arrays of Josephson junctions*, J. P. Pekola, J. J. Toppari, M. Aunola, M. T. Savolainen, and D. V. Averin, Phys. Rev. B **60**, R9931 (1999), also available as cond-mat/9904264. https://doi.org/10.1103/PhysRevB.60.R9931

[**P2**] *Arrays of Josephson junctions in an environment with vanishing impedance*, M. Aunola, J. J. Toppari, and J. P. Pekola, Phys. Rev. B **62**, 1296 (2000), also available as cond-mat/9911368. https://doi.org/10.1103/PhysRevB.62.1296

[**P3**] *Tunneling-charging Hamiltonian of a Cooper-pair pump*, M. Aunola, Phys. Rev. B **63**, 132508 (2001), also available as cond-mat/0011408.
https://doi.org/10.1103/PhysRevB.63.132508

The author of this thesis has written the publications [P2] and [P3] and participated in the writing of the publication [P1]. The author has derived all theoretical results in [P2] and [P3], as well as the general expressions for the pumped charge and the supercurrent in [P1]. Further development of the renormalisation approach and the block-diagonalisation scheme was done by the author. The author has developed and written all the numerical routines used for numerical analysis in [P3] and most of the routines used in [P2]. The interpretation and analysis of the results in [P2] and [P3] have been performed by the author.

CONTENTS

## LIST OF FIGURES

## LIST OF TABLES

# I. INTRODUCTION

## 1. Superconductivity

The phenomenon of *superconductivity* was first observed in 1911 by H. Kamerlingh Onnes and his student G. Holst in Leiden [4]. Mercury was refrigerated by liquefied helium and at temperature of approximately 4 K the electrical resistance of the sample vanished. The transition temperature $T_c$ was found to depend on the metal, and subsequently superconductivity was discovered in alloys. The so-called high-$T_c$ superconductors, first discovered in 1986 [5] fall outside the present discussion.

A superconductor is also a *perfect diamagnet*, so that magnetic field lines only penetrate the surface of the sample up to a certain depth, typically about 500 Å. The Meissner effect was found by Meissner and Ochsenfeld in 1933 [6] and it does not follow from perfect conductance which only requires that the magnetic field is stationary, i.e. time-independent.

It was found that the superconductivity can be treated *thermodynamically*. The difference between Helmholz free energy densities in the superconducting and the normal state can be expressed as

$$F_n(T) - F_s(T) = B_c^2(T)/2\mu_0. \tag{1}$$

The *critical magnetic field strength* behaves approximately as $B_c(T) = B_c(0)[1 - (T/T_c)^2]$ and determines the boundary in the $(B, T)$-phase diagram. At $T_c$ the *phase transition* is of the second order and the heat capacity is discontinuous. For non-zero magnetic field strengths the first order transition is associated with latent heat.

The Meissner effect was first explained by F. and H. London who derived the London equation [7]

$$\vec{\nabla} \times \vec{j} = -\frac{n_s e^2}{m}\vec{B}, \tag{2}$$

by choosing a specific solution of the Maxwell equations. Here $n_s$ is the density of superconducting electrons in the *two-fluid model* as some of the electrons are assumed to remain in the normal state. No static current densities or magnetic fields are allowed inside a bulk sample of superconducting material. The attenuation of magnetic field and surface currents is described by $e^{-x/\lambda_0}$, where $x$ is the depth into the sample and $\lambda_0 = (n_s e^2/m\mu_0)^{1/2}$ is the characteristic *London penetration depth*. Actually, the penetration depth $\lambda(T)$ is always larger than $\lambda_0$, which is an ideal limit when $T \to 0$.

A nonlocal generalisation of the London model was presented by Pippard in 1950 [8]. In this model the supercurrent density $\vec{j}_s(\vec{r})$ is determined by the vector potential $\vec{A}(\vec{r})$ within a volume of radius of the order of $\xi$. The *coherence length* $\xi$ is determined by an intrinsic

length $\xi_0$ and the *mean free path* $\ell$ according to

$$\frac{1}{\xi} = \frac{1}{\xi_0} + \frac{1}{\ell}. \tag{3}$$

Here $\xi_0 = a\hbar v_F / k_B T_c$ is qualitatively justified by the uncertainty principle and $a$ is a constant of the order of unity. The length $\xi_0$ can be understood as the smallest size of the wave packet of the superconducting charge carriers.

If the ordinary mean free path is shorter than $\xi_0$, the measured coherence length $\xi$ is considerably reduced from the ideal value. Using a single value $a = 0.15$ Pippard was able to fit several sets of data. Later microscopic calculations by Bardeen, Cooper and Schrieffer gave a result $a \approx 0.18$ [9].

Above it has been assumed that $\lambda < \xi$ so that the penetration layer is thin as compared to the size of the carriers of the supercurrent. Then the transition between the normal and superconducting phases occurs simultaneously in the whole sample. In the opposite case $\xi < \lambda$ (*type II superconductors*), the superconducting state is not completely destroyed as in the Pippard or *type I superconductors*, rather the magnetic flux penetrates the sample gradually as predicted by Abrikosov in 1957 [10].

The London superconductors with $\xi < \lambda$ have two critical fields strengths, $B_{c1}$ and $B_{c2}$. Below the first critical field the sample behaves as type I superconductor and above the second critical field the superconductivity is lost. High-field superconducting magnets are possible because $B_{c2}$ can be much larger than the thermodynamical critical field $B_c$ in Eq. (1) and the supercurrent carrying property remains.

Between $B_{c1}$ and $B_{c2}$, a mixed state occurs and the flux penetrates the sample via flux tubes or vortices. Each tube carries a *quantum of flux*

$$\Phi_0 = \frac{h}{2e} = 2.07 \cdot 10^{-15}\ \text{Tm}^2. \tag{4}$$

These tubes form a regular triangular array in the mixed phase which was experimentally confirmed in 1967 [11].

## 2. The Ginzburg–Landau and BCS theories of superconductivity

In 1950 Ginzburg and Landau [12] proposed a variational theory based on a complex *order parameter* $\psi$ in order to describe the electrodynamical properties of superconductors. The order parameter is related to the density of superconducting electrons by $n_s(\vec{r}) = |\psi(\vec{r})|^2$.

By expressing the free energy as a power series in $\psi$ and its gradient they derived the famous *Ginzburg–Landau equation*

$$\frac{(\vec{p} - e^*\vec{A})^2}{2m^*}\psi + \alpha\psi + \beta|\psi|^2\psi = 0, \tag{5}$$

where $\vec{p} = -i\hbar\vec{\nabla}$, $e^*$ is the charge and $m^*$ is the mass of the particle. Variational principle ensures that the correct macroscopic wave function minimises the free energy. The expression for the supercurrent reads

$$\vec{j}_s = (e^*/2m^*)[(\vec{p}\psi)^*\psi + \psi^*(\vec{p}\psi)] - [(e^*)^2/m^*]|\psi|^2\vec{A}. \tag{6}$$

The Ginzburg–Landau theory is able to accommodate variations of $n_s$ and it also explains penetration of magnetic field into thin slabs of superconducting material.

Well below $T_c$ the temperature-dependent coherence length

$$\xi(T) = \hbar/|2m^*\alpha(T)| \tag{7}$$

approaches the value $\xi_0$ from Pippard's theory. Near $T_c$ both $\xi(T)$ and the penetration depth $\lambda(T)$ diverge as $(T_c - T)^{-1/2}$. Because the ratio is approximately constant it defines the *Ginzburg–Landau parameter* $\kappa = \lambda/\xi$. For type I superconductors $\kappa$ is typically much less than unity and consequently formation of vortices is inhibited by a positive surface energy. Abrikosov found that the transition between type I and type II superconductors occurs at $\kappa = 1/\sqrt{2}$.

In the Ginzburg–Landau theory the flux quantization condition can be expressed as $\Phi' = n\Phi_0$, where the *fluxoid* is defined by

$$\Phi' := \oint \vec{A} \cdot d\vec{s} + \frac{m^*}{(e^*)^2} \oint \frac{\vec{j}_s \cdot d\vec{s}}{|\psi|^2}. \tag{8}$$

The first part describes the ordinary magnetic flux through the loop, while the second part is directly due to the supercurrent. If the density of supercurrent vanishes, the quantisation of the magnetic flux in integer multiples of $\Phi_0$ is regained. This property was experimentally confirmed in 1961 [13]. In the mixed state of type II superconductors only the fluxoid $\Phi'$ is strictly quantised.

The first microscopic theory of superconductivity was presented by Bardeen, Cooper and Schrieffer (BCS) in 1957 [9]. The BCS theory predicts formation of the so-called *Cooper pairs* due to the weak, but attractive interaction between electrons induced by the electron-phonon interaction. The spatial dimension of a Cooper pair is of the order of $\xi_0$, so that they can be interpreted as the charge carriers of the preceding theories.

The pairing interaction leads to an *energy gap* of $E_g = 2\Delta(T)$ in the single-particle spectrum. Simultaneously $E_g$ is the minimum energy required to break a Cooper pair and create two quasiparticles. The size of the gap increases from zero at $T_c$ to the maximum value

$$E_g(0) = 2\Delta(0) \approx 3.528 k_B T_c \tag{9}$$

for $T \ll T_c$. The energy gap immediately explained the exponential behaviour of the specific heat $c_s$ below $T_c$. The discontinuity in the specific heat at $T_c$ was found to agree with the BCS prediction $(c_s - c_n)/c_n \approx 1.43$ [14].

The original BCS theory and its extensions can be regarded as the theory of ordinary superconductors. The BCS transformation which defines the quasiparticles has been successfully applied e.g. in nuclear physics [15–17] and to the description of superfluid $^3$He [18, 19].

## 3. The Josephson effects

The validity of the Ginzburg–Landau wave function $\psi(\vec{r})$ combined with the formation of Cooper pairs in the BCS theory indicates that the many-particle quantum system can be described collectively with a macroscopic wave function $\psi(\vec{r}) = |\psi(\vec{r})|e^{i\theta(\vec{r})}$. The Cooper pairs are the bosons of the condensate which is similar, but not identical to the Bose-Einstein condensate.

A *Josephson junction* [20] is formed when two superconductors are separated by a weak link which is often an insulating layer. When the superconductors are described by constant phases $\theta_1$ and $\theta_2$, Josephson predicted that a current flows through the junction in the absence of an external voltage. The supercurrent is given by

$$I = I_c \sin(\phi), \tag{10}$$

where $I_c$ is a constant, the critical current of the junction, and $\phi := \theta_2 - \theta_1$ is the phase difference across the junction. This is known as the *dc Josephson effect.*

A further prediction was that the phase difference is related to the voltage across the junction $V$ via $d\phi/dt = -2eV/\hbar$. Consequently, in the *ac Josephson effect* a dc bias voltage induces an ac current with angular frequency

$$\omega = 2eV/\hbar. \tag{11}$$

Both effects were soon confirmed experimentally. A quantum mechanical description of the dc Josephson effect is given in [21], where static tunnelling in ultrasmall Josephson junctions is discussed in detail. The ac Josephson effect can be used in high-precision voltage measurements and it was also used in the determination of the ratio $e/h$ between two fundamental constants, as soon as in 1969 [22]. The coupling between Josephson junctions and the magnetic field is used in SQUIDs or *Superconducting QUantum Interference Devices.* The most common of such devices are the two-junction *dc SQUID*, where the current $I$ is modulated by the enclosed flux $\Phi$ according to $I_0 \sin(\pi\Phi/\Phi_0)/(\pi\Phi/\Phi_0)$, and the single-junction *rf SQUID*, which is monitored at a radio frequency (typically of the order of 20

MHz). The theory and applications of SQUIDs are discussed in numerous references, e.g in a book by Ruggieri and Rudman [23]. A text book by Tinkham [24] examines the physics and properties of small Josephson junctions.

The *canonical Hamiltonian* of a Josephson junction when only *electrostatic effects* and *Cooper pair tunnelling* are included is discussed e.g. in [21, 24–26] and it reads

$$H_{\mathrm{JJ}} = (2e^2/C)(n-q)^2 - E_{\mathrm{J}} \cos\phi, \tag{12}$$

where $n$ is the number of tunnelled Cooper pairs across the junction as compared to the equilibrium case at zero external voltage. Here $E_{\mathrm{J}}$ is known as the *Josephson coupling energy* and $q$ is the optimal deviation of $n$. The formulation is based on the complementary nature of the particle number $N$ and the phase difference $\phi$, which are assumed to be *canonical conjugate variables*, i.e. to satisfy the relation $[\phi, N] = i$. The corresponding uncertainty relation is important when the properties of Josephson devices are examined. It should be noted that even the *quasiparticle tunnelling* has been neglected above.

If an island separates two Josephson junctions and the number of Cooper pairs on the island can be controlled, a *Cooper pair transistor* is formed. If the electrostatic effects dominate, the device is somewhat analogous to a *single electron transistor* (SET), see e.g. [27] in which the tunnelling rate can be controlled by the island gate voltage and the external bias voltage. Nevertheless, the quantum-mechanical nature of the superconducting junctions means that many of the properties are quite unlike those of a SET. A thorough examination of Cooper pair transistors is given in [28] and the references therein further complement the study.

In this thesis *Cooper pair pumps*, or linear arrays of Josephson junctions, where the charge on each intervening island can be controlled, are examined by generalising the Hamiltonian (12) accordingly. The description is not as advanced as in the case of the Cooper pair transistor [28], but the simple model will be rather exhaustively studied in the following chapters.

### 4. Block diagonalisability and compatible observables

The introductory part is concluded by a remark that highlights the simplicity of leading theoretical ideas in this thesis. First, any finite-dimensional Hamiltonian $H$ is completely diagonalisable as a Hermitian operator. Thus the orthonormal eigenstates and corresponding eigenvalues can be found.

Second, in case of *compatible operators*, say $A$ and $B$, such that $[A, B] = 0$, simultaneous eigenstates for both operators can be found, see e.g. [29]. If the Hamiltonian $H$ commutes with $A$, the observable corresponding to $A$ is a *conserved quantity* and the associated

quantum number is referred to as a *good quantum number*. A well-known example is the conservation of angular momentum in case of a central field.

An important special case occurs if $A$ is an *orthogonal projection operator*, i.e. $A^2 = A$ and $A^\dagger = A$, so that the eigenvalues of $A$ are 0 and 1. Because the Hamiltonian also commutes with $\hat{1} - A$, the projection operator block diagonalises $H$ as a direct sum $H = AHA \oplus (1-A)H(1-A)$. In other words, the operator $A$ assigns each eigenstate an additional label, which is either 1 or 0. All eigenstates are obtained by diagonalising the Hamiltonian in each subspace separately. If the required eigenstate is known to correspond to the label 1, it suffices to diagonalise the operator $AHA$. One of the main results of this thesis is the construction of such a projection operator and the evaluation of the corresponding matrix elements.

Third, in case of an infinite-dimensional Hamiltonian, such as the tunnelling-charging Hamiltonian of a Cooper pair pump, the full Hilbert space must be compatible with the choice of the projection $A$. Thus $A$ is always a conserved quantity and the eigenstates, the eigenvalues, and the expectation values of observables should converge with respect to the dimension of the representation.

Finally, because each symmetry is associated with a conserved quantity it is the theoretician's job to identify them, one after the other. Different geometrical and dynamical symmetries, both exact and approximate, are constantly identified in all fields of physics. Examples of collected works on the subject are given by Tinkham's ageless text book "Group Theory and Quantum Mechanics" [30] and Talmi's book on the shell model and bosonic models in nuclear physics [31]. The role and the importance of symmetry in physics is beautifully highlighted in both books. In short, one should never underestimate "the force of symmetry", see e.g. [32].

## II. ADIABATIC TRANSPORT OF COOPER PAIRS

In this chapter the charge transfer in gated arrays of Josephson junctions is discussed. First the *model Hamiltonian* is defined and some introductory examples are examined. The renormalisation method used in this chapter is explained and applied in case of uniform arrays and different choices with respect to the included charge states. The leading order expressions for the supercurrent and the Cooper pair pumping are obtained and confirmed numerically.

Further on, more detailed an analysis based on the renormalisation approach is carried out. First, the basis-dependent effects and next-to-leading order corrections are examined. The calculations are extended to intermediate coupling strengths. The model is generalised so that inhomogeneous, i.e. non-uniform, arrays can be considered. The leading order contributions due to inhomogeneity are evaluated and parametrised. The effects due to deviations in the gating sequence are briefly scanned. In all, the model yields a quantitative, testable prediction of the Cooper pair pumping based on experimentally motivated parameters. An outlook which includes discussion on possible applications finishes the chapter.

### 1. An overview of the model

In the main part of this thesis a model describing the direct supercurrent and *adiabatic transport of Cooper pairs* through one-dimensional Cooper pair pumps, is developed. In short, a Cooper pair pump is a linear array of Josephson junctions, where the amount of charge on each island can be controlled by an external *gate voltage* $V_{\mathrm{g},k}$ as shown in Fig. 1. The Josephson junctions are assumed to be independent and described by the Hamiltonian

$$H_k = H_{\mathrm{C},k} + H_{\mathrm{J},k}. \tag{13}$$

The *charging Hamiltonian* $H_{\mathrm{C},k} := (2e)^2 m_k^2/C$, where $m_k$ is the relative number of Cooper pairs across the junction, describes electrostatic charging effects. The *tunnelling Hamiltonian* $H_{\mathrm{J},k} := -E_{\mathrm{J},k}\cos(\phi_k)$ is also related to the supercurrent through the junction via the *supercurrent operator* $I_{\mathrm{S},k} = I_{\mathrm{c},k}\sin(\phi_k) = (-2e/\hbar)dH_{\mathrm{J},k}/d\phi_k$, where $I_{\mathrm{c},k}$ is the critical current of the junction. The supercurrent operator is proportional to a Gâteaux derivative of $H_{\mathrm{J},k}$ with respect to $\phi$ [33, 34], i.e.

$$I_{\mathrm{S},k}(\phi_k) = (-2e/\hbar)\lim_{d\phi_k\to 0}\frac{H_{\mathrm{J},k}(\phi_k + d\phi_k) - H_{\mathrm{J},k}(\phi_k)}{d\phi_k}, \tag{14}$$

where $\phi_k$ is understood to be a continuous and $2\pi$-periodic parameter of the Hamiltonian.

Because $m_k$ and $\phi_k$ are canonical conjugate variables, i.e. $[\phi_k, m_k] = i$, the canonical representation $m_k = -i\partial/\partial\phi_k$ casts Hamiltonian in the form $H = -E_{\mathrm{C},k}\partial^2/\partial(\phi_k)^2 -$

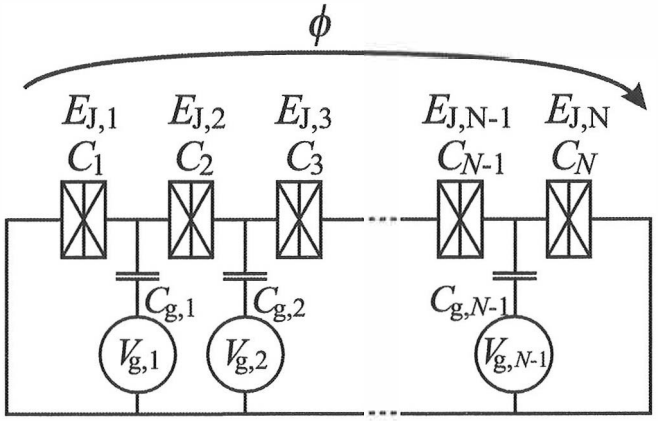


FIG. 1: A schematic drawing of a gated array of $N(\geq 3)$ Josephson junctions described by capacitances $C_k$, Josephson coupling energies $E_{\mathrm{J},k}$ and phase differences $\phi_k$. The total phase difference is given by $\phi = \sum_{k=1}^{N} \phi_k$. The gate voltages $V_{\mathrm{g},k}$ are used in order to control the optimal amount of charge on each island. In terms of Cooper pairs this is given by the normalised gate charges $\vec{q}$, where $q_k := -C_{\mathrm{g},k} V_{\mathrm{g},k}/2e$.

$E_{\mathrm{J},k}\cos(\phi_k)$. The corresponding eigenvalue equation can be written in terms of the *Mathieu equation*

$$\frac{d^2y}{dv^2} + [(-E/4E_{\mathrm{C},k}) + (E_{\mathrm{J},k}/4E_{\mathrm{C},k})\cos(2v)]y = 0, \tag{15}$$

where $E$ is the eigenvalue and $v := \phi_k/2$ [26, 35]. This framework has been generalised to include damping and external circuits and it is widely used in literature [36]. A recent paper by Anglin et al. [35] highlights some problems of this approach as compared to the bosonic Hamiltonian written in terms of creation and destruction operators, e.g. in [37, 38]. In short, the problem boils down to the existence and definition of a *quantum phase operator* [39, 40]. In this thesis, the existence of such a phase operator $\phi_k$ is taken for granted and number of Cooper pairs $m_k$ is assumed to be the canonical conjugate variable of $\phi_k$, i.e. $[\phi_k, m_k] = i$.

All calculations will be performed after considerable simplifications. The *quasiparticle degree of freedom* is neglected, and only Cooper pairs are taken into account. The independence of the junctions means that the total Hamiltonian can be expressed as

$$H = \sum_{k=1}^{N} (H_{\mathrm{C},k} + H_{\mathrm{J},k}). \tag{16}$$

The charging Hamiltonians have to be corrected for the fact that the amount of free charge

on each island, $(-2e)u_k$, is controlled by the gate voltage $V_{g,k}$, so $u_k$ is not necessarily an integer. It is implicitly assumed that the number of Cooper pairs on each island is large enough so that many pairs can be removed without destroying the condensate. Thus the number of Cooper pairs is evaluated relative to the equilibrium case, when all gate voltages are set to zero. The number of Cooper pairs on each island and the *normalised gate charges* ($q_k := -C_{g,k}V_{g,k}/2e$) are specified by $\vec{n} = (n_1, n_2, \ldots, n_{N-1})$ and $\vec{q} = (q_1, q_2, \ldots, q_{N-1})$, respectively.

The *capacitive charging energy* of the array is given by $E_{ch} = \frac{1}{2}\sum_{k=1}^{N} C_k V_k^2$, where $V_k$ is the voltage across the $k$th junction, in turn related to the phase difference $\phi_k$ via $d\phi_k/dt = -2eV_k/\hbar$. The voltage across each junction can be solved for a definite charge state $\vec{n}$, provided the voltage across the array, $V_b = \sum_{k=1}^{N} V_k$, is fixed by ideal biasing, i.e. $V_b$ is a constant. If the bias voltage vanishes, the charging Hamiltonian $H_C$ depends only on the gate charges $\vec{q}$ and the charging energy of a given state only on the free charge $\vec{u} := \vec{n} - \vec{q}$. This simultaneously fixes the total phase difference across the array, $\phi := \sum_{k=1}^{N} \phi_k$, which is shown in Fig. 1.

The assumption of ideal biasing can be justified if the impedance of the environment is negligible. The rate of change of gate charges $\vec{q}$ is slow as compared to the evolution of the condensates, which are assumed to be in equiliblium with respect to the value of $\vec{q}$. The resulting *Born-Oppenheimer approximation*, where $\vec{q}$ is a parameter of the Hamiltonian, is analogous to the molecular approximation of stationary, massive nuclei [41]. Any fluctuations of the gate charges are neglected, so the eigenenergies and the eigenstates, corresponding to specific values of the supercurrent, are solved separately for each value of $\vec{q}$. If the rate of change is slow enough, the *Landau–Zener tunnelling* between instantaneous eigenstates can also be neglected.

Any effects due to the *electromagnetic environment*, *sporadic quasiparticle tunnelling*, or external circuits are neglected, so that any transport of Cooper pairs must be directly evaluated from the *tunnelling-charging Hamiltonian* $H$, which does not contain effects due to the *Cooper pair co-tunnelling*.

If the array is uniform, $C_k := C$ for all $k$, the charging energy in case $V_b = 0$ can be expressed in terms of the free charge $\vec{u}$. The conservation of charge requires that

$$v_k - v_{k+1} = u_k, \tag{17}$$

whence a relatively easy calculation yields the result [1]

$$E_{ch}^{\vec{n},\vec{q}} = \frac{E_C}{N}\left[\sum_{k=1}^{N-1} k(N-k)u_k^2 + 2\sum_{l=2}^{N-1}\sum_{k=1}^{l-1} k(N-l)u_k u_l\right], \tag{18}$$

where $E_C := (2e)^2/2C$ is defined as the (unit of) *charging energy*. The generalisation corresponding to non-uniform, or inhomogeneous arrays, will be derived later as the model

is developed further. The uniformity also implies that the Josephson coupling strengths $E_{\mathrm{J},k}$ are identical, denoted by $E_{\mathrm{J}}$, so the tunnelling Hamiltonian simplifies to

$$H_{\mathrm{J}} = -\frac{E_{\mathrm{J}}}{2}\sum_{k=1}^{N}\cos(\phi_k). \tag{19}$$

Original canonical variables $\{\phi_k, m_k\}$, where $m_k$ is the number of tunnelled Cooper pairs through junction $k$, satisfy *canonical commutation relations*

$$[\phi_j, m_k] = i\delta_{jk}, \quad [\phi_j, \phi_k] = [m_j, m_k] = 0, \tag{20}$$

where $\delta_{jk}$ is the Kronecker delta symbol. A canonical transformation to a new set of variables, $\{\theta_k, n_k, \phi, M\}$, containing both $\vec{n}$ and the *overall phase difference* $\phi$, is given by Ingold and Nazarov [43]. Here $\theta_k$ is the phase on the $k$th island, $M = (1/N)\sum_k m_k$ is the average number of tunnelled Cooper pairs, and $\phi_k = \theta_k - \theta_{k-1} + \phi/N$. As $E_{\mathrm{ch}}^{\vec{n},\vec{q}}$ does not depend on the overall phase difference, $\phi$ is a constant of motion of the *model Hamiltonian*

$$H = H_{\mathrm{C}}(\vec{q}) + H_{\mathrm{J}}, \tag{21}$$

unless externally controlled by $V_{\mathrm{b}}$. In case of a superconducting loop, when the whole ring is superconducting, the *magnetic flux* can be used for controlling $\phi$, as explained e.g. in [26, 42]. The matrix elements of the charging Hamiltonian are given by the charging energies, so that

$$\langle \vec{n}, \phi | H_{\mathrm{C}} | \vec{n}', \phi \rangle = E_{\mathrm{ch}}^{\vec{n},\vec{q}}\delta_{\vec{n},\vec{n}'}. \tag{22}$$

The matrix elements of the tunnelling Hamiltonian $H_{\mathrm{J}}$ are most easily evaluated using the inverse of the Euler's formula $\cos(x) = (e^{ix}+e^{-ix})/2$ and $\sin(x) = (e^{ix}-e^{-ix})/2i$ and so-called *tunnelling vectors* $\{\vec{\delta}_k\}_{k=1}^{N}$. Tunnelling of one Cooper pair through the $k$th junction changes $|\vec{n}\rangle$ by $\vec{\delta}_k$, where the non-zero components are (if applicable) $(\vec{\delta}_k)_k = 1$ and $(\vec{\delta}_k)_{k-1} = -1$. Direct evaluation then yields [1]

$$H_{\mathrm{J}} = -\sum_{k=1}^{N}\frac{E_{\mathrm{J},k}}{2}\sum_{\vec{n}}\left(|\vec{n}+\vec{\delta}_k\rangle\langle\vec{n}|e^{i\phi/N} + |\vec{n}\rangle\langle\vec{n}+\vec{\delta}_k|e^{-i\phi/N}\right), \tag{23}$$

so each tunnelling in the "forward" direction is related to a phase difference $\phi/N$ as shown by the relation expressing $\phi_k$ in terms of the new canonical variables.

In any eigenstate of the model Hamiltonian the expectation value of all supercurrent operators

$$I_{\mathrm{S},k} = \frac{ieE_{\mathrm{J},k}}{\hbar}\sum_{\vec{n}}\left(|\vec{n}+\vec{\delta}_k\rangle\langle\vec{n}|e^{i\phi/N} - |\vec{n}\rangle\langle\vec{n}+\vec{\delta}_k|e^{-i\phi/N}\right), \tag{24}$$

must be identical due to the conservation of charge. In [1] the supercurrent and pumping have been evaluated for single junctions, but most of the time the *average supercurrent operator* $I_S$ defined by

$$I_S := \frac{1}{N}\sum_{k=1}^{N} I_{S,k} = \frac{(-2e)}{\hbar}\frac{\partial H}{\partial \phi} \tag{25}$$

is more appropriate. Because $I_S$ is a Gâteaux derivative of the full Hamiltonian, the common expectation value is just $(-2e/\hbar)\partial E/\partial\phi$, where $E$ is the eigenenergy of the stationary state.

The most important parameter of the model is the *coupling strength*, defined as the ratio between the Josephson energy and the charging energy,

$$\varepsilon_J := E_J/E_C. \tag{26}$$

When $\varepsilon_J \ll 1$ the charging effects dominate and the distribution of charge on islands is narrow. The average number of Cooper pairs on island $k$ is the expectation value in a stationary state $|\psi\rangle = \sum_{\vec{n}} c_{\vec{n},\phi}|\vec{n},\phi\rangle$, i.e.

$$\langle n_k\rangle = \sum_{\vec{n}} (\vec{n})_k |c_{\vec{n},\phi}|^2. \tag{27}$$

As usual, the uncertainty in $n_k$ is defined as the root mean square deviation $\Delta n_k = (\langle n_k^2\rangle - \langle n_k\rangle^2)^{1/2}$, which grows for all islands as $\varepsilon_J$ becomes larger. On the other hand, if $\varepsilon_J \gg 1$ the phases $\phi_k$ are well defined and the system is dominated by the supercurrent through the array. Both properties must be considered in detail if the coupling is neither insignificant nor dominant.

In principle, the pumping of Cooper pairs can be arranged by operating gate voltages cyclically when $\varepsilon_J \ll 1$. One presumes that as the nature of the ground state changes sharply when the optimal charge state changes, this also corresponds to tunnelling of a single Cooper pair and eventually yields a current $I = -2ef$, where $f$ is the operating frequency of the gate voltages. The reported study of a three-junction Cooper pair pump by Geerligs et al [44], did not reproduce this result, although current plateaus near this value were observed. They accounted deviations in terms of Landau–Zener tunnelling, Cooper pair co-tunnelling and sporadic quasiparticle tunnelling.

In general, when a potential well propagates adiabatically along an electron system that is effectively one-dimensional, it carries with it additional electron density, and induces dc electric current through the system. Such a pumping effect has been widely studied in small metallic tunnel junctions in the Coulomb blockade regime [45–47]. Semiconductor quantum dots [48] and one-dimensional ballistic channels [49] have also been used. The propagation of the well is arranged either by phase-shifted gate voltages [45, 47, 48] or by an acoustoelectric effect [46, 49].

If the well carries precisely $n$ electrons and the pumping frequency is $f$, the induced current is given by the fundamental relation $I = -nef$. In the case of normal state Coulomb blockade pumps, the obtainable accuracy may become sufficient for metrological applications [47]. The origin of the inaccuracy for normal state pumps, i.e. deviation from $I = -nef$, has also been examined, e.g. in [47, 50, 51]. The pumping of Cooper pairs has gained interest due to new ideas in quantum measuring and computing [52, 53]. In principle, the Cooper pair pump could also be used when studying geometrical phases in superconducting nanocircuits as discussed in [54]. The geometrical Berry's phase [55] is an additional phase factor an adiabatically evolving eigenstate must acquire in order to satisfy the Schrödinger's equation.

Below, a model describing adiabatic transport of Cooper pairs in gated arrays of Josephson junctions is developed. The model also relates to the direct supercurrent flowing through the array. It must be stressed that the model is highly idealised, disregarding any enviromental effects and describing only the gated array itself. The model can be used as a building block when developing a more realistic model. In the last part of this thesis, the properties of the model Hamiltonian are examined in detail.

## 2. Naive expression for the pumped charge

Initial ideas for the model revolved around occupation propabilities of different charge states. The capacitive charging energy for a three-junction pump used by Geerligs et al. in [44] reads explicitly

$$E_{\rm ch}^{\vec{n},\vec{q}} = (2E_{\rm C}/3)\left[(q_1 - n_1)^2 + (q_2 - n_2)^2 + (q_1 - n_1)(q_2 - n_2)\right], \tag{28}$$

when the array is assumed to be uniform. The lowest-lying charge states and suggested gating paths are shown in Fig. 2. The circular path encircles the so-called resonance point where supercurrent is maximal because the charging energies for three charge states are identical. This path has been used experimentally as it is relatively easy to realise by using two phase-shifted, harmonic gate voltages superposed on dc gate biases. The triangular path also shown in the figure gives maximal energy separation of the degenerate charge states from other states at the crossing point.

A naive argument relating the occupation probabilities $P_{ij} := |c_{ij}|^2$ and their changes due to the charge transfer gives the *differential pumped charge*

$$dQ_{\rm p} = (-2e/3)\sum_{ij}[P_{i-1,j} - P_{i+1,j} + P_{i+1,j-1} - P_{i-1,j+1} + P_{i,j+1} - P_{i,j-1}]dP_{ij}. \tag{29}$$

Thus the change in the occupation probability $P_{ij}$ is weighted by probabilities of the states that can be reached by a single Cooper pair tunnelling. The sign is positive if the tunnelling

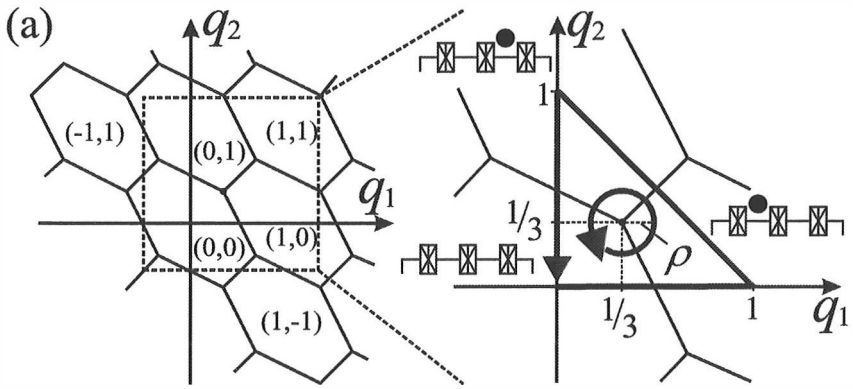


FIG. 2: (a) The lowest-lying charge states for a homogeneous three-junction Cooper pair pump in a small region of $(q_1, q_2)$-plane. The close-up shows a circular path with radius $\rho$ and a triangular gating path, both enclosing the node at $(\frac{1}{3}, \frac{1}{3})$. Both paths are suitable for pumping Cooper pairs and they correspond to transport of approximately one pair per cycle when $\varepsilon_J \ll 1$.

corresponds to $e^{i\phi/N}$ and the denominator 3 is the length of the array because a Cooper pair has to tunnel thrice in order to go through the array.

A simple example is offered by the circular path $\vec{q} = (\frac{1}{3} + \rho \sin x, \frac{1}{3} + \rho \cos x)$, where the parameter $x$, $0 \leq x < 2\pi$, determines the point on the trajectory. In the limit $\varepsilon_J \to 0$ and small radius $\rho$, only three charge states, namely $\{|00\rangle, |10\rangle, |01\rangle\}$, should be of importance. The corresponding truncated Hamiltonian matrix $H$, in units of $E_C$, is given by

$$\begin{pmatrix} \frac{2}{3}[q_1^2 + q_2^2 + q_1 q_2] & -\frac{1}{2}\varepsilon_J e^{-i\phi/3} & -\frac{1}{2}\varepsilon_J e^{i\phi/3} \\ -\frac{1}{2}\varepsilon_J e^{i\phi/3} & \frac{2}{3}[(q_1-1)^2 + q_2^2 + (q_1-1)q_2] & -\frac{1}{2}\varepsilon_J e^{-i\phi/3} \\ -\frac{1}{2}\varepsilon_J e^{-i\phi/3} & -\frac{1}{2}\varepsilon_J e^{i\phi/3} & \frac{2}{3}[q_1^2 + (q_2-1)^2 + q_1(q_2-1)] \end{pmatrix} \quad (30)$$

and the expression for the pumped charge simplifies to

$$dQ_p = (-2e/3)[(P_{00} - P_{01})dP_{10} + (P_{10} - P_{00})dP_{01} + (P_{01} - P_{10})dP_{00}]. \quad (31)$$

The obvious limit $Q_p \to 1$, when $\varepsilon_J \to 0$, is satisfied for all reasonable paths encircling the resonance point. For $\phi = 0$, and a small circular path around the node $(\frac{1}{3}, \frac{1}{3})$, the first order perturbation theory yields

$$Q_p \approx (-2e)\pi(\rho/\varepsilon_J)^2(128/729) + \mathcal{O}(\rho/\varepsilon_J)^4 \quad (32)$$

per cycle. Nevertheless, this approach suffers from a serious drawback. The direct supercurrent is evaluated as an expectation value but the suggested pumped charge (29) can not

be expressed as a matrix element of any linear operator because it contains the amplitudes $c_{ij}$ up to the fourth order. Consequently, the picture is inconsistent as the pumped charge and the supercurrent in the same process should be treated on the same footing.

### 3. The direct supercurrent and the pumped charge

The problem is solved by applying the *adiabatic approximation*, in the limit of slowly-varying gate voltages. The time-dependent Schrödinger equation yields the evolution of eigenstates and the expectation value of the supercurrent operator may be calculated for corresponding eigenstates. The expectation value is divided into the *direct supercurrent* and an additional, geometric part induced by operating the gates, which is consequently identified as the *pumped current*. Simultaneous quantum mechanical description of both currents is obtained.

The derivation proceeds as follows. For each instant of time $t$ the instantaneous eigenstates $\{|m_{(t)}\rangle\}$ corresponding to the eigenenergies $\{E_m^{(t)}\}$ of the Hamiltonian (21) for a given set of gate charges $\vec{q}(t)$ can be found. For slowly varying gate voltages the solution of the time-dependent Schrödinger equation satisfying the initial condition $|\psi_{(t_0)}\rangle = |m_{(t_0)}\rangle$ reads

$$\begin{aligned} |\psi_{(t_0+\delta t)}\rangle \;=\; & e^{-iE_m^{(t_0)}\delta t/\hbar}|m_{(t_0)}\rangle + \sum_{l(\neq m)} \frac{(e^{-iE_l^{(t_0)}\delta t/\hbar} - e^{-iE_m^{(t_0)}\delta t/\hbar})}{i(E_l^{(t_0)} - E_m^{(t_0)})/\hbar} \\ & \times \langle l_{(t_0)}|\vec{\nabla}_{\vec{q}}\, m_{(t_0)}\rangle \cdot (\partial\vec{q}/\partial t)|l_{(t_0)}\rangle := |m_{(t_0)}^{\delta t}\rangle + |\delta m_{(\delta t)}\rangle, \end{aligned} \tag{33}$$

where the term $\langle l_{(t_0)}|\vec{\nabla}_{\vec{q}}\, m_{(t_0)}\rangle \cdot (\partial\vec{q}/\partial t)$ is the directional derivative of the state $|m_{(t_0)}\rangle$ with respect to the change in gate charges $\vec{q}$. The amount of charge passing through the $k$th junction during a short time interval $\delta t$ is given by

$$\delta Q_k = \int_{t_0}^{t_0+\delta t} \langle\psi_{(t)}|I_{\mathrm{S},k}|\psi_{(t)}\rangle dt - \delta t\langle I_{\mathrm{S},k}\rangle_{|m_{(t_0)}\rangle} + 2\mathrm{Re}\left[\int_{t_0}^{t_0+\delta t} \langle m_{(t_0)}|I_{\mathrm{S},k}|\delta m_{(t-t_0)}\rangle dt\right], \tag{34}$$

where the term quadratic in $|\delta m\rangle$ has been neglected. When $\delta t \gg \hbar/|E_l - E_m|$ holds for all $l$, the oscillatory term can be neglegted and integration gives the induced (pumped) charge

$$\delta Q_{k,\mathrm{ind}} = -2\hbar \sum_{l(\neq m)} \mathrm{Im}\left[\frac{\langle m|I_{\mathrm{S},k}|l\rangle\langle l|\delta m\rangle}{E_l - E_m}\right], \tag{35}$$

where $|\delta m\rangle$ is the change in the instantaneous eigenstate induced by the change in gate charges $\vec{q}(t_0) \to \vec{q}(t_0 + \delta t)$.

For a closed path $\Gamma$ the total transferred charge must be equal for all junctions due to the conservation of charge. In terms of the average supercurrent operator $I_{\mathrm{S}}$ the total transferred

charge $Q = Q_\mathrm{s} + Q_\mathrm{p}$ reads

$$\frac{Q}{-2e} = \frac{1}{\hbar}\int_0^\tau \frac{\partial E_m^{(t)}}{\partial \phi} dt + \frac{\hbar}{e}\oint_\Gamma \sum_{l(\neq m)} \mathrm{Im}\left[\frac{\langle m|I_\mathrm{S}|l\rangle\langle l|dm\rangle}{E_l - E_m}\right]. \tag{36}$$

Here $\tau$ is the duration of a cycle and $Q_\mathrm{s}$, the *charge transported by the direct supercurrent*, is proportional to the dynamical phase of the wave function, $-\int_0^\tau (E_m^{(t)}/\hbar)dt$, since $I_\mathrm{S} = (-2e/\hbar)\partial H/\partial\phi$. Because the supercurrent vanishes for $\phi = 0$, so does $Q_\mathrm{s}$. The *pumped charge* $Q_\mathrm{p}$ depends only on the traversed path $\Gamma$, while $Q_\mathrm{s}$ depends also on the rate of change of the gate voltages.

The most important application of $Q_\mathrm{p}$ is clearly given by the ground-state pumping in which the system begins in its lowest eigenstate and remains in this state for the whole duration of pumping. Roughly speaking, the adiabatic approximation is valid if $h/\tau := hf \ll E_\mathrm{J}$, where $f$ is the gating frequency, so that the probability for Landau–Zener transitions to excited states is negligible. More precise expressions can be given once the energy denominators in $Q_\mathrm{p}$ have been evaluated. Naturally pumping for excited states can be evaluated but the inclusion of relaxation and excitation into an adiabatic model is quite complicated.

The evaluation of the pumped charge $Q_{\mathrm{p},k}$ for a single junction only can be done and it is sometimes very instructing. An alternative way to express the pumped charge through the junction $k$ is given by [1]

$$Q_{\mathrm{p},k} = 2\mathrm{Re}\left[\oint_\Gamma \langle m|\hat{Q}_k|dm\rangle\right], \tag{37}$$

where $\hat{Q}_k = \int I_{\mathrm{S},k}(t)dt$ is the time-dependent operator for charge through junction $k$, whose off-diagonal matrix elements are given by

$$\langle m|\hat{Q}_k|l\rangle = \frac{i\hbar\langle m|I_{\mathrm{S},k}|l\rangle}{E_l - E_m}. \tag{38}$$

The pumped charge can be associated with the geometrical *Berry's phase* $\xi = i\oint\langle m|dm\rangle$ [55], which ensures that the adiabatically evolving state satisfies the time-dependent Schrödinger equation. In the case $E_\mathrm{J} \ll E_\mathrm{C}$ it is stated in [1]: "As in the case of Berry's phase, the second term in Eq. (4) [$= Q_{\mathrm{p},k}$] does not vanish because the integration contour encloses a singularity where the energies of several charge states coincide. This degeneracy occurs when $q_k = 1/N$ for all k." The association is not direct as in the case of dynamical phase but it can be considerably simplified. It must be noted that deriving $Q_\mathrm{p}$ using fully adiabatic wave functions which contain the Berry's phase is neither very simple nor straightforward.

## 4. The two-level approximation

As $\varepsilon_J$ becomes vanishingly small the lowest eigenstate $|\psi\rangle$ corresponds very accurately to a single charge state $|\vec{n}\rangle$, in turn determined by $\vec{q}$. Unless several charge states become degenerate or nearly degenerate, a level crossing can be examined as a two-state process, at least in the lowest order. This non-multiple degeneracy condition holds for the circular path (except for some specific radii) and the triangular path or its generalisations shown in Fig. 3. Parametrisation for the gate charges for each leg can be written as

$$\vec{q}_{\rm leg}(x) = \sum_{k=1}^{\rm leg-1} \vec{\delta}_k + x \cdot \vec{\delta}_{\rm leg}, \quad {\rm leg} = 1, \ldots, N, \; x : 0 \to 1, \tag{39}$$

which closes after $N$ legs for an $N$-junction Cooper pair pump. As shown below, this path corresponds to the maximal charging energy differences at the degeneracy point $x = 1/2$. For obvious reasons, the names *sawtooth gating sequence* and *sawtooth path* are adopted for these cycles.

The Hamiltonian is truncated to include the charge states that become degenerate on the $k$th leg $|\vec{n}_1\rangle$ and $|\vec{n}_2\rangle := |\vec{n} + \vec{\delta}_k\rangle$. All other charge states are discarded and the Hamiltonian matrix reads

$$H = \begin{pmatrix} \epsilon_1 & -w^* \\ -w & \epsilon_2 \end{pmatrix}, \tag{40}$$

where $w := ve^{i\phi/N} := e^{i\phi/N} E_J^{(k)}/2$ and $\epsilon_i$ is the charging energy for charge state $i = 1, 2$. Solving for the eigenenergies and choosing the amplitude for state $|\vec{n}_1\rangle$ to be real yields

$$E_{1/2} = (\epsilon_1 + \epsilon_2)/2 \mp v\sqrt{1+\eta^2}, \tag{41}$$

$$a_{1/2,1} = 2^{-1/2}\left(1 \pm \eta/\sqrt{1+\eta^2}\right)^{1/2}, \tag{42}$$

$$a_{1/2,2} = \pm 2^{-1/2} e^{i\phi/N}\left(1 \mp \eta/\sqrt{1+\eta^2}\right)^{1/2}, \tag{43}$$

where $\eta = (\epsilon_2 - \epsilon_1)/2v$. The pumped charge for the two-level system simplifies to

$$Q_{\rm p} = (-2e){\rm Re}\left[\int_{\eta_i}^{\eta_f} \frac{-2(a_{1,2}^* a_{2,1} w - a_{1,1}^* a_{2,2} w^*)(a_{2,1}^* da_{1,1} + a_{2,2}^* da_{1,2})}{2v\sqrt{1+\eta^2}}\right]. \tag{44}$$

Since $(a_{1,2}^* a_{2,1} w - a_{1,1}^* a_{2,2} w^*) = v$ and an easy diffentiation shows that $(a_{2,1}^* da_{1,1} + a_{2,2}^* da_{1,2}) = \frac{1}{2} d\eta/(1+\eta^2)$, the integration results in

$$Q_{\rm p} = e\left[\eta_f (1+\eta_f^2)^{-1/2} - \eta_i (1+\eta_i^2)^{-1/2}\right], \tag{45}$$

which depends only on the initial and final charging energy differences and is independent of the total phase difference $\phi$. For small values of $\varepsilon_J$ the pumping is usually almost complete,

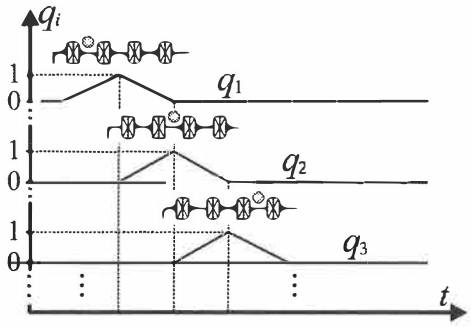


FIG. 3: A train of normalised gate charges for the generalisation of the triangular path, also called the sawtooth path. The optimal charge states at the endpoints of the first three legs are also shown.

i.e. $-2e[1-\mathcal{O}(\varepsilon_{\rm J})^2]$. Any $\phi$-dependence is induced by the other charge states that become active as $\varepsilon_{\rm J}$ becomes significant, but as most of the pumping occurs in the vicinity of the degeneracy points, it should be possible to evaluate $Q_{\rm p}$ accurately from the properties of the system at the level crossing.

The pumping of Cooper pairs can be described by the two-level approximation when each level crossing is treated separately, using appropriate charge states. A Cooper pair must tunnel once through each junction in the same direction in order to pass through the array. Either the average supercurrent operator $I_{\rm S}$ is used for all level crossings, so the result (45) has to be divided by $N$, or $Q_{{\rm p},k}=0$ except for the level crossing when $I_{{\rm S},k}$ is active. The validity of the approximation is questionable if the pumped charges for single junctions vary considerably. Then the full path should be taken into account.

## 5. Elementary renormalisation method and the first results

A level crossing of charge states $|\vec{n}_1\rangle$ and $|\vec{n}_2\rangle$ is sharp if all other amplitudes in the corresponding eigenstate are small at and in the vicinity of the degeneracy point. In other words the eigenstate $|\psi\rangle$ can be decomposed as

$$|\psi\rangle := |\psi(2)\rangle + |\psi(>2)\rangle = a_1|\vec{n}_1\rangle + a_2|\vec{n}_2\rangle + \sum_{j(>2)} a_j|\vec{n}_j\rangle, \tag{46}$$

where all non-dominant charge states in the truncated Hamiltonian are included in the small part $|\psi(>2)\rangle$, such that $\| \, |\psi(>2)\rangle\| \ll 1$. The amplitudes are obtained from the Schrödinger

equation

$$
\begin{aligned}
(E_{\mathrm{ch},1} - E)a_1 - w^* a_2 + \sum_{j>2} \langle \vec{n}_1 | H_\mathrm{J} | \vec{n}_j \rangle a_j &= 0, \\
-w a_1 + (E_{\mathrm{ch},2} - E)a_2 + \sum_{j>2} \langle \vec{n}_2 | H_\mathrm{J} | \vec{n}_j \rangle a_j &= 0, \\
(E_{\mathrm{ch},j} - E)a_j + \sum_{k=1}^{N} (w^* a_{\vec{n}_j + \vec{\delta}_k} + w a_{\vec{n}_j - \vec{\delta}_k}) &= 0, \quad j > 2,
\end{aligned}
\tag{47}
$$

where $w := ve^{i\phi/N} = e^{i\phi/N} E_\mathrm{J}/2 \ll E_\mathrm{C}$. The two lowest-lying eigenstates $|1\rangle$ and $|2\rangle$ can now be used for re-evaluating the integral (44), when coefficients $a_{1/2,j>2}$ are expressed in terms of the dominant coefficients $a_{1/2,1}$ and $a_{1/2,2}$. The contribution from other states is suppressed by large energy denominators at the level crossing as well as small amplitudes for charge states $\vec{n}_1$ and $\vec{n}_2$.

A suitable truncation in case of the three-junction pump, i.e. $N = 3$, includes the charge states $\{|00\rangle, |10\rangle, |01\rangle, |1,-1\rangle, |11\rangle, |-1,1\rangle\}$. Three additional states are included due to their involvement in the leading order correction. The Hamiltonian matrix for $\phi = 0$ is given by

$$
H = \begin{pmatrix}
E_{\mathrm{ch},1} & -v & -v & 0 & -v & -v \\
-v & E_{\mathrm{ch},2} & -v & -v & 0 & -v \\
-v & -v & E_{\mathrm{ch},3} & -v & -v & 0 \\
0 & -v & -v & E_{\mathrm{ch},4} & 0 & 0 \\
-v & 0 & -v & 0 & E_{\mathrm{ch},5} & 0 \\
-v & -v & 0 & 0 & 0 & E_{\mathrm{ch},6}
\end{pmatrix}. \tag{48}
$$

Three level crossings, $|00\rangle \to |10\rangle$, $|10\rangle \to |01\rangle$, and $|10\rangle \to |00\rangle$, occur as shown in Fig. 2. Their locations are determined by $E_{\mathrm{ch},j}$ which depend on the gate charges $\vec{q}$. Elimination of the non-dominant coefficients yields a *renormalised Hamiltonian matrix* which gives the correct coupling between dominant charge states, naturally up to the evaluated order. The two-level Hamiltonian matrix is given by

$$
\tilde{H} \approx \begin{pmatrix}
E_{\mathrm{ch},1|2|3} - v^2(\delta_{3|1|2} + \delta_{5|6|4} + \delta_{6|4|5}) & -v[1 + v(\delta_{3|1|2} + \delta_{6|4|5})] \\
-v[1 + v(\delta_{3|1|2} + \delta_{6|4|5})] & E_{\mathrm{ch},2|3|1} - v^2(\delta_{3|1|2} + \delta_{6|4|5} + \delta_{4|5|6})
\end{pmatrix}, \tag{49}
$$

where $\delta_j = (E_{\mathrm{ch},j} - E)$ and $E$ is the correct eigenenergy at the crossing. The notation $k_1|k_2|k_3$ indicates that the energy difference is evaluated with respect to the charge state $k_1$, $k_2$ and $k_3$ at the first, the second and the third crossing, respectively. As proposed in Sec. II.4, the charge transfer is modified mostly near the degeneracy point, where the $\tilde{H}$ is evaluated and integration of the $Q_\mathrm{p}$ is subject to these modifications.

Full charge transfer in the framework of the two-level model, mainly due to to higher-lying excited states, is assumed, i.e. $Q_\mathrm{p} = -2e$ or $\eta \to \infty$ in Eq. (45), Deviations from

$Q_{\rm p} = -2e$ are assumed to arise from the changes in the effective Hamiltonian near the level crossing.

When $E_{\rm J} \ll E_{\rm C}$, $E$ is well approximated by the degenerate charging energy, and corrections in the diagonal matrix elements are of the order of $(E_{\rm J}/E_{\rm C})^2$. The magnitude of coupling constant changes already in the first order and $v_{\rm eff}/v = 1+v(\delta_{3|1|2}+\delta_{6|4|5})$. This reduces the amount of transferred charge in the dominant junction because $\langle \vec{n}_{2|3|1}|I_{{\rm S},1|2|3}|\vec{n}_{1|2|3}\rangle \propto -iv$. Thus $Q_{\rm p,dom} \approx (-2e)[1-v(\delta_{3|1|2}+\delta_{6|4|5})]$. For the non-dominant junctions, the pumped charge arises from expanding the non-dominant coefficients in the matrix element. The resulting contribution is of the form $2ev(\delta_{3|1|2}+\delta_{6|4|5})$, where only the contribution in the order of $-2e$ is missing.

The predicted pumped charge over a full cycle for any of the junctions is given by

$$Q_{\rm p} = (-2e)[1 - w(\delta_3^{(1)} + \delta_6^{(1)} + \delta_1^{(2)} + \delta_4^{(2)} + \delta_2^{(3)} + \delta_5^{(3)})], \tag{50}$$

where the superscript $^{(j)}$ corresponds to the crossing in question. This is the complete leading order correction. The result does not depend on the interpretation. One may as well follow a single junction for the duration of a cycle or directly evaluate the average charge transport for each junction.

Inserting energy denominators for the triangular gating sequence results in

$$Q_{\rm p}^{\Delta}/(-2e) := 1 - 9\varepsilon_{\rm J}. \tag{51}$$

On the other hand, the pumped charge for a circular path with radius $\rho$ reads [1]

$$\frac{Q_{\rm p}^{\bullet}}{-2e} := 1 - \frac{3\varepsilon_{\rm J}}{2}\left(\frac{1}{3\sqrt{2}\rho} + \frac{1}{2-3\sqrt{2}\rho} + \frac{\sqrt{5}}{3\rho} + \frac{\sqrt{5}}{\sqrt{5}-3\rho}\right), \tag{52}$$

which diverges when $\rho \to 0$ or $\rho \to \sqrt{2}/3$, because the assumption of a sharp level crossing is violated in the vicinity of the resonance points $(\frac{1}{3},\frac{1}{3})$ and $(\frac{2}{3},\frac{2}{3})$. These are the first quantitative evaluations of the quantum inaccuracy, i.e. the deviation from $Q_{\rm p} = -2e$.

The predicted inaccuracies for $\phi = 0$ are large, of the order of 10 % for $\varepsilon_{\rm J} = 0.01$ and about 25 % for $\varepsilon_{\rm J} = 0.03$, which are very small values of $\varepsilon_{\rm J}$ from the experimental point of view. The results for $\varepsilon_{\rm J} \geq 0.1$ definitely require more charge states to be included, even when evaluated numerically from Eq. (36). Numerical calculations for the triangular path show that the actual inaccuracy is reduced by about 3 % or 10 % from the prediction (51), when $\varepsilon_{\rm J} = 0.01$ or 0.03. For even stronger coupling, $\varepsilon_{\rm J} = 0.1$, the numerically obtained pumped charge is $0.366 \cdot (-2e)$, while the simple prediction gives $0.1 \cdot (-2e)$.

The results for $Q_{\rm p}$ of the circular path and the inaccuracy as a function of $\rho$ are shown in Fig. 4. Optimal charge transfer is seen to occur near radius $\rho \approx 0.3$. In the limit $\rho \to 0$ the analytical result

$$Q_{\rm p}^{o} \approx (-2e)\pi(\rho/\varepsilon_{\rm J})^2(64/729) + \mathcal{O}(\rho/\varepsilon_{\rm J})^4 \tag{53}$$

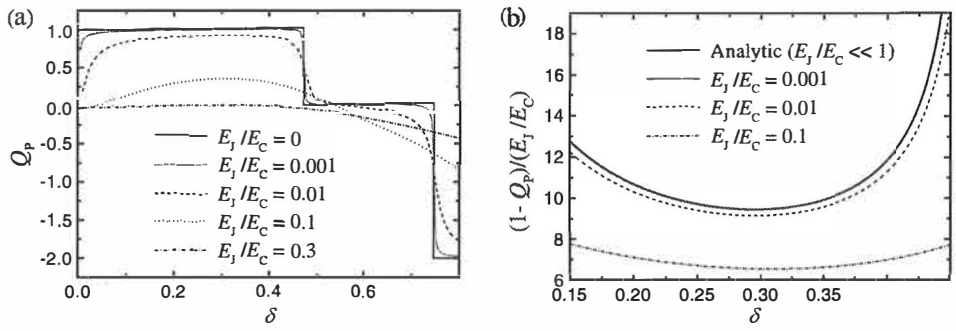


FIG. 4: (a) Numerical results for the pumped charge from Eq. (36) as a function of $\rho$ and $\varepsilon_J$. $Q_p$ for $E_J = 0$ vanishes at $\rho = \sqrt{2}/3$ because the degeneracy point at $\vec{q} = (\frac{2}{3}, \frac{2}{3})$ is circulated and the direction of charge transfer is opposite to that of $\vec{q} = (\frac{1}{3}, \frac{1}{3})$. Additional transfer of $-2$ Cooper pairs occurs at $\rho = 1/\sqrt{3}$. (b) A closeup on the inaccuracy and comparison against the analytical result (52). At $\varepsilon_J = 0.001$ the curves practically coincide. Taken from [1], where the symbol $\delta$ was used instead of $\rho$.

is exactly one half of the naive result (32). This shows that the simple description works qualitatively, but not quantitatively. For very small values of $\varepsilon_J$, the eigenenergies relative to the degenerate charging energy are given by $E_k = -E_J \cos[(\phi - 2\pi k)/N]$ and thus the ground state supercurrent is given by

$$I(\phi) = (I_c/N)\sin(\phi/N), \quad \phi \in (-\pi, \pi), \tag{54}$$

exhibiting a cusp at $\pm\pi$ due to a level crossing between decoupled eigenstates of the model Hamiltonian [1]. Consequently, the adiabatic approximation is not valid in the the region of this resonance point for $\phi \approx \pm\pi$.

In order to systematically apply the renormalisation method described above, an identification is necessary. The renormalised Hamiltonian corresponds to the Feshbach *effective interaction* [56, 57] and the evaluation of matrix elements to the use of respective *effective operators*. Due to its simplicity, the theory of Feshbach can easily be applied in case of a Cooper pair pump.

## 6. Mathematical interlude I: Effective operators

The theory of effective operators or renormalisation is widely used in nuclear, atomic and molecular physics [58–66]. An effective interaction strives to obtain correct eigenenergies and

eigenstates of a system in a *finite-dimensional model space*. In some cases the full eigenstate of the system can be reconstructed. In short, renormalisation means mapping the system onto the model space, as accurately as possible.

Many renormalisation schemes have been proposed, some of them straightforward, others quite complicated. The quality of an effective interaction is determined by the accuracy of the eigenvalues and eigenstates as compared to those of the full system. In many cases, e.g. in nuclear and particle physics, part of the problem is that the actual full Hamiltonian is not exactly known. In the present case the model Hamiltonian is well defined but not very realistic. Nevertheless, understanding even a simple model may give insight regarding the physical system.

The matrix elements of an effective operator operating on the model space should be as close as possible to those of the corresponding operator in the full space. Sometimes this is relatively easy, sometimes very difficult. Theory of effective interactions and operators in nuclei are studied in review articles by Kuo [60] and Ellis and Osnes [61]. Both works contain a suitable introduction to the subject and the latter also compares perturbative approaches and renormalisation.

The following derivation of the Feshbach effective interaction goes along the lines set by Kuo [60]. A complete Hilbert space $\mathcal{H}$ is divided into two parts by orthogonal projection operators $P$ and $Q$ such that $P + Q = \hat{1}$, and $PQ = 0$. The aim is to solve the full Schrödinger equation $H|\psi\rangle = E|\psi\rangle$ in the finite-dimensional ($= d_P$) model space ($P$-space) in such a manner that correct eigenenergies and wave functions are obtained. The rest of the full space, the $Q$ space or the excluded space, enters in the equation as a renormalisation of the Hamiltonian in the $P$-space.

The Schrödinger equation can be decomposed as

$$\begin{array}{rcrcl} PHP|\psi\rangle & + & PHQ|\psi\rangle & = & EP|\psi\rangle \\ QHP|\psi\rangle & + & QHQ|\psi\rangle & = & EQ|\psi\rangle \end{array}, \tag{55}$$

where $H = H_0 + V$ and $[H_0, P] = [H_0, Q] = 0$. Often it is common to choose $H_0$ to be diagonal with respect to the basis states, so that the residual interaction $V$ corresponds to coupling between states. Thus $H_0|\nu_l\rangle = \epsilon_l|\nu_l\rangle$ and it is convenient to choose $|\nu_l\rangle$ in the $P$-space when $l < d_P$. If the inverse of operator $Q(E - H)Q$ exists, this leads to an effective Schrödinger equation for $P|\psi\rangle$

$$P\left[H_0 + V + V(Q(E - H)Q)^{-1}V\right]P|\psi\rangle = EP|\psi\rangle. \tag{56}$$

Expanding $[Q(E - H_0 - V)Q]^{-1}$ as a power series leads to the Feshbach form of the $P$-space effective interaction [56]

$$\tilde{V}_{\text{eff}}(E) = P\left[\sum_{n=0}^{\infty}\left(V[Q(E - H_0)Q]^{-1}\right)^n\right]VP, \tag{57}$$

which is especially convenient if $H_0$ is diagonal so that $[Q(E-H_0)Q]^{-1}$ corresponds to energy denominators of the type $E - \epsilon_{l(>d_P)}$. If $E$ is an eigenvalue of the effective Hamiltonian

$$\tilde{H}(E) = H_0 + \tilde{V}_{\text{eff}}(E), \tag{58}$$

then $E$ is also an eigenvalue of the full problem and the solution $P|\psi\rangle$ can be expanded into the full space according to

$$|\psi\rangle = \left[\sum_{n=0}^{\infty} \left([Q(E-H_0)Q]^{-1}V\right)^n\right] P|\psi\rangle, \tag{59}$$

where the zeroth power ($n = 0$) of an operator is simply the identity operator $\hat{1}$. An alternative derivation of $\tilde{V}_{\text{eff}}(E)$ in the present case, where $H = H_{\text{C}} + H_{\text{J}}$ with $H_{\text{C}}|\vec{n}_l\rangle = \epsilon_l|\vec{n}_l\rangle$ and $V = H_{\text{J}}$, follows. Inserting the expansion $|\psi\rangle = \sum_l a_l|\vec{n}_l\rangle$ into the Schrödinger equation yields an infinite set of linear equations

$$\epsilon_l a_l + \sum_{m(\neq l)} V_{lm} a_m = E a_l. \tag{60}$$

In the first $d_P$ equations coefficients $a_{l(>d_P)}$ are repeatedly replaced by

$$a_{l(>d_P)} = \sum_{m=1}^{d_P} \frac{V_{lm}a_m}{E-\epsilon_l} + \sum_{m(>d_P)} \frac{V_{lm}a_m}{E-\epsilon_l}. \tag{61}$$

A sufficient condition for convergence and subsequent elimination of $a_{l(>d_P)}$ is given by

$$\max\left[\min\left(\sum_{m(>d_P)} \frac{|V_{lm}|}{|E-\epsilon_l|}, \sum_{m(>d_P)} \frac{|V_{lm}|}{|E-\epsilon_m|}\right),\ l > d_P\right] < 1. \tag{62}$$

The resulting set of $d_P$ linear equations is identical to the eigenvalue problem related to the effective Hamiltonian (58) which establishes that $E$ is a common eigenvalue of the renormalised and the full Hamiltonian. This follows from the diagonalisability of Hermitian operators in a finite-dimensional space. It is possible for another eigenvalue of $\tilde{H}$ to match an eigenvalue of the full Hamiltonian, but such a degeneracy is almost always accidental.

Evaluation of the effective interaction (57) up to the infinite order with arbitrary precision is often impossible, especially if the dimension of the Hamiltonian is not finite. Infinite sets of linear equations, as well as eigenvalue problems related to infinite matrices have been rigorously studied in mathematics, see e.g. [67, 68], where general results concerning the existence and accuracy of eigenvalues have been obtained. More specific results were obtained in case of tridiagonal matrices, which have also been studied in physics [69]. Examples of recent studies on infinite eigenvalue problems are related to the double points of Mathieu

equation [70], where two eigenvalues become degenerate, and the eigenvalues of quartic, sextic and octic anharmonic oscillators, which can be iteratively evaluated with an arbitrary precision [71].

Consequently, the evaluation of $\tilde{V}_{\rm eff}$ is truncated at the $k$th order, i.e. at $n = k$, and eigenvalues of resulting $\tilde{V}_{{\rm eff},k}$ are obtained recursively starting from an initial guess $E^{(0)}$ and repeatedly inserting the sought eigenenergy into the effective interaction. Sufficient criteria for convergence have been evaluated [72]. Limits for the accuracy of eigenvalues are also given. In order to obtain accurate eigenvalues one should have $\ll 1$ instead of only $< 1$ in Eq. (62) which is a sufficient condition for the existence of $\tilde{V}$. Actual convergence is usually considerably faster and may occur even if this convergence condition is violated. The ground state energy of the full system is bounded from above by the smallest eigenvalue of $P(H_0 + V)P$ which often also improves the limits for convergence.

Once approximate eigenenergies $\{E_i\}$ and corresponding renormalised states $\{P|\psi_i\rangle\}$ have been found, the expansion (59) can be used for evaluation of matrix elements of an arbitrary operator $T$. If the normalisation factors are given by $N_i := \langle\psi_i|\psi_i\rangle^{-1/2}$ the matrix element $\langle\psi_i|T|\psi_j\rangle$ reads

$$N_i N_j \langle\psi_i|P \left[\sum_{n=0}^{\infty} \left(V[Q(E_i - H_0)Q]^{-1}\right)^n\right] T \left[\sum_{n'=0}^{\infty} \left([Q(E_j - H_0)Q]^{-1}V\right)^{n'}\right] P|\psi_j\rangle. \qquad (63)$$

Usually a consistent matrix element corresponding to a fixed value of $k$ is given by including terms up to and including $n+n' \leq k$. For the present model some contributions are evaluated separately corresponding to different orders of renormalisation, because specific properties are sought after. This holds both for the direct supercurrent and the pumped charge.

## 7. Approximations concerning the effective interaction

The zeroth order Feshbach effective interaction $\tilde{V}_{\rm eff}^{(0)} := PVP$ corresponds to the $P$-space truncation of the Hamiltonian operator. Eigenvalues of the $n$th order renormalised Hamiltonian with effective interaction

$$\tilde{V}_{\rm eff}^{(n)}(E) := P \left[\sum_{n'=0}^{n} \left(V[Q(E - H_0)Q]^{-1}\right)^{n'}\right] VP \qquad (64)$$

are called the $n$th order eigenvalues. If the iteration has been performed and $E$ is an eigenvalue of Eq. (64), $E$ is an $n$th order "individual" choice eigenvalue. Skipping the iteration means that the "individual-0" choice eigenvalue $E$ corresponds to an eigenvalue $E_j$ of $PHP$. These choices are often used when evaluating the supercurrent proportional to the derivative of the eigenenergy.

The eigenstates obtained for "individual" choices are not orthogonal in $P$-space as they correspond to different effective Hamiltonian operators. One has to re-expand the states in order to regain orthogonality. If the residual interaction is weak enough it is possible to use a single effective interaction for the whole $P$-space without making any significant errors. This choice is referred to as the "average" choice as the average $P$-space energy $(1/d_P)\sum_{j=1}^{d_P}\tilde{H}_{jj}$ is used for renormalisation. Thus one does not have to diagonalise the effective Hamiltonian until at the final step and the obtained eigenstates are orthogonal. Skipping the iterative process leads to "average-0" choice which was already used in Sec. II.5. Evaluation of the matrix element of the supercurrent operator was performed using an "average-0" choice effective operator.

Finally it must be emphasised that renormalisation and full diagonalisation in a restricted basis are just two similar although nonidentical approaches to the eigenvalue problem. In renormalisation the full problem is projected onto a smaller space while in diagonalisation the problem is truncated by discarding all basis states outside the restricted basis.

### 8. Mathematical interlude II: Few-state dominance

The concept of "few-state dominance" is important for the present model because it often implies good convergence for the effective interaction as well as for effective operators. In "few-state dominant" systems some of the basis states are separated from all the others by an energy $\Delta E$ which is large as compared to the coupling between any two states in the system. Thus certain eigenstates of the full system can be approximated by the eigenstates of the "few-state dominant" part only.

Let $H = H_0 + V$ such that $H_0|\nu_l\rangle = \epsilon_l|\nu_l\rangle$, and $V$ is the residual interaction defining the coupling between eigenstates of $H_0$. The matrix elements of $V$ can often be considerably suppressed by a proper choice of the basis states. Explicitly, a part of the Hamiltonian can be called $d_P$-state dominant if there are $d_P$ basis states that satisfy the conditions

$$\begin{aligned} |\epsilon_l - \epsilon_m| &\geq \Delta E, \quad \text{if } l \leq d_P < m, \\ |V_{nn'}| &\ll \Delta E, \quad \text{for all } n, n'. \end{aligned} \tag{65}$$

By choosing $P$-space to contain these $d_P$ states the connection to renormalisation becomes obvious. The requirements are graphically depicted in Fig. 5 showing some of the energy levels for two examples of a 5-state dominant system. Note that $V_{\max}$, the magnitude of the largest element in $V$, can be much smaller than the energy spread of the separated basis states.

In the regime $\varepsilon_J \ll 1$ a Cooper pair pump demonstrates several different types of few-state dominance depending on the normalised gate charges $\vec{q}$. If $\vec{q} \approx \vec{n}$ for a charge state $|\vec{n}\rangle$ the

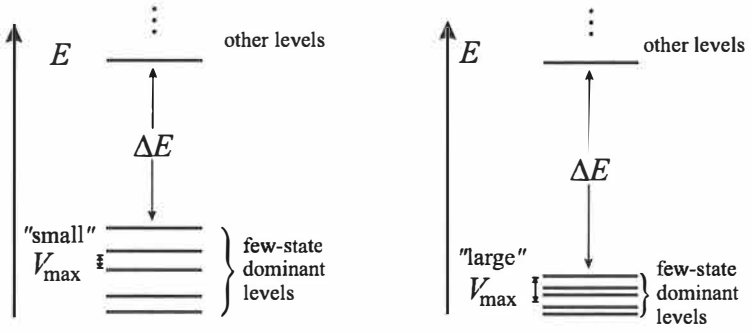


FIG. 5: Schematic view of two 5-state dominant systems. On the right-hand-side all low-lying levels are closely packed in energy while on the left-hand-side the spread is large as compared to $V_{\max}$, the magnitude of the largest element in $V$. Thus even the few-state dominant levels are weakly coupled on the left.

system is one-state dominant. The ground-state energy and consequently the supercurrent can be evaluated without any diagonalisation. At any sharp level crossing the system is usually two-state dominant. Thus the two-dimensional effective Hamiltonian can be used in order to evaluate the pumped charge or the supercurrent through the array.

The so-called resonance points which correspond to maximal supercurrent of the system are located at $\vec{q}_{\pm} = \vec{n} \pm (1/N, \ldots, 1/N)$ in case of homogeneous arrays and close to these points in case of inhomogeneous arrays with non-equal $E_{\mathrm{J},k}$. At these points the system is $N$-state dominant and circulating a $\vec{q}_{+}$ ($\vec{q}_{-}$) in the counterclockwise (clockwise) direction corresponds to adiabatic transfer of one Cooper pair when $\varepsilon_{\mathrm{J}} \to 0$. The optimal paths, in the sense of validity of adiabatic approximation, are given by the sawtooth gating path (39) which assures maximal energy separation at each level crossing.

If more than two charge states become degenerate or nearly degenerate the validity of adiabatic approximation becomes questionable as the energy separation between eigenstates of the Hamiltonian is greatly diminished. In principle, any permutation of $\{\vec{\delta}_k\}$ in Eq. (39) could be used for pumping, but actual realisation of any path other than the suggested one or its mirror image would be unnecessarily complicated.

### 9. Sawtooth gating and the $N$-state basis

The most important charge states on each leg are the optimal charge states with respect to the gate charges $\vec{q}$. For the sawtooth gating all such states are given by Eq. (39) at $x = 0$.

A general $N$-state basis contains charge states $\{|\vec{n}_j\rangle\}_{j=1}^{N}$, where $\vec{n}_1 = 0$ and the non-zero component in other states is $(\vec{n}_{j(>1)})_{j-1} = 1$. The truncated Hamiltonian matrix reads

$$H = \begin{pmatrix} E_{\mathrm{ch},1} & -w^* & 0 & \cdots & -w \\ -w & E_{\mathrm{ch},2} & -w^* & \cdots & 0 \\ 0 & -w & E_{\mathrm{ch},3} & \cdots & 0 \\ \vdots & \vdots & \vdots & \ddots & \vdots \\ -w^* & 0 & 0 & \cdots & E_{\mathrm{ch},N} \end{pmatrix}. \tag{66}$$

The effective Hamiltonian at the first crossing is given by

$$\tilde{H} \approx \begin{pmatrix} E_{\mathrm{ch},1} - \mathcal{O}(\delta_{j>2})^2 & -w^*(1 + v^{N-2}e^{-i\phi}\Pi_{j=3}^{N}\delta_j) \\ -w(1 + v^{N-2}e^{i\phi}\Pi_{j=3}^{N}\delta_j) & E_{\mathrm{ch},1} - \mathcal{O}(\delta_{j>2})^2 \end{pmatrix}, \tag{67}$$

where $\delta_j = 1/(E_{\mathrm{ch},j} - E)$ for the corresponding gate voltages and both $w$ and $v$ are defined in Sec. II.4. The results for other crossings are obtained by a cyclic permutation of the state indices, i.e. $1 \to 2 \to \cdots \to N \to 1$.

The magnitude of the effective coupling constant, the off-diagonal matrix element, now explicitly depends on $\phi$, unlike in case of the pure two-level approximation. Consequently, the pumped charge and the direct supercurrent must be functions of $\phi$. Using $I_{\mathrm{S}}$ when evaluating the pumped charge as $(-2e/N)|w/w_{\mathrm{eff}}|$ yields

$$Q_{\mathrm{p}}^{\Delta} \approx (-2e)\left[1 - v^{N-2}\cos(\phi)\sum_{\mathrm{leg}=1}^{N}\left(\Pi_{j=1}^{N}\delta_j\right)/(\delta_{\mathrm{leg}}\delta_{\mathrm{leg}+1})\right], \tag{68}$$

where the energy denominators are evaluated at the degeneracy points and $\delta_{N+1} = \delta_1$. This hints that the quantum inaccuracy or the deviation scales as $\varepsilon_{\mathrm{J}}^{N-2}\cos(\phi)$. The energy denominators are equal for all legs and in units $E_{\mathrm{C}}/N$ they are $(3,4,3)$, and $(5,8,9,8,5)$ in cases $N = 5$ and $N = 7$. For $\phi = 0$ the quantum inaccuracies $(625/288)\varepsilon_{\mathrm{J}}^3$ and $(117649/460800)\varepsilon_{\mathrm{J}}^5$ correspond to the numerical results rather well.

The above result and the effects due to inclusion of a second set of $N$ states were evaluated on a term-by-term basis. This is extremely complicated so the renormalisation must be performed in a systematic way. An important lesson taught by this calculation is that the formula used in obtaining Eq. (68) is slightly incorrect. The magnitude of $w_{\mathrm{eff}}$, which obtains a contribution in the order $\varepsilon_{\mathrm{J}}^2$, is not as crucial as the dependence of $w_{\mathrm{eff}}$ as a function of $\phi$, i.e. the ratio between terms proportional to $e^{i(\phi/N-\phi)}$ and $e^{i\phi/N}$. An explicit calculation of the matrix elements shows cancellation of possibly dangerous $\varepsilon_{\mathrm{J}}^2$ terms. The quantum inaccuracy is multiplied by an $N$-dependent integer, which is also numerically verified.

TABLE I: The predicted (#paths $\times$ term) and numerical inaccuracies for $\phi = 0$ in units $(\varepsilon_{\rm J})^{N-2}$ for different bases with different number of charge states. The value of $\varepsilon_{\rm J}$ in numerical calculations was 0.01.

| $N$ | states | paths | prediction | numerical |
|---|---|---|---|---|
| 4 | 8 | 3 | 12 | 11.982 |
| 4 | 16 | 6 | 24 | 23.950 |
| 4 | 28 | 6 | 24 | 23.947 |
| 5 | 40 | 24 | 52.083 | 52.002 |
| 5 | 60 | 24 | 52.083 | 51.994 |

## 10. The leading order quantum inaccuracy and the direct supercurrent

In order to evaluate the general leading order quantum inaccuracy for sawtooth gating the charging energy differences must be evaluated near and at the crossing points. Additionally, all charge states contributing in this order must be identified. For a closed cycle, the pumped charges through all junctions are identical so the average supercurrent operator $I_{\rm S}$ can be used. In addition, for homogeneous arrays and triangular gating paths the contribution from each leg is identical, so one leg suffices, and $1/N$ pumped Cooper pairs are pumped per leg in the limit $\varepsilon_{\rm J} \to 0$. The states $|\vec{n}_k\rangle$ and $|\vec{n}_{k+1}\rangle$ (with $N+1 \to 1$) of the $N$-state basis become degenerate on the $k$th leg.

For the $N$-state basis the leading order correction is caused by $N-1$ tunnellings in the opposite direction starting from $|\vec{n}_k\rangle$ and ending at $|\vec{n}_{k+1}\rangle$. The Cooper pair must tunnel once through each of the non-dominant junctions and the general result is obtained when all such terms are included. On the first leg the renormalised Hamiltonian is approximately given by

$$\tilde{H} = \begin{pmatrix} E_{\rm ch,1} - E_{\rm C} \cdot \mathcal{O}(\varepsilon_{\rm J})^2 & -w^*[1 + \mathcal{O}(\varepsilon_{\rm J})^2 + v^{N-2} e^{i\phi} \sum(\Pi\delta_j)] \\ -w[1 + \mathcal{O}(\varepsilon_{\rm J})^2 + v^{N-2} e^{-i\phi} \sum(\Pi\delta_j)] & E_{\rm ch,2} - E_{\rm C} \cdot \mathcal{O}(\varepsilon_{\rm J})^2 \end{pmatrix}. \quad (69)$$

The summation goes over all possible paths and $\Pi\delta_j$ is the product of the corresponding energy denominators. The off-diagonal matrix element contains two corrections, the first one in the order $\mathcal{O}(\varepsilon_{\rm J})^2$ strengthens the coupling and has the same phase difference $e^{i\phi/N}$ as the basic coupling $w$. The other one carries an additional phase factor $e^{-i\phi}$ which modifies the magnitude of the off-diagonal matrix elements as a function of $\phi$. The leading order inaccuracy in the pumped charge is given directly by the term proportional to $\varepsilon_{\rm J}^{N-2}$, because

$1/(1+b\cos\phi) \approx 1 - b\cos\phi$. This behaviour is in accordance with Eq. (45) in the limit of complete charge transfer. The phase factor $e^{i\phi/N}$ corresponds to $1/N$ Cooper pairs per leg, and only a modification of the phase dependence changes $Q_{\rm p}$.

For homogeneous arrays all energy denominators are identical for all legs, explicitly $(2,2)$ for $N=4$ and $(3,4,3)$ for $N=5$, in units of $E_{\rm C}/N$. By calculating the number of terms for each basis, the prediction for each basis is obtained. For $\phi = 0$ the expected deviation is the number of paths times $4\varepsilon_{\rm J}^2$ and $(625/288)\varepsilon_{\rm J}^3$. In Table I this dependence is clearly shown. The number of $N-1$-step paths has been evaluated for different truncations corresponding to a varying number of charge states when $N=4$ and $N=5$. The result is compared against the numerical integration of Eq. (36) when $\varepsilon_{\rm J} = 0.01$.

The predicted $\phi$-dependence is demonstrated for $\varepsilon_{\rm J} = 0.01$ and $N=5$ for 40-states. At $\phi = \pi/2$ the inaccuracy is very close to zero, $-0.17$ in units of $\varepsilon_{\rm J}^3$. For phase differences 0, $\pi/8$, $\pi/4$, $5\pi/8$, $3\pi/4$ and $\pi$ the inaccuracy normalised by $(625/12)(\varepsilon_{\rm J})^3\cos\phi$ are 0.99843, 0.99839, 0.99838, 0.99854, 0.99851, and 0.99850, respectively. Due to symmetry the results are even in $\phi$.

All paths are taken into account if the truncation contains $N\cdot 2^{N-2}$ states, that is $\sum_{k=1}^{N-2}\binom{N-2}{k} = 2^{N-2}-1$ states on top of each of the $N$ charge states $|\vec{n}_j\rangle$, which are visited during a full cycle. The total number of paths in the leading order is $(N-1)!$, and the truncation is called an $a$ basis for given $N$. At each crossing $2^{N-1}$ states participate in the leading order inaccuracy and $k$ tunnellings from dominant states the number is $\binom{N-1}{k}$. The $a$ basis for $N=5$, verifying both classifications, is tabulated in Table II. The energy denominators and corresponding intermediate states for different legs are obtained by cyclic permutations of the columns $\Delta E_{\rm ch}$.

The general case is derived as follows. Due to symmetry the pumped charge and direct supercurrent are identical for all legs of the sawtooth gating cycle. Therefore it suffices to consider the first leg only. Let $(s)$ denote a sum of $s$ different $\vec{\delta}_j$ that does not include $\vec{\delta}_1$, i.e.

$$(s) := \sum_{j=1}^{k} \vec{\delta}_{s_j}, \quad 1 < s_1 < \ldots < s_s \le N. \tag{70}$$

Each $(s)$ corresponds to $\binom{N-1}{s}$ different representatives $\vec{s}$. Because $\sum_{k=1}^{N}\vec{\delta}_k$ vanishes, the classes $(s)$ and $-(N-1-s)-\vec{\delta}_1$ coincide.

In addition to the states that become degenerate, denoted by $\vec{0}$ and $\vec{1} := \vec{\delta}_1$, the leading order inaccuracy depends on classes $\vec{1}+(s)$. The charging energy differences relative to charge $\vec{0}$ are required, and they read

$$\Delta E_{\vec{1}+(s),x} = (E_{\rm C}/N)(s+1-2x)(N-1-s), \quad s=0 \text{ for } \vec{1}. \tag{71}$$

At the degeneracy point, $x=\frac{1}{2}$, these differences simplify to $\Delta E_{\vec{1}+(s),\frac{1}{2}} = s(N-1-s)E_{\rm C}/N$

TABLE II: The charge states in the $a$ basis for $N = 5$ and the corresponding energy differences at the first degeneracy point in units of $E_C/5$. For brevity $\vec{n}$ are given without punctuation apart from separating negative values of $n_k$. The energy differences for other crossings are obtained by cyclic permutations of the columns $\Delta E_{ch}$. The number of intermediate state related to the leading order correction in columns 3 – 5 is 4, 6, and 4, just as expected.

| $\vec{n}$ | $\Delta E_{ch}$ | $\vec{n}$ | $\Delta E_{ch}$ | $\vec{n}$ | $\Delta E_{ch}$ | $\vec{n}$ | $\Delta E_{ch}$ | $\vec{n}$ | $\Delta E_{ch}$ |
|---|---|---|---|---|---|---|---|---|---|
| 0000 | 0 | 1000 | 0 | 0100 | 3 | 0010 | 4 | 0001 | 3 |
| 1001 | 5 | $-1,100$ | 5 | $1,-1,10$ | 3 | $01,-1,1$ | 4 | $001,-1$ | 3 |
| $-1,101$ | 10 | $0,-1,10$ | 5 | $10,-1,1$ | 3 | $010,-1$ | 4 | 1010 | 8 |
| $0,-1,11$ | 10 | $00,-1,1$ | 5 | $100,-1$ | 3 | 1100 | 8 | $-1,110$ | 13 |
| $101,-1$ | 5 | 0101 | 10 | $-1,010$ | 8 | $1,-1,01$ | 4 | $01,-10$ | 3 |
| $-1,11,-1$ | 10 | $1-1,11$ | 10 | $-1,1,-1,1$ | 8 | $1,-1,1,-1$ | 4 | $11,-1,1$ | 8 |
| 0110 | 15 | $-1,011$ | 15 | $0,-1,01$ | 8 | $10-10$ | 4 | $110-1$ | 8 |
| $11,-1,0$ | 5 | $011,-1$ | 10 | $-1,001$ | 13 | $-1,001$ | 9 | $1,-1,00$ | 3 |

and the product of any energy denominators contributing to the leading order inaccuracy is identical to $(NE_C)^{N-2}/[(N-2)!]^2$. The total number of such terms is $(N-1)!$ and the Josephson couplings correspond to a factor $(E_J/2)^{N-2}$. In all, this amounts to the pumped charge [1]

$$\frac{Q_p^{\Delta}}{-2e} \approx 1 - \frac{N(N-1)}{(N-2)!}(N\varepsilon_J/2)^{N-2}\cos\phi. \tag{72}$$

These couplings also carry most of the supercurrent on the gating path induced by renormalising the coupling between two states. The resulting contribution, proportional to the derivative of the ground-state eigenenergy with respect to $\phi$, reads [1]

$$\langle I_S\rangle_x \approx I_c \frac{(N-1)}{2(N-2)!}\frac{(N\varepsilon_J/2)^{N-2}}{[1+((1-2x)(N-1)/(N\varepsilon_J))^2]^{1/2}}\sin\phi, \tag{73}$$

where the numerical factor at $x = \frac{1}{2}$ is seen to be the inaccuracy multiplier in Eq. (72) divided by $2N$.

An $a$ basis is not very complete as one pair of nearest neighbours for each of the states $\{|\vec{n}_j\rangle\}_{j=1}^N$ is missing. As an example, the charge states $|-1,000\rangle$ and $|000,-1\rangle$, which can be reached by a single tunnelling from $|0000\rangle$, do not appear in Table II.

When $N = 3$ the leading order inaccuracy is linear in $\varepsilon_J$ and the renormalisation calculation shows that the next direct terms occur in the order $(\varepsilon_J)^3$. By approximating $(1+3\varepsilon_J)^{-1}$ up to the second order the pumped charge becomes

$$Q_p^{\Delta,3}/(-2e) \approx 1 - 9\varepsilon_J \cos\phi + 27(\varepsilon_J \cos\phi)^2, \tag{74}$$

which approximates the evaluated inaccuracies for $\phi = 0$ much better than the linear approximation and the observed $\phi$-dependence is reasonably reproduced.

In the general case there is an additional source that reduces the inaccuracy at $\phi = 0$. The energies of the two low-lying eigenstates decrease as $\varepsilon_J$ grows consequently making the energy denominators larger. Although more connections become active the total effect works against the inaccuracy. By explicitly evaluating the terms proportional to $E_J(\varepsilon_J)^N$ one can evaluate the next to leading correction in inaccuracy as a power series in $\varepsilon_J$ as a sort of an intelligent guess. In cases $N = 3$ and $N = 4$ also terms proportional to $\cos^2\phi$ and $\cos^3\phi$ contribute. The predictions correspond rather well to the results of the numerical calculations but theoretical derivation or justification of the expansion is yet insufficient.

Due to symmetry of the Hamiltonian the pumped charge for each junction is identical which is also confirmed by numerical integration. In addition, the pumped charge through the $k$th junction on the first leg equals the pumped charge through the first junction on the $k$th leg. But, unlike the prediction of the renormalisation calculations the pumped charges through the non-dominant junctions are not identical. For $N = 5$, $a$ basis, and $\phi = 0$ the numerical pumped charges $\{Q_{p,k}/(-2e)\}_{k=1}^5$ on the first leg are given by $(0.9996, 7.32 \cdot 10^{-5}, -8.24 \cdot 10^{-5}, -8.24 \cdot 10^{-5}, 7.32 \cdot 10^{-5})$ and $(0.9981, -3.02 \cdot 10^{-5}, -6.51 \cdot 10^{-4}, -6.51 \cdot 10^{-4}, -3.02 \cdot 10^{-5})$, where $\varepsilon_J = 0.02$ and $\varepsilon_J = 0.04$, respectively. Nevertheless in scaled units of $\varepsilon_J^3$ the total quantum inaccuracy is predicted correctly, being 51.785 and 51.006 of the expected 52.083. In case of the stronger coupling the higher order effects are beginning to emerge.

In case of longer arrays the quantum inaccuracy diminishes quickly for $\varepsilon_J < 1$. When $N = 5$ the numerically evaluated inaccuracy for $\phi = 0$ is 4.63 % and 0.139 % at $\varepsilon_J = 0.1$ and 0.03, respectively. For $N = 7$ the corresponding values are 0.160 % and $4.40 \cdot 10^{-6}$. The analytical result (72) overestimates the inaccuracy by about 15 % at $\varepsilon_J = 0.1$ and by some 1.5 % at $\varepsilon_J = 0.03$. It is obvious that higher order corrections work against the inaccuracy, the important question being by how much and if the suppression can be predicted.

Alternative derivations for the pumped charge also exist. An obvious possibility is to evaluate the ratio and angle between dominant "forward" and "reverse" (N-1)-step tunnellings using perturbation theory. This method also works when evaluating supercurrent, and gives the correct ratio $1/2N$ between the coefficients. The derivation of $Q_p$ given in [1] is rather vague, if not incorrect, but the results were confirmed numerically as well as by

two independent analytical calculations.

In the following sections the framework is generalised so that inhomogeneous arrays can be examined. Then next-to-leading order corrections and some specific higher order contributions are derived. Finally effects due to inhomogeity of the array and non-ideal pumping sequences are examined in the leading order.

## 11. Hamiltonian revisited

The original expression for the charging energy, Eq. (18), is unnecessarily complicated. The junction capacitances $\{C_k\}$ correspond to an average capacitance $C$ via $\sum_{k=1}^{N} C_k^{-1} = N/C$. The *relative junction capacitances* $\vec{c}$, where $c_k = C_k/C$, are considered to be parameters of the Hamiltonian. Then it is easy to evaluate the charging energies when $\phi$ is assumed to be fixed, or equivalently $V_\mathrm{b} = 0$. In order to be precise, only the charging energy differences matter in the model Hamiltonian.

Defining quantities $v_k$ by $Q_k = (-2e)v_k$, where $Q_k$ is the charge across the $k$th junction, simplifies capacitive charging energy of the array to $E_\mathrm{ch}^{\vec{n},\vec{q}} = E_\mathrm{C} \sum_{k=1}^{N} v_k^2/(2c_k)$ where the condition of ideal biasing requires that $\sum_{k=1}^{N} v_k/c_k = 0$. The charge conservation with respect to the free charge $\vec{u}$ implies that Eqs. (17) must also hold. The unique solution is given by $v_k = \tilde{v}_k + y$, where

$$\tilde{v}_k = \sum_{j=k}^{N-1} u_j - \frac{1}{N} \sum_{j=1}^{N-1} j u_j, \quad y = -\frac{1}{N} \sum_{k=1}^{N} \frac{\tilde{v}_k}{c_k}, \tag{75}$$

so that $\sum_k \tilde{v}_k = 0$. Substitution yields the diagonal matrix elements of the charging Hamiltonian

$$\langle \vec{n}, \phi | H_\mathrm{C} | \vec{n}, \phi \rangle = E_\mathrm{C} \left[ \sum_{k=1}^{N} \frac{v_k^2}{c_k} - \frac{1}{N} \left( \sum_{k=1}^{N} \frac{v_k}{c_k} \right)^2 \right], \tag{76}$$

where $v_k = \tilde{v}_k + \bar{y}$ for arbitrary $\bar{y}$ since the expression (76) is invariant under the transformation $\{v_k\} \to \{v_k + \bar{y}\}$. It is worth noting that for a homogeneous array ($c_k := 1$) the charging energy differences are not affected by non-zero bias voltage over the array. A voltage $V_\mathrm{b}$ only introduces an additional energy $CV_\mathrm{b}^2/2N$ corresponding to $N$ identical capacitors in a series. The combination of inhomogeneity and non-zero bias voltage does change the energy differences.

More problematic question is the validity of adiabatic approximation since the driving frequency of the total phase difference $\phi$ is approximately $V_\mathrm{b}\,[\mu\mathrm{V}] \times 0.5$ GHz. If the impedance of the enviroment is small, the structure of the wave function must change with extreme rapidity near the level crossings, unlike the adiabatic approximation requires. Because this

question can not be examined unless environment is explicitly treated, it shall be skipped and the ideal biasing is assumed. It is also possible that a suitable environmental coupling cures this problem, either completely or at least partially.

The inhomogeneity or nonuniformity of an array is quantified by the *inhomogeneity index* $X_{\mathrm{inh}}$, defined as the root mean square deviation of the inverses of the components of $\vec{c}$

$$X_{\mathrm{inh}} := \left[ \frac{1}{N} \sum_{k=1}^{N} (c_k^{-1})^2 \right]^{1/2} . \tag{77}$$

General considerations imply that the quantity $E_{\mathrm{J}} E_{\mathrm{C}}$ is approximately constant for all junctions in an array. The Josephson coupling energy $E_{\mathrm{J}}$ is inversely proportional to the normal state resistance $R_{\mathrm{T}}$ of the junction and $E_{\mathrm{C}}$ is inversely proportional to the capacitance $C$ of the junction. Since $R_{\mathrm{T}}$ is inversely proportional and $C$ is directly proportional to the area of the junction, the product is approximately constant for different junctions in the array. (This argument works for junctions fabricated in the same batch; otherwise the constants of proportionality are different.) The current technology can ensure a reasonable homogeneity, $X_{\mathrm{inh}} \leq 0.15$ to $0.2$, at capacitances of the order of 1 fF, or even better.

Thus $X_{\mathrm{inh}}$ is closely related to the rms-deviation of the normalised junction resistances, defined as a parameter $[\delta R/R_0]_{\mathrm{rms}}$ in Ref. [73]. In principle, $X_{\mathrm{inh}}$ can be measured by using the array as a Coulomb blockade thermometer, an absolute thermometer with linear dependence in $T$ [74]. The coefficient multiplying $T$ is modified by a term quadratic in $X_{\mathrm{inh}}$ if the array is inhomogeneous.

Setting $E_{\mathrm{J},k} := c_k E_{\mathrm{J}}$ in Eq. (23) uniquely and consistently defines the model Hamiltonian $H = H_{\mathrm{J}} + H_{\mathrm{C}}$ when combined with Eq. (76). The full set of model parameters is given by the coupling ratio $\varepsilon_{\mathrm{J}}$, the total phase difference $\phi$, the relative capacitances $\vec{c}$ and normalised gate charges $\vec{q}$. As $\phi$ is a constant of motion its conjugate variable $M$, the average number of tunnelled Cooper pairs is completely undetermined in stationary states.

From now on, only the average supercurrent operator, Eq. (25), will be applied as both the supercurrent through the array and adiabatically pumped charge $Q_{\mathrm{p}}$ can be evaluated using $I_{\mathrm{S}}$. The matrix elements of $I_{\mathrm{S}}$ between two different stationary states $|m\rangle$ and $|l\rangle$ can be expressed simply as

$$\langle m|I_{\mathrm{S}}|l\rangle_{\phi} = \frac{(-2e)(E_m - E_l)}{\hbar} \lim_{\phi' \to \phi} \frac{\phi\langle m|l\rangle_{\phi'}}{\phi' - \phi} . \tag{78}$$

The stationary states must be locally single-valued and continuous with respect to $\phi$ so that the limit exists. This simplifies the expression for pumped charge $Q_{\mathrm{p}}$ in Eq. (36) to

$$\frac{Q_{\mathrm{p}}}{-2e} = 2 \oint_{\Gamma} \sum_{l(\neq m)} \mathrm{Im} \left[ \lim_{\phi' \to \phi} \frac{\phi\langle m|l\rangle_{\phi'}}{\phi' - \phi} \langle l|dm\rangle \right] . \tag{79}$$

One can interpret this as if the pumped current is mediated by the induced mixing of other components into the initial state and modified depending on how the relative phases of the eigenstates change with respect to the differential change in $\phi$ [2].

This expression can be further simplified by removing the identity operator $\sum_l |l\rangle\langle l|$ and using the canonical representation $M = -i\partial/\partial\phi$ to obtain [3]

$$\frac{Q_{\mathrm{p}}}{-2e} = 2 \oint_{\Gamma} \mathrm{Re}\left[\langle m|\hat{M}|dm\rangle\right]. \tag{80}$$

A single eigenstate for phase differences $\phi$ and $\phi + d\phi$ is required for each integration point. The above expression identifies $\hat{M}$ as the link between $Q_{\mathrm{p}}$ and the geometrical Berry's phase, $\gamma_m(\Gamma) = i \oint_{\Gamma} \langle m|dm\rangle$ [55]. The connection was stated without explicit identification in Ref. [1] and it has been mentioned in Ref. [54]. Further discussion of the connection will be postponed until Chap. III, where the symmetries of the model are explicitly examined.

Expression (80) becomes increasingly more favourable as compared to Eq. (79) when the dimension of the truncated Hamiltonian grows. In case of the two-state model, presented in Sec. II.5 and generalised below, this difference is not as prominent.

### 12. The generalised two-level model

When a level crossing is sharp, i.e. $\varepsilon_{\mathrm{J}} \ll 1$, the two-level truncation consisting of two charge states only is used. Any two-level Hamiltonian can be decomposed as

$$H = \begin{pmatrix} \epsilon_1 & -ve^{-i\theta(\phi)} \\ -ve^{i\theta(\phi)} & \epsilon_2 \end{pmatrix}. \tag{81}$$

For the truncated two-level system this amounts to $\theta(\phi) = \phi/N$, $v = c_k E_{\mathrm{J}}/2$ and $\epsilon_j = E_{\mathrm{ch},j}$, $j = 1, 2$. Here $c_k$ is the relative capacitance of the dominant junction so that the proper decomposition of the renormalised Hamiltonian reads [2]

$$\tilde{H} \approx \begin{pmatrix} E_{\mathrm{ch},1} - a^{(1)} \cdot E_{\mathrm{C}} & -v|b(\phi)|e^{-i(\phi/N+\phi_b)} \\ -v|b(\phi)|e^{i(\phi/N+\phi_b)} & E_{\mathrm{ch},2} - a^{(2)} \cdot E_{\mathrm{C}} \end{pmatrix} \tag{82}$$

where $v = E_{\mathrm{J}}/2$, $a^{(j)} = a_0^{(j)} + a_1^{(j)} \cos\phi$, $j = 1, 2$, $b = b_0 + b_{-1}e^{-i\phi} + b_1 e^{i\phi}$ and $e^{i\phi_b} = b/|b|$. The leading components for these coefficients are $a_0 \propto \varepsilon_{\mathrm{J}}^2$, $a_1 \propto \varepsilon_{\mathrm{J}}^N$, $b_0 - c_k \propto \varepsilon_{\mathrm{J}}^2$, $b_{-1} \propto \varepsilon_{\mathrm{J}}^{N-2}$ and $b_1 \propto \varepsilon_{\mathrm{J}}^N$. Thus $\tilde{H}$ clearly approaches the truncated Hamiltonian in the natural limit $\varepsilon_{\mathrm{J}} \to 0$.

In the context of this two-level model the *renormalisation coefficients* $a$ and $b$ have the following interpretation. The diagonal coefficient $a_0$ corresponds to those tunnelling sequences that end in the same state inside the active $P$-space and without transporting any Cooper

pairs through the array. Coefficients $a_1$ correspond to those sequences that transport one Cooper pair in forward or backward direction, thus yielding the $\cos(\phi)$-dependent term. The coefficients $b$ arise from the sequences that connect the two charge eigenstates via the $Q$-space, transporting $-1$, 0 or 1 Cooper pairs through the array. Each intermediate state $|\vec{n}\rangle$ naturally introduces an energy denominator $E - E_{\mathrm{ch}}^{\vec{n},\vec{q}}$.

This interpretation is illuminating and extremely helpful when evaluating the renormalisation coefficients but it is, nevertheless, false. The virtual transition sequences are not real, but they appear when the existence of high-lying states is treated as described in Secs. II.6. Quantum mechanics implies that if $\varepsilon_J \neq 0$ all charge eigenstates simultaneously coexist although the amplitude of most of these states is negligible in the low-lying eigenstates of the system.

The evaluation of the pumped charge in Sec. II.4 is locally affected only by the appearance of a factor $d\theta/d\phi$, to be evaluated at each point of integration. For the truncated system $d\theta/d\phi = 1/N$, which leads to the original result, Eq. (44), where $E_{\mathrm{J}}$ should be replaced by $E_{\mathrm{J}}c_k$. The sign of the parameter $\eta$ was unfortunately wrong in Ref. [2].

In the limit $\varepsilon_{\mathrm{J}} \to 0$ the pumped charge tends to $(-2e/N)$ per leg regardless of the inhomogeneity in the array. It is bluntly assumed that the charge transfer in the limit $\theta \to \phi/N$ is exactly $Q_{\mathrm{p}} = -2e$. This assumption is partially justified by allowing for the missing charge transfer via higher excited states and noting that the identification of the initial and final states changes after each leg. Ultimately, the validity is determined by comparison against numerical calculations based on Eqs. (79) and (80).

For the renormalised system $d\theta_{\mathrm{ren}}/d\phi$ may be evaluated analytically yielding

$$\frac{d\theta_{\mathrm{ren}}}{d\phi} = \frac{1}{N} + \frac{b_0(-b_{-1} + b_1)\cos\phi - b_{-1}^2 + b_1^2}{|b(\phi)|^2}. \tag{83}$$

The pumping inaccuracy for a homogeneous array is given by a weighted average of $N d\theta_{\mathrm{ren}}/d\phi$ on a single leg. In case of an inhomogeneous array each leg has to be treated separately. The weights can be obtained from Eq. (44) or actually its renormalised version, but for practical purposes it usually suffices to evaluate Eq. (83) at the degeneracy point. The coefficients are obtained by using the "average" choice for the eigenenergy $E$. In most cases the renormalisation includes all terms up to the third order and coefficients $a_1$ and $b_{\mp 1}$ up to and including order $\varepsilon_{\mathrm{J}}^N$.

In units of $E_{\mathrm{C}}$ the renormalised eigenenergies are given by

$$\left.\begin{matrix}\tilde{E}_- \\ \tilde{E}_+\end{matrix}\right\} = \frac{\epsilon_1 + \epsilon_2}{2} \mp \tfrac{1}{2}\sqrt{(\epsilon_1 - \epsilon_2)^2 + \varepsilon_{\mathrm{J}}^2 |b(\phi)|^2} \tag{84}$$

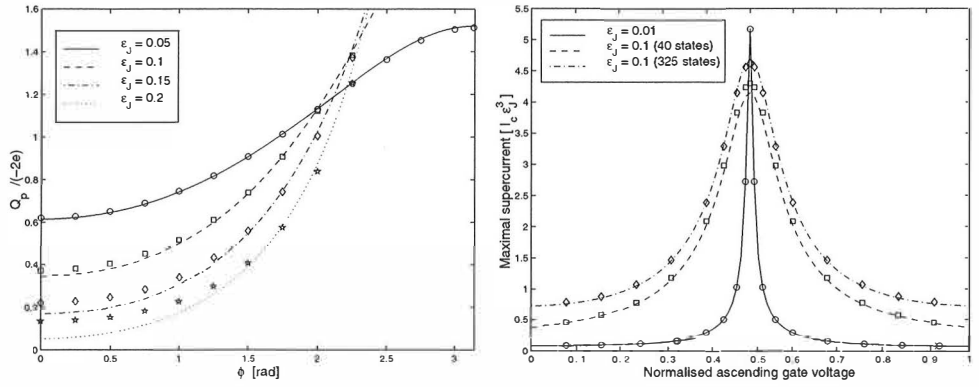


FIG. 6: (a) The pumped charge $Q_{\rm p}/(-2e)$ as a function of $\phi$ for some values of $\varepsilon_{\rm J}$ and $N = 3$. Curves denote renormalised values and symbols numerical values which were obtained for a 41-state basis. Pumped charge is symmetric in $\phi$ and its period is $2\pi$.

(b) The maximal value for the supercurrent in units $I_{\rm C}\varepsilon_{\rm J}^3$ for $N = 5$ and $\phi = \pi/2$. The normalised ascending gate voltage corresponds to $x$ in Eq. (39). Curves denote renormalised values and symbols numerical values corresponding to $a$ basis and $c$ basis with 40 and 325 charge states, respectively. In case $\varepsilon_{\rm J} = 0.01$ the differences between bases can hardly be seen even at the degeneracy point. Taken from [2].

The ground state supercurrent is obtained by deriving $\tilde{E}_-$ with respect to $\phi$ with the result

$$\langle I_{\rm S}\rangle = (I_c \sin\phi)\left[\frac{a_1^{(1)}+a_1^{(2)}}{2\varepsilon_{\rm J}} + \frac{b_0(b_{-1}+b_1)+2b_{-1}b_1\cos\phi-(a_1^{(1)}-a_1^{(2)})\Delta\epsilon/\varepsilon_{\rm J}}{(2/\varepsilon_{\rm J})\sqrt{(\Delta\epsilon)^2+\varepsilon_{\rm J}^2|b(\phi)|^2}}\right]. \qquad (85)$$

In Fig. 6 (a) the pumped charge $Q_{\rm p}$ for $N = 3$ is studied as function of the phase difference $\phi$. The renormalised and numerical results are in good agreement and they clearly indicate that the deviations from the leading order result $[Q_{\rm p}/(-2e) = 1 - 9\varepsilon_{\rm J}\cos\phi]$ are important even when $\varepsilon_{\rm J}$ is rather small. The maximum value for the numerical and renormalised pumped charges are 2.14 and 2.18, 2.87 and 2.98, 3.70 and 3.89 for $\varepsilon_{\rm J} = 0.1$, 0.15 and 0.2, respectively.

Both the minimum and the maximum values of $Q_{\rm p}$ correspond to a vanishing supercurrent which suggests that, in principle, the phase differences $\phi = 0$ and $\phi = \pi$ can be distinguished from each other and the ratio $Q_{\rm p,max}/Q_{\rm p,min}$ could be used in order to approximately determine $\varepsilon_{\rm J}$. More realistic models are required in order to find out if this signature can persist when effects due to the electromagnetic environment are included.

In Fig. 6 (b) the renormalised and numerical supercurrents are shown for $N = 5$. The renormalisation using the "individual" choice reproduces the supercurrent well in all three cases. For clarity the $a$ basis with 40 states was used although it is not large enough to produce the leading order ($\propto \varepsilon_{\mathrm{J}}^{N-1}$) supercurrent fully. The slight underestimation of the supercurrent at the degeneracy point is explainable since only leading order terms were used in the renormalisation. Below we study various effects related to restricted bases.

### 13. Numerical, renormalised and analytical results

In the following sections the results are referred to as numerical, renormalised or analytical results. Numerical results are obtained by diagonalising the Hamiltonian operator in a given truncated basis and using the corresponding eigenstates in order to evaluate the required observable. The pumped charge $Q_{\mathrm{p}}$ is obtained by numerically integrating the second term in Eq. (36).

The renormalised results are obtained by a semianalytical process where the renormalised matrix elements in Eq. (82) and its counterparts for a given $E$ are expressed analytically but the iteration process is naturally done numerically. Although restricting renormalisation into a given basis is rather difficult it facilitates direct comparison between the renormalised and numerically obtained results.

The analytical results are obtained by renormalisation in such a manner that they can be expressed in a closed form. The analytical results for the supercurrent are given by the relation $(-2e/\hbar)\partial E/\partial\phi$, while the pumped charge is evaluated using Eq. (79).

### 14. The basis-dependent effects

In order to reliably evaluate the pumped charge or the supercurrent one must first select a proper basis in which the calculations are performed. The basis should be as large as possible so that the discarded states are not important but on the other hand such calculations may require prohibitive amounts of CPU-time. These problems can be partially circumvented by the use of renormalisation techniques.

Numerical calculations have been mainly performed in three classes of bases named as $a$, $b$ and $c$ bases. In this section the superscript in parenthesis $^{(k)}$ is reserved for the $\varepsilon_{\mathrm{J}}^{k}$-dependent part of any coefficient and the distinction between charge states $\vec{n}_1$ and $\vec{n}_2$ is taken to be complied implicitly. As previously explained an $a$ basis contains all states contributing to the leading order inaccuracy ($b_{-1}^{(N-2)}$). A larger $b$ basis produces the leading component of the supercurrent ($a_1^{(N)}$) fully. Even larger $c$ basis contains all states required for the next-to-leading correction of the inaccuracy ($b_{-1}^{(N)}$, $b_1^{(N)}$).

For each length of the array $N$ these bases can be created as follows. The leading component of the inaccuracy (supercurrent) is carried by the $N-1$-step ($N$-step) "paths" containing at most one tunnelling through each junction that connects the initial state to the final state (itself) for each leg. The total number of charge states is $2^{N-2}N$ and $2^{N-1}N$ for an $a$ basis and a $b$ basis, respectively. A short reasoning confirms that a state should be included in a $c$ basis if it can be reached from a state in the corresponding $b$ basis by a single tunnelling. In this sense a $c$ basis is the first order expansion of a $b$ basis, or $b$ basis[1]. The number of states included in a $c$ basis has not been generally resolved but in cases $N = 4 - 8$ the $c$ basis contains 100, 325, 966, 2695 and 7176 states, respectively. In any case for $N \geq 6$ they are too large to be diagonalised repeatedly up to $10^5$ or $10^6$ times as required for accurate evaluation of Eq. (36). The supercurrent can be evaluated even for the $N = 8$ $c$ basis since only one eigenstate is needed. Due to computational necessities some modifications of the above-mentioned bases have been used.

The differences between bases can be illuminated by performing an "average-0" choice renormalisation at the degeneracy point of the triangular gating path. Inserting the coefficients $b_j^{(k)}$ ($j = 0, \pm 1$) and respective powers of $\varepsilon_J$ into Eq. (83) one obtains a power expansion of the inaccuracy for small values of $\varepsilon_J$. This expansion has to be corrected for the drop in ground state energy induced by the terms $a_0^{(k)}$.

In order to include all contributions up to the next-to-leading order $\varepsilon_J^N$ the coefficients $a_0^{(2)}$, $b_0^{(2)}$, $b_{-1}^{(N-2)}$, $b_{-1}^{(N)}$ and $b_1^{(N)}$ are required. Simple expressions are obtained for

$$\begin{aligned}
a_{0,\mathrm{a}}^{(2)} &= \frac{N-2}{4} + \frac{N(N-1)}{4(N-2)}, \\
a_{0,\mathrm{b}+}^{(2)} &= \frac{N-1}{4} + \frac{N(N-1)}{4(N-2)} + \frac{N}{4(2N-2)}, \\
b_{0,\mathrm{a}}^{(2)} &= N/2, \quad b_{0,\mathrm{b}+}^{(2)} = N(N-1)/2(N-2), \\
b_{-1,\mathrm{a}+}^{(N-2)} &= \left(\frac{N}{2}\right)^{N-2} \frac{N-1}{(N-2)!}
\end{aligned}$$

where the indices a and b correspond to $a$ and $b$ bases, respectively, and + implies that the coefficient does not change when new states are introduced. The analytical expressions for the coefficients $b_{-1}^{(N)}$ and $b_1^{(N)}$ are composed of several multiple summations. Some of the evaluated values of $b_{-1}^{(N)}$ for different bases and $b_1^{(N)}$ for $c$ basis are given in Table III.

The power expansion of the pumped charge finally reads

$$\frac{Q_\mathrm{p}}{-2e} \approx 1 - N\varepsilon_J^{N-2} \cos\phi \left[ b_{-1}^{(N-2)} + \varepsilon_J^2 \left( b_{-1}^{(N)} - b_1^{(N)} - (Nl(N)a_0^{(2)} + b_0^{(2)}) b_{-1}^{(N-2)} \right) \right] \qquad (86)$$

where $l(N) \approx 1$ stems from the energy denominators. Its value is 1, 1, 11/12, 5/6 and 137/180 in cases $N = 3$ to $N = 7$, respectively. For $N = 3$ and $N = 4$ the strong deviations from $\cos(\phi)$-dependence are explained by additional terms $27(\varepsilon_J \cos\phi)^2 - 81(\varepsilon_J \cos\phi)^3$ and

TABLE III: Analytically and semianalytically evaluated "average-0" choice coefficients $b_{-1}^{(N)}$ for $a$, $b$ and $c$ bases and the $c$ basis value of $b_1^{(N)}$ in cases $N = 3 - 9$. Many of the values have been truncated to five-digit precision. Taken from [2].

| $N$ | $b_{-1,\mathrm{a}}^{(N)}$ | $b_{-1,\mathrm{b}}^{(N)}$ | $b_{-1,\mathrm{c}}^{(N)}$ | $b_{1,\mathrm{c}}^{(N)}$ |
|---|---|---|---|---|
| 3 | 9/4 | 57/8 | 69/8 | 3/4 |
| 4 | 63/2 | 436/10 | 513/10 | 5/2 |
| 5 | 83.189 | 106.44 | 125.54 | 53375/9216 |
| 6 | 176.78 | 217.07 | 261.52 | 459/40 |
| 7 | 339.51 | 405.5 | 497.62 | 20.834 |
| 8 | – | – | 894.45 | 35.781 |
| 9 | – | – | 1544.9 | 59.135 |

$144(\varepsilon_\mathrm{J}^2 \cos\phi)^2$, respectively ($4 \cdot 6^2 = 144$, so there is a typo in [2]). The expansion (86) for $N = 3$ does not compare well against numerical results in Fig. 6 but addition of these terms improves agreement considerably, at least up to $\varepsilon_\mathrm{J} \approx 0.1$.

A closer look at the case $N = 5$ is offered by Fig. 7, where the power expansions for the $b$ basis and the 240-state basis (an almost full $c$ basis) as well as the results for "average" renormalisation are compared to numerical results for $\phi = 0$. The use of non-standard basis was necessary because well-converged data was already available and data of similar quality for 325-state $c$ basis would have required prohibitive amounts of CPU-time in change of just minor improvements. The inaccuracy is given in units $\varepsilon_\mathrm{J}^3$ which allows a more detailed comparison of the predictions. The renormalised values follow the numerical results more closely than the power expansions but the differences between bases are still reproduced well up to $\varepsilon_\mathrm{J} \approx 0.1$. In addition, the inaccuracy for an $a$ basis is correctly placed in between the presented bases.

Similar overestimation can be seen in the inset showing the numerical and renormalised inaccuracies for $N = 7$. Although the results may not seem to be so good at the first glance, one should bear in mind that the 336-states basis for which the numerical convergence is the best corresponds to even smaller an inaccuracy than the $N = 7$ $b$ basis. Actual inaccuracy should be evaluated for much larger a basis, the $c$ basis, which turns out to be nearly impossible to do. The scaling of the inaccuracy by $\varepsilon_\mathrm{J}^5$ certainly exaggerates the error. It may be stated that the renormalisation seems to be able to reproduce the behaviour of the

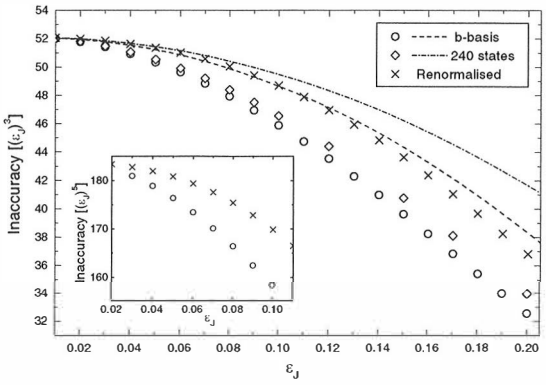


FIG. 7: The inaccuracy of the pumped charge $Q_p/(-2e)$ as a function of $\varepsilon_J$ for different bases and $N = 5$. Curves denote analytical power expansions and symbols numerical or renormalised values. The inaccuracy is given in units $\varepsilon_J^3$ and the phase difference used is $\phi = 0$. The inset shows renormalised and numerical results for the $N = 7$, 336-state basis. Taken from [2].

inaccuracy reasonably well for any $N$ and $\varepsilon_J \leq 0.2$.

The enhancement of the supercurrent has been studied at the resonance point but similar behaviour occurs also in its vicinity. The truncated supercurrent for an $N$-state ring is given by $I_{res}^{(0)}(\phi) := I_C \sin(\phi/N)/N$, stemming from an identical nearest-neighbour coupling after setting all $E_{ch,j}$ to zero in Eq. (66). For very small values of $\varepsilon_J$ next-to-nearest neighbour coupling is induced corresponding to a total supercurrent $1+N\varepsilon_J \cos(\phi/N)$ in units of $I_{res}^{(0)}(\phi)$. Higher order corrections are also induced but the convergence of the effective interaction $\tilde{V}_{eff}$ weakens rapidly for longer arrays and stronger couplings.

It must be stressed that at the resonance point the Hamiltonian for a homogeneous array decouples into $N$ blocks phase shifted by multiples of $2\pi/N$. When convergence is guaranteed, all $N$ lowest eigenstates and eigenenergies can be obtained by extending $\phi$ to the full range of $[0, 2N\pi)$. The same result also holds for larger $P$-spaces. Enlarging the $P$-space is the most straightforward way of improving convergence of $\tilde{V}_{eff}$. The stronger couplings have been evaluated using semianalytical third order renormalisation with $2N(N-1)$-state $P$-space.

The results can be compared to the supercurrent obtained by direct diagonalisation of the truncated Hamiltonian matrix. For $\phi \approx \pi$ and $6 \leq N \leq 10$ the comparison is shown in Table IV. The differences between bases for $\varepsilon_J = 0.1$ are not significant but for $\varepsilon_J = 0.2$ they are growing. The renormalisation calculations indicate that for $\varepsilon_J = 0.1$ the convergence is fast both with respect to the order of renormalisation as well as the basis. Thus

TABLE IV: The maximal supercurrent ($\phi \approx \pi$) in units $I_{\rm res}^{(0)}(\phi)$ for relatively long arrays and strong couplings. For different bases the results were obtained by diagonalisation and the renormalised value is for the third order renormalisation and $2N(N-1)$-state $P$-space. Taken from [2].

| $N$ | $\varepsilon_{\rm J}$ | $a$ basis | $b$ basis | $c$ basis | renormalised | $\varepsilon_{\rm J}$ | $a$ basis | $b$ basis | $c$ basis | renormalised |
|---|---|---|---|---|---|---|---|---|---|---|
| 6 | 0.1 | 1.485 | 1.488 | 1.491 | 1.492 | 0.2 | 1.881 | 1.897 | 1.913 | 1.914 |
| 7 | 0.1 | 1.589 | 1.591 | 1.596 | 1.601 | 0.2 | 2.072 | 2.087 | 2.113 | 2.117 |
| 8 | 0.1 | 1.689 | 1.691 | 1.697 | 1.708 | 0.2 | 2.256 | 2.271 | 2.303 | 2.316 |
| 9 | 0.1 | 1.786 | 1.788 | – | 1.815 | 0.2 | 2.435 | 2.448 | – | 2.508 |
| 10 | 0.1 | 1.881 | 1.883 | – | 1.923 | 0.2 | 2.601 | 2.621 | – | 2.690 |

the enhancement is important for large $N$ and $\varepsilon_{\rm J}$ although it will not cancel the overall suppression $\sim 1/N^2$ of the maximal supercurrent.

### 15. Inhomogeneous arrays and the pumping inaccuracy

One of the most important questions related to the present model is how, if at all, does inhomogeneity of the array affect pumping inaccuracy in the regime of interest, i.e. $\varepsilon_{\rm J} \ll 1$? The obvious guess, based on experience from other similar systems, is that the homogeneous case corresponds to the best available accuracy, or at least an extremum of the pumped charge. The two-level model implies that the inaccuracy is enhanced for smaller values of relative capacitance, and vice versa. Consequently the average value, i.e. a homogeneous pump, stands a fair chance of minimising the inaccuracy. There is some ambiguity in choosing $X_{\rm inh}$, but the current choice gives representative results.

Let an array be characterised by $\varepsilon_{\rm J}$ and relative capacitances $\vec{c}$ corresponding to an inhomogeneity index $X_{\rm inh}$ and defining convenient quantities $g_k := c_k^{-1} - 1$. Classes $s$ and vectors $\vec{s}$ defined in Eq. (70) are usable as they stand provided leg-dependent capacitances are defined. The new $\vec{c}^{\,(\rm leg)}$ is a cyclic permutation of $\vec{c}$ satisfying $(\vec{c}^{\,(\rm leg)})_1 = c_{\rm leg}$, e.g. for $\vec{c} = (c_1, c_2, c_3, c_4)$ this means $\vec{c}^{\,(3)} = (c_3, c_4, c_1, c_2)$.

Writing $\vec{c}$ short for $\vec{c}^{\,(\rm leg)}$ gives the charging energies of the dominant states as

$$E_{\vec{0},x} = E_{\vec{1},1-x} = E_{\rm C} x^2 [c_1^{-1} - c_1^{-2}/N], \tag{87}$$

where the crossing still occurs at $x = \frac{1}{2}$. Due to the reflection symmetry, the relation $E_{\vec{1}-\vec{n},x} = E_{\vec{0}+\vec{n},1-x}$ holds for arbitrary $\vec{n}$. Let $\sigma$ denote a permutation of the set $\{2, 3, \ldots, N\}$,

$\sigma(s)$ the set of $s$ first elements in $\sigma$ and $\sigma_k$ the $k$th element in $\sigma$. Each $\sigma(s)$ defines exactly one vector $\vec{s}$ and two states with charging energies

$$E_{\pm\sigma(s),x} := E_{\pm\vec{s},x} = \frac{E_{\rm C}}{N}\left\{\left(N/c_1 - 1/c_1^2\right)x^2 + (s + G_\sigma^s)\left[(N-s) \pm 2x(1+g_1) - G_\sigma^s\right]\right\}, \quad (88)$$

where $G_\sigma^s := \sum_{k=1}^{s} g_{\sigma_k}$ leading to a generalisation $G_\sigma^{s,\rm leg}$ evaluated from $\vec{c}^{\,(\rm leg)}$. The states $-\vec{s}$ could be picked from class $\vec{1} + (N-1-s)$ but this will not be necessary. Although the above charge states are related to coefficients $b_{-1}$ and $a_1^{(1)}$, this appears to be sufficient.

The leading order pumped charge $Q_{\rm p}^{\vec{c}}$ can be obtained using the "average-0" choice at the degeneracy point for each leg, which is exact in the limit $\varepsilon_{\rm J} \to 0$. A more convenient quantity is the ratio between inhomogeneous and homogeneous inaccuracy

$$W_{\rm inh}^{\vec{c}} := (Q_{\rm p}^{\vec{c}} + 2e)/(Q_{\rm p}^{\Delta} + 2e), \quad (89)$$

which is nearly independent of $\phi$. Inserting the homogeneous inaccuracy $-N(N-1)(N\varepsilon_{\rm J}/2)^{N-2}\cos(\phi)/(N-2)!$ and setting $r$ as the leg index yields

$$W_{\rm inh}^{\vec{c}} = \frac{(N-2)!\prod_{k=1}^{N} c_k}{N(N-1)} \sum_{r=1}^{N}\sum_{\sigma}\left[c_r^{-2}\Big/\left(\prod_{s=1}^{N-2}\Delta E_{r,-\sigma(s)}\right)\right], \quad (90)$$

where the energy denominators are given by

$$\Delta E_{r,-\sigma(s)} := (N/E_{\rm C})(E_{-\vec{s},1/2}^{(r)} - E_{0,1/2}^{(r)}) = (s + G_\sigma^{s,r})(N - s - 1 - g_r - G_\sigma^{s,r}). \quad (91)$$

Clearly $W_{\rm inh} \to 1$ when $X_{\rm inh} \to 0$ as all products of denominators are of the form $[(N-2)!]^2$. The ratio $W_{\rm inh}(\geq 1)$ should be interpreted as the theoretical ratio between inhomogeneous and homogeneous inaccuracy which can be compared against numerical results. The interpretation is obvious since for small values of $\varepsilon_{\rm J}$ the higher order corrections are not very important and even then their behaviour is relatively similar to the leading contribution.

The inaccuracies for single legs can be evaluated by fixing the index $r$ in Eq. (90) and the results agree reasonably well with numerical calculations, although such a measurement can not be performed. Nevertheless, this agreement is important from the viewpoint of theoretical description. The inaccuracies are largest for legs with the smallest relative capacitances and vice versa. The comment in Ref. [2] about junctionwise inaccuracies is incomplete and inadvertent. The conservation of charge ensures that for a full cycle $Q_{{\rm p},k}$ are identical, and it most likely tries to refer to some kind of dominant leg behaviour. The numerical calculation converges better when $I_{\rm S}$ is used. If the total inaccuracy for $\phi = 0$ is large, e.g. more than 30 %, the validity of the leading order approximation should be checked more carefully.

In Fig. 8 (a) the ratio $W_{\rm inh}$ is plotted as a function of $X_{\rm inh}$ corresponding to specific sets of relative capacitances $\vec{c}$ for $N = 4$ and $N = 5$. The numerical results have been obtained

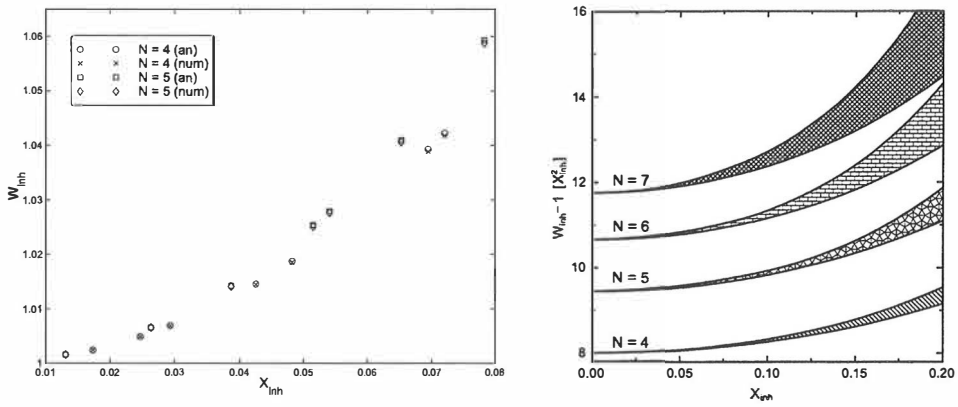


FIG. 8: (a) The ratios $W_{\rm inh}$ between inhomogeneous and homogeneous inaccuracies from analytical expression (90) and numerical calculations as functions of $X_{\rm inh}$. Nearly coinciding numerical results were obtained for $b$ bases with $\varepsilon_{\rm J} = 0.02$ and $\varepsilon_{\rm J} = 0.03$ for $N = 4$ and $N = 5$, respectively.
(b) The limits for the ratio $(W_{\rm inh} - 1)/(X_{\rm inh})^2$ as a function of $X_{\rm inh}$ for array lengths $N = 4$ – 7. Both upper and lower limits approach the asymptotical value $a_N^{\rm (inh)}$ defined in Eq. (94). Taken from [2].

for $b$ bases. The agreement between analytical and numerical results is excellent showing that the effects due to inhomogeneity of the array can be reliably treated as a correction factor when relative capacitances $c_k$ are given.

The effects due to inhomogeneity can be parametrised by obtaining explicit limits for $W_{\rm inh}$ as a function of $X_{\rm inh}$. For $X_{\rm inh} = |g|$ this is achieved by considering the even distribution of inhomogeneity ($g_{\rm odd} = g$, $g_{\rm even} = -g$ for even $N$ and $g_{\rm odd} = g\left(\frac{N-1}{N+1}\right)^{1/2}$, $g_{\rm even} = g\left(\frac{N+1}{N-1}\right)^{1/2}$ for odd $N$) yielding a lower limit and maximally distorted distribution ($g_1 = g\tilde{N}$, $g_{k(\geq 2)} = g/\tilde{N}$, $\tilde{N} = \sqrt{N-1}$) corresponding to an upper limit. The upper limit yields a simple, analytical result

$$W_{\rm inh}(X_{\rm inh}, N) \leq \max[f(X_{\rm inh}, N), f(-X_{\rm inh}, N)] \tag{92}$$

where

$$f(g,N) = \frac{[1-g/\tilde{N}]^{5-3N}}{N(1+g\tilde{N})}\left[(1+g\tilde{N})^2 + (1-g/\tilde{N})^2 \sum_{k=1}^{N-1}\left[\prod_{s=N-k}^{N-2}\frac{s}{s+\gamma}\prod_{s=k}^{N-2}\frac{s}{s+\gamma}\right]\right] \tag{93}$$

with $\gamma = Ng/(N-g)$. The analytical expression for the lower limit is obtained by explicitly inserting the even distribution in Eq. (90) and using the symmetry in order to reduce the

number of terms to be calculated. Even simpler a lower limit can be obtained by considering the asymptotical behaviour of the inhomogeneity, which yields

$$W_{\rm inh}(X_{\rm inh}, N) \geq 1 + a_N^{\rm (inh)} X_{\rm inh}^2. \tag{94}$$

The $N$-dependent constant $a_N^{\rm (inh)}$ can be evaluated from Eq. (93) having values 8, 85/9, 1279/20, 42317/3600, 40267/3150, and 13.769 when $N = 4 - 9$, respectively.

In Fig. 8 the allowed values of $(W_{\rm inh} - 1)/X_{\rm inh}^2$ are shown as functions of $X_{\rm inh}$ in cases $N = 4 - 7$. The allowed range of possible values is quite narrow up to $X_{\rm inh} \approx 0.1$ and not very far from the asymptotical limit $a_N^{\rm (inh)}$. Then measuring of $X_{\rm inh}$, or equivalently $[\delta R/R_0]_{\rm rms}$, is sufficient to fix the prediction of the model. The drawn lower limit is not valid in the strict, mathematical sense but the violation is extremely weak and it only occurs for $X_{\rm inh} \leq 0.03$. The asymptotical limit (94) cannot be violated.

For larger values of $X_{\rm inh}$ and especially longer arrays the spread increases considerably. For the chosen experimental upper limit of $X_{\rm inh} = 0.15$ the maximal increase in inaccuracy as compared to the homogeneous array is approximately 20 %, 24 %, 28 % and 32 % for $N = 4 - 7$, respectively. It is important to remember that the predicted ratio $W_{\rm inh}$ is most reliable for phase differences $\phi = 0$ and $\phi = \pi$, or vanishing supercurrent and maximal inaccuracy. Additional requirement is that the model itself should be valid.

### 16. The leading order supercurrent for inhomogeneous arrays

The leading order renormalised supercurrent may be evaluated using the "individual-0" choice by evaluating the corresponding coefficients $b_{-1}$, $a_1^{(1)}$ and $a_1^{(2)}$ which contribute to the $\phi$-dependence of the eigenenergies. The renormalisation uses eigenenergies of the truncated Hamiltonian for the $r$th leg given by

$$\left.\begin{matrix}\tilde{E}_1 \\ \tilde{E}_2\end{matrix}\right\} = \frac{E_{\vec{0},x} + E_{\vec{0},1-x}}{2} \mp \tfrac{1}{2}\sqrt{\Delta_x^2 + c_r^2 E_{\rm J}^2} \tag{95}$$

where $\Delta_x := E_{\vec{0},x} - E_{\vec{0},1-x}$ corresponds to $\vec{c}^{\,(\rm leg)}$. Inserting $\tilde{E}_1$ into the denominators yields an expression

$$I_{r,x} = (I_c \sin\phi)\,(E_{\rm J}/2)^{N-1} \left(\prod_{k=1}^{N} c_k\right) \sum_{\sigma} \sum_{l=1}^{N} \left[\left(\prod_{m=1}^{l-1} \Delta E_\sigma^{(m)}\right)\left(\prod_{m=l}^{N-1} \Delta E_\sigma^{(r,m)}\right)\right]^{-1} \tag{96}$$

where energy differences are given by $\Delta E_\sigma^{(s)} = E_{s,x} - \tilde{E}_1$, for $s = 1, \ldots, N-1$ and $\Delta E_\sigma^{(r,s)} = E_{\bar{s},x} - \tilde{E}_1$, $\bar{s} = -(N-s-1)$ corresponding to the last elements of $\sigma$. The remaining energy difference $\Delta E_\sigma^{(r,0)} = \tilde{E}_2 - \tilde{E}_1$ corresponds to the coefficient $b_{-1}$ at $x$. All other terms amount

to $a_1^{(1)}$ at $x$ which is not the complete supercurrent. In the range $x \in [0, 0.5]$ the supercurrent is described rather well by this expression and evaluation $I_{r,1-x}$ for $x > 0.5$ as the actual supercurrent is nearly symmetric, especially when $\varepsilon_J$ is very small.

Both expressions slightly overestimate the supercurrent. The justification for using $I_{r,\bar{x}}$, where $\bar{x} = \min(x, 1-x)$ is the following. Close to the degeneracy point $x = \frac{1}{2}$ where the charging energy difference between two states $|\vec{n}_r\rangle$ and $|\vec{n}_{r+1}\rangle$ is of the order of $\varepsilon_J$ the coefficients $a_1^{(1)}$ and $a_1^{(2)}$ are nearly identical and either of them can be used.

As the charging energy difference grows, the lower truncated eigenstate corresponds more and more dominantly to one of the charge states only. The leading component of the $\phi$-dependence in the truncated eigenergy is given by sequences containing $\tilde{E}_2 - \tilde{E}_1$, simultaneously decoupling the truncated eigenstates. As the state is nearly a pure charge state, the eigenenergy is further renormalised by $N$-step paths outside the two-state $P$-space, corresponding to the rest of the terms in $I_{r,\bar{x}}$.

In Fig. 9 the analytical prediction (96) is compared against numerically evaluated supercurrent for $N = 6$ $b$ basis. Each curve corresponds to a randomly chosen set $\{c_k\}$ $\varepsilon_J \in [0.02, 0.06]$ as seen from the different widths of the peak. The numerical and analytical results practically coincide.

Finally, by using Eq. (96) the $a$ basis supercurrent in Fig. 6 can be explained. For a homogeneous array $g_k = 0$ and the charging energies $E_{\pm s,x}$ are identical so the summation over $\sigma$ yields a prefactor $(N-1)!$. The omission of certain states amounts to disallowing some paths and the numerator has to be corrected by a factor $(l-1)/(N-1)$, where $l$ is the summation index in Eq. (96), which is how the supercurrent for an $a$ basis can be approximately evaluated. The comparison does not work as well when the array is inhomogeneous.

### 17. Pumping inaccuracy and nonideal gating sequences

If gate voltages are assumed to be independent, the deviations from the ideal gating sequence can be quantitatively included in the present model. Instead of the ideal gating path defined in Eq. (39), the initial offset of the gate charges and the normalised sweep voltages for each gate are used. For zero sweep voltages the initial gate charges at the beginning of the first leg can be written as

$$\vec{q}_{(1)} = \vec{n}_1 + \vec{q}_{\text{off}}, \tag{97}$$

where $\vec{q}_{\text{off}}$ is the offset error. The normalised sweeping voltages $\vec{q}_{\text{sw}} = (q_{\text{sw},1}, \ldots, q_{\text{sw},N-1})$ are applied when parametrising the full cycle as

$$\vec{q}_{\text{leg}}(x) = \vec{q}_{(1)}' + x \cdot q_{\text{sw,leg}} \vec{\Delta}_{\text{leg}}(0) + (1-x) \cdot q_{\text{sw,leg}-1} \vec{\Delta}_{k-1}, \quad \text{leg} = 1, \ldots, N, \; x : 0 \to 1, \tag{98}$$

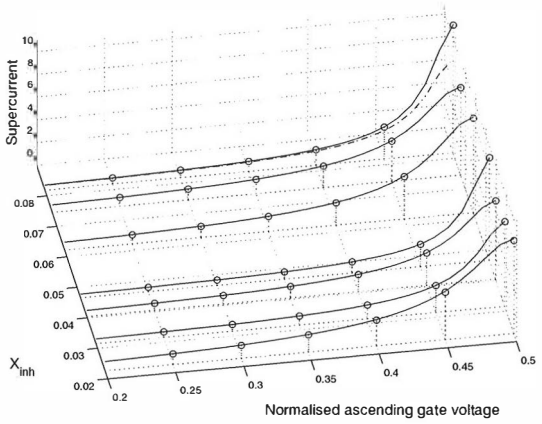


FIG. 9: A three-dimensional plot of the maximal supercurrent for $N = 6$ $b$ basis in units $I_c\varepsilon_J^4$ for several sets $\{c_k\}$ corresponding to different $X_{\text{inh}}$. The gate voltages are chosen from the first leg of the saw-tooth gating path. Junction capacitances have been chosen randomly as well as the ratios $\varepsilon_J$ which lie between 0.02 and 0.06. Solid curves denote analytical values and discrete symbols numerical values. The modifications of the supercurrent are well reproduced even for larger inhomogeneities. The dash-dot curve represents the supercurrent for a homogeneous array as compared to the supercurrent for the most inhomogeneous array shown. Taken from [2].

where $\vec{\Delta}_k = \sum_{j=1}^{k} \vec{\delta}_k$. In general, the sweeping voltages can be determined more precisely than the offset voltages, and for most of the calculations the precision has been set to 1 % and 2 %, respectively.

As in the case of inhomogeneity the charging energy differences at the degeneracy point must be evaluated. The coordinates of the degeneracy point on the $r$th leg must be expressed as

$$\vec{q}_{(\text{deg},r)} = \vec{n}_1 + \vec{\Delta}_{r-1} + \tfrac{1}{2}\vec{\delta}_r + \sum_{j=1}^{N} \mu_j \vec{\delta}_j, \tag{99}$$

where $\mu_r = 0$. The degeneracy condition $E_{\vec{0}} = E_{\vec{1}}$ can be solved easily yielding

$$\sum_{j=1}^{N} (\mu_j / c_j) = 0, \tag{100}$$

which defines a hyperplane in the space of gate charges $\vec{q}$. On the $r$th leg the level crossing occurs when the gate charges $\vec{q}_r(s)$ lie on the hyperplane. This clearly implies that the

correct nonideality parameter is

$$X_{\mathrm{non}} = \left[ \frac{1}{N} \sum_{\mathrm{leg}=1}^{N} \sum_{j=1}^{N} \left( \frac{\mu_j^{(\mathrm{leg})}}{c_j} \right)^2 \right]^{1/2} \tag{101}$$

which can easily be evaluated once the offset charges and sweeping voltages are known.

The leading order inaccuracy may be evaluated using the charging energies (76) at the degeneracy point and inserting the corresponding energy differences (multiplied by $N/E_{\mathrm{C}}$) into Eq. (90). The energy differences are usually calculated numerically as the degeneracy point has to be solved first. The resulting ratio $W_{\mathrm{non}}$ is the total increase in inaccuracy and it may include a contribution due to the inhomogeneity of the array. For small values of $X_{\mathrm{non}}$ and homogeneous arrays the asymptotic behaviour can be derived as in the case of $W_{\mathrm{inh}}$. Direct calculation gives the result

$$W_{\mathrm{non}} \sim 1 + a_N^{(\mathrm{non})} X_{\mathrm{non}}^2, \tag{102}$$

where $a_N^{(\mathrm{non})}$ is a constant whose value is 40/3, 1225/108, 41/4, 258181/27000, 6136/675 in cases $N = 4 - 8$, respectively.

For homogeneous arrays $X_{\mathrm{non}}$ is clearly the correct parameter. Twenty sets of offset charges and normalised sweeping voltages, corresponding to $0.01 \leq X_{\mathrm{non}} \leq 0.024$ were created, ten for both $N = 4$ and $N = 5$. All renormalised predictions for $W_{\mathrm{non}}$ lie on the asymptotical limit (102). Numerically evaluated ratios $W_{\mathrm{non}}$ agree in general, but some deviations do occur. The largest deviation occurs for $X_{\mathrm{non}} = 0.016$ where the renormalised increase in inaccuracy is about 0.3 %, while the numerical increase is only about 0.15 %. Nevertheless, the inaccuracy always increases due to nonideal gating.

The full inaccuracy may be approximately understood in terms of the contribution from the inhomogeneity and nonideality. By treating both effects separately the ratio $W_{\mathrm{non,prod}} := W_{\mathrm{non}} \cdot W_{\mathrm{inh}}$ is obtained. Simultaneous renormalisation treatment corresponds to the ratio $W_{\mathrm{non,ren}}$ and numerical integration yields the ratio $W_{\mathrm{non,num}}$. Randomly chosen $\vec{q}_{\mathrm{off}}$ and $\vec{q}_{\mathrm{sw}}$ were combined with inhomogeneous arrays already used in Fig. 8 (a). The results have been collected in Table V which also includes the corresponding parameters $X_{\mathrm{inh}}$ and $X_{\mathrm{non}}$. The agreement between renormalised and numerical results is rather good showing that both inhomogeneity and nonideal gating sequences can be treated simultaneously.

The parameter $X_{\mathrm{non}}$ is linked to the offset charges and sweeping voltages by more complicated a connection than the respective connection between relative capacitances $\vec{c}$ and $X_{\mathrm{inh}}$. Thus there is no straighforward way to obtain $X_{\mathrm{non}}$ from the experimental data, but an approximate upper limit can be derived. A sort of a worst-case scenario occurs, when the precision for each gate voltage is limited by $x_{\mathrm{non}}$, including both the offset and sweeping

TABLE V: The ratios $W_{\rm non}$ corresponding to nonideal gating in an inhomogeneous array. The numerical values $W_{\rm non,num}$ have been obtained by numerical integration for the $N = 5$ $a$ basis with $\varepsilon_{\rm J} = 0.04$ or $b$ basis with $\varepsilon_{\rm J} = 0.03$. The values of $W_{\rm non,ren}$ and $W_{\rm non,prod}$ are obtained by renormalisation when inhomogeneity and nonideal gating sequences are treated simultaneously and separately, respectively. Taken from [2].

| $X_{\rm inh}$ | $X_{\rm non}$ | $W_{\rm non,num}$ | $W_{\rm non,ren}$ | $W_{\rm non,prod}$ |
|---|---|---|---|---|
| 0.0131 | 0.0377 | 1.0178 | 1.018 | 1.018 |
| 0.0263 | 0.0130 | 1.0082 | 1.0085 | 1.0085 |
| 0.0292 | 0.0173 | 1.0095 | 1.0115 | 1.0115 |
| 0.0387 | 0.0163 | 1.0169 | 1.0173 | 1.0173 |
| 0.0515 | 0.0174 | 1.0277 | 1.0287 | 1.0289 |
| 0.0541 | 0.0244 | 1.0339 | 1.0346 | 1.0349 |
| 0.0653 | 0.0237 | 1.0463 | 1.048 | 1.0477 |
| 0.0741 | 0.0201 | 1.0572 | 1.0577 | 1.058 |
| 0.0783 | 0.0315 | 1.0697 | 1.0706 | 1.0714 |

errors. The actual parameter $X_{\rm non}$ should be bounded from above by

$$X_{\rm non}(N) \approx x_{\rm non} 6^{-1/2} (14 + 11N + 4N^2 + N^3)^{1/2}/N, \tag{103}$$

which is not too restrictive unless $x_{\rm non}$ is rather small. Inserting this into Eq. (102) and multiplying the result with the allowed range of $W_{\rm inh}$ corresponding to the estimated value of $X_{\rm inh}$, yields a quantitative prediction for the increase in inaccuracy. Finally, the measured value of $\varepsilon_{\rm J}$ and the corresponding homogeneous inaccuracy complete the prediction of the present model. The prediction is, naturally, a range inside which the inaccuracy is expected to lie, but it remains to be seen whether the electromagnetic environment or other effects strongly modify the present results.

### 18. Predictions of the model and outlook

A theory for pumping of Cooper pairs for an unbiased array of Josephson junctions in an environment with vanishing impedance has been developed. The present model, which includes only Cooper pair charging effects and tunnelling, can be reliably solved yielding

relatively simple predictions for the direct supercurrent and the accuracy of the pumping of Cooper pairs. Further theoretical studies should be performed using more realistic models which also include the electromagnetic environment and enable dissipative effects.

Next-to-leading order corrections for homogeneous arrays can be reliably predicted or calculated numerically by using the adiabatic approximation. In addition, the behaviour of the direct supercurrent in the ground state is explained rather convincingly. The effects due to inhomogeneous arrays or nonideal gating sequences can be quantitatively treated by defining parameters $X_{\mathrm{inh}}$ and $X_{\mathrm{non}}$ and respective correction factors $W_{\mathrm{inh}}$ and $W_{\mathrm{non}}$. The parameters $\varepsilon_{\mathrm{J}}$ and $X_{\mathrm{inh}}$ can be experimentally measured and the precision of the gate voltages yields limits for $X_{\mathrm{non}}$. Thus the present model can give an explicit prediction for the expected range of the experimental inaccuracy.

The predictions are most likely to be of use when the direct supercurrent vanishes, i.e. when $\phi$ is a multiple of $\pi$, and the expected inaccuracy ($\propto \cos(\phi)$) is largest. The theoretical predictions have been verified by numerical calculations, but whether the model is realistic enough to give quantitatively, or least qualitatively correct results will be ultimately tested in experiments. The adiabatic approximation works best on the suggested sawtooth gating path because the energy difference between the ground state and excited states is always at least $E_{\mathrm{J}}$, regardless of the value of $\phi$. Near the resonance points the separation can be much smaller and at the resonance point a degeneracy occurs for $\phi = \pi(2l+1)$, where $l \in \mathbb{Z}$.

In order to relate these results to possible future experiments, the decoherence calculations by Pekola and Toppari must be discussed [75]. They have evaluated the dephasing frequency $f_{\mathrm{C}}$ for arrays of Josephson junctions coupled to a dissipative electromagnetic environment. Technically, $f_{\mathrm{C}}$ is defined as the inverse of the dephasing time $\tau_\phi$ after which the rms-fluctuations of initially sharply defined total phase difference exceed $\pi/2$. This sets a lower limit for the operating frequency of a Cooper pair pump below which the phase differences average out, i.e. $\langle \cos\phi \rangle = 0$. For very small frequencies the current will become too small to be measured. An upper limit for the operating frequency is forced by the loss of adiabaticity induced by Landau-Zener transitions. This frequency can be estimated by $f_{\mathrm{LZ}} \approx E_{\mathrm{J}}^2/(hE_{\mathrm{C}})$, typically of the order of 10 GHz. The dephasing frequency $f_{\mathrm{C}}$ is expected to be lower than 200 MHz, so the regimes are well separated. Especially for the three junction Cooper pair pump, a regime of coherent pumping with $I/(-2ef) \approx 1 - 9(E_{\mathrm{J}}/E_{\mathrm{C}})\cos\phi$ is expected in the range $f_{\mathrm{C}} < f < f_{\mathrm{LZ}}$. It might even be possible to create Josephson qubits if the dephasing time is of the order of 1 $\mu$s.

Quantitative predictions for the leading order inaccuracy corrections and supercurrent as well as the explanation for the $\cos^2\phi$- and $\cos^3\phi$-dependent terms in the inaccuracy for short arrays have been obtained. The power expansion of the inaccuracy for arrays of arbitrary length is a by-product of the process. Although numerical calculations have

been extended up to $\varepsilon_J \sim 0.2 - 0.3$, from the theoretical point of view this is not that impressive. Full diagonalisation of large matrices still consumes prohibitive amounts of CPU-time. Introducing Eq. (80) for the pumped charge will help, but the symmetries of the Hamiltonian have not been applied efficiently enough, yet.

In the next chapter the symmetries of the model Hamiltonian are examined in detail. By explicitly implementing these symmetries quite general properties of important observables can be found. Numerical calculations can be extended to far longer arrays and stronger couplings, for short arrays even up to $\varepsilon_J \approx 1$.

# III. ANALYSIS OF THE TUNNELLING-CHARGING HAMILTONIAN OF A COOPER PAIR PUMP

In this chapter the discussion concentrates on the symmetries of the Hamiltonian operator and their implications. After a brief glance on the model in general, several symmetries are discussed and explictly formulated. It is shown that an eigenstate can be written as a Fourier series. This property is immediately reflected by the main observables, the pumped charge and the direct supercurrent. An efficient block-diagonalisation scheme is constructed in order to extend the analysis towards stronger couplings by simplifying the numerical calculations.

Finally, the general systematics of the pumped charge are examined and stated. Most of the properties can be justified, although not rigorously proven. For homogeneous arrays, the ratios between consequtive Fourier coefficients are found to be negative and the magnitude of the ratios is diminishing sequence, which is bounded from below. This is clearly an indication of a hidden symmetry, presently unidentified. Because the identification, a most intriguing problem, has not been solved, the chapter can not be concluded decisively.

## 1. The model Hamiltonian

Below, the symmetries of the model Hamiltonian

$$H = H_{\mathrm{C}}(\vec{q}) + H_{\mathrm{J}} \tag{104}$$

and the behaviour of important observables due to these symmetries will be discussed. The matrix elements of $H_{\mathrm{C}}$ are determined by Eq. (76) and $H_{\mathrm{J}}$ is given by Eq. (23), in the basis of charge states augmented by the total phase difference $\phi$, i.e. $\{|\vec{n}, \phi\rangle\}$. All other degrees of freedom except capacitive charging effects and Cooper pair tunnelling are neglected.

To recap, the full set of model parameters is given by the coupling ratio $\varepsilon_{\mathrm{J}} := E_{\mathrm{J}}/E_{\mathrm{C}}$, $\phi$, the normalised gate charges $\vec{q}$, and the relative junction capacitances $\vec{c}$. The relative importance between $H_{\mathrm{C}}$ and $H_{\mathrm{J}}$ is determined by $\varepsilon_{\mathrm{J}}$. The exact value of $\phi$ in stationary states implies complete indeterminacy of $M = -i\hbar\partial/\partial\phi$, the average number of tunnelled Cooper pairs. The degree of inhomogeneity of the array is quantified by $X_{\mathrm{inh}}$ in Eq. (77).

The supercurrent through the array is determined by a Gâteaux derivative [33, 34] of the full Hamiltonian, i.e. $I_{\mathrm{S}} = (-2e/\hbar)(\partial H/\partial\phi)$, for fixed $\vec{q}$ and $\phi$. In the limit of adiabatically evolving system described by a time-dependent eigenstate $|\psi(t)\rangle$, the total transferred charge is simply an integral of the expectation value $\langle\psi(t)|I_{\mathrm{S}}|\psi(t)\rangle$ over the corresponding period of time. In addition to the dynamical phase $\xi(t) = -\int_0^\tau (E(t)/\hbar)dt$, the time-dependent

state acquires the geometrical Berry's phase $\gamma(t) = i\int_\Gamma \langle m|dm\rangle$ [55], where $|m\rangle$ is a locally single-valued instantaneous eigenstate of the Hamiltonian (104).

The time-dependent expectation value has not been rigorously integrated out, but with the help of time-dependent Schrödinger equation the total charge transfer for a closed cycle can be expressed as $Q = Q_\mathrm{s} + Q_\mathrm{p}$, where $Q_\mathrm{s}/(-2e) = \int_0^\tau [(\partial E(t)/\partial\phi)/\hbar]dt$ and the pumped charge in natural units of $-2e$ is given by

$$Q_\mathrm{p} = 2\oint_\Gamma \mathrm{Re}\left[\langle m|\hat{M}|dm\rangle\right]. \tag{105}$$

Here $\Gamma$ is the path traversed by the gate charges $\vec{q}(t)$. The charge transported by direct supercurrent, $Q_\mathrm{s}$, is determined by the evolution of the corresponding eigenenergy, while the pumped charge, $Q_\mathrm{p}$, is almost identical to the Berry's phase $\gamma(\tau)$, the only difference being an additional operator $M = -i\partial/\partial\phi$ and multiplicative factors [1–3].

The adiabatic approximation is valid if the Landau-Zener transition probability is small. If all level crossings are sharp, in other words two-level crossings with adequate separation from other charge states, the minimum energy separation between the ground state and the lowest-lying excited state is approximately $E_\mathrm{J}$ for all values of $\phi$. Consequently, the operating frequency of the gate voltages, $f$, should satisfy $hf \ll E_\mathrm{J}^2/E_\mathrm{C}$, as explained in Sec. II.18. In case of multiple charge-state degeneracies or near such a degeneracy the separation can be large enough for some values of $\phi$, yet insufficient for other values.

In case of pure two-level approximation the ground state can be expressed as $[(1-a^2)^{1/2},\ ae^{i\phi/N}]^\mathrm{T}$, where $a$ changes from the initial value $a_i(\approx 0)$ to the final value $a_f(\approx 1)$. Thus the pumped charge is given by

$$Q_\mathrm{p} = 2\int_{a_i}^{a_f} \mathrm{Re}\left([(1-a^2)^{1/2},\ ae^{-i\phi/N}]\begin{bmatrix} 0 \\ (e^{i\phi/N}/N)da \end{bmatrix}\right) = \int_{a_i}^{a_f}\frac{d(a^2)}{N} = \frac{a_f^2 - a_i^2}{N}, \tag{106}$$

which matches the previously obtained result (45) exactly.

### 2. General symmetries of the Hamiltonian operator

Instead of labelling the charge states by using the number of Cooper pairs on islands, i.e. $\vec{n}$, it is more appropriate to choose a reference state $|\vec{n}_0\rangle$ and label states by integers $\vec{y}_{\vec{n}} := (y_1, \ldots, y_N)$, such that

$$\vec{n} = \vec{n}_0 + \sum_{k=1}^{N} y_k\vec{\delta}_k, \quad 0 \le Y_{\vec{n}} := \sum_k y_k < N. \tag{107}$$

The additional label $Y_{\vec{n}}$ is required for uniqueness, since $\sum_{k=1}^N \vec{\delta}_k = 0$. The numbers $y_k$ tabulate the number and direction of tunnellings through different junctions on the path

from $\vec{n}_0$ to $\vec{n}$. If $\vec{q} = \vec{n}_0$, the quantities $v_k^{\vec{n}}$ defined in Eqs. (17) can be chosen as $\vec{y}_{\vec{n}}$. In both cases $\vec{n}$ indicates the charge state in question. Consequently, analytical evaluation of the charging energies from Eq. (76) is easy if the difference $\vec{q} - \vec{n}_0$ is expressible in terms of less than three of the vectors $\vec{\delta}_k$.

The distance between two charge states $\vec{n}_1$ and $\vec{n}_2$ is defined as the smallest total number of tunnellings from $\vec{n}_1$ to $\vec{n}_2$, regardless of the direction. Explicitly the distance is given by

$$\tilde{d}(\vec{n}_1, \vec{n}_2) := \min\left(\sum_{k=1}^{N} |y_k^{(1)} - y_k^{(2)} + l| : l \in \mathbb{Z}\right), \tag{108}$$

which is clearly independent of the reference state $\vec{n}_0$. If $\tilde{d}(\vec{n}_1, \vec{n}_2) = 1$ $(= k)$, then $|\vec{n}_1\rangle$ and $|\vec{n}_2\rangle$ are ($k$th) *nearest neighbours*. The discrete-valued metric $\tilde{d}$ is useful when choosing truncations, as it immediately gives an estimate of the relative importance of a charge state. The estimate is most reliable when coupling between the charge states is weak, i.e. $\varepsilon_{\mathrm{J}} \ll 1$.

The most obvious symmetry of the charging energy in the Hamiltonian (104) is the reflection symmetry, i.e. invariance with with respect to the transformation $\vec{v}^{\vec{n}} \to -\vec{v}^{\vec{n}}$. In terms of the charge states this means that if $\vec{n}_1 + \vec{n}_2 = 2\vec{q}$, the diagonal matrix elements are identical. Such a symmetry holds on the sawtooth gating path (39) both at $x = 0$ and at $x = \frac{1}{2}$ of each leg.

A more fundamental symmetry is that the charging energy is completely independent of the order of the components $v_k^{\vec{n}}$, when the relative capacitances $\vec{c}$ are subject to the same permutation. The corresponding symmetry on the sawtooth path means that the full Hamiltonian is invariant under cyclical permutations of the relative capacitances $\vec{c}$, apart from the naming of the charge states.

The $r$th leg contribution to the pumped charge $Q_{\mathrm{p}}$ can be evaluated using the gate charges for the first leg combined with the relative capacitances $\vec{c}^{(r)} = (c_r, \ldots, c_N, c_1, \ldots, c_{r-1})$, which were defined in Sec. II.15. In case of homogeneous arrays, i.e. when $c_k := 1$, this symmetry is much stronger, because the charging energy is unchanged by an arbitrary permutation of the components $v_k^{\vec{n}}$. Additionally, in the tunnelling Hamiltonian $H_{\mathrm{J}}$ only the direction of the tunnelling is important due to the phase factor $e^{\pm i\phi/N}$.

The most symmetric case occurs when $\vec{q} = \vec{n}_1$ for some charge state $|\vec{n}_1\rangle$. Then the charge states carrying the label

$$\vec{y} = (z_1^{(1)}, ..., z_1^{(m_1)}, z_2^{(1)}, \ldots, z_2^{(m_2)}, \ldots, z_{j_{\max}}^{(m_{j_{\max}})}), \tag{109}$$

where $z_1 < \cdots < z_{j_{\max}}$ and $m_1 + \cdots + m_{j_{\max}} = N$, or any distinct permutation of $\vec{y}$, correspond to an identical charging energy

$$E_{\mathrm{ch}}^{\vec{m}_{\vec{z}}} = E_{\mathrm{C}}\left[\sum_{j=1}^{j_{\max}} m_j z_j^2 - \frac{1}{N}\left(\sum_{j=1}^{j_{\max}} m_j z_j\right)^2\right]. \tag{110}$$

Here $\bar{m}_{\bar{z}}$ is the short-hand notation for all such states. Thus each label $\bar{m}_{\bar{z}}$ corresponds to $d_{\bar{m}_{\bar{z}}} := N!/(\prod_{j=1}^{j_{\max}} m_j!)$ charge states. In this scheme, the new label of $\vec{n}_0$ is $N_0$, and its nearest neighbours fall into classes $(N-1,1)_{(0,1)}$ and $(1,N-1)_{(0,1)}$. Altogether these three labels cover $2N+1$ charge states which are the dominant ones in the ground state wave function at $\vec{q} = \vec{n}_0$.

On the ideal gating path the situation is nearly as symmetric: As noted above it suffices to consider only the first leg when gate charges can be expressed as $\vec{q} = \vec{n}_0 + x \cdot \vec{\delta}_1$. Thus all components in $\vec{y}$ except the first one are interchangeable and new labels $z_0; \bar{m}_{\bar{z}}$ are introduced. Now $\bar{m}_{\bar{z}}$ refers to the remaining $N-1$ components, $0 \le z_0 + \sum_{i=1}^{N-1} m_i z_i < N$. The charging energy reads

$$E_{\rm ch}^{x,z_0;\bar{m}_{\bar{z}}} = E_{\rm C}\left[(z_0-x)^2 + \sum_{j=1}^{j_{\max}} m_j z_j^2 - \frac{1}{N}\left((z_0-x) + \sum_{j=1}^{j_{\max}} m_j z_j\right)^2\right]. \qquad (111)$$

The number of charge states corresponding to each label is given by $d_{z_0;\bar{m}_{\bar{z}}} = (N-1)!/(\prod_{j=1}^{j_{\max}} m_j!)$.

The states $n_0$ and $n_0 + \vec{\delta}_1$, or equivalently $0;(N-1)_0$ and $1;(N-1)_0$, become degenerate at $x = \frac{1}{2}$. The full set of their nearest neighbours are labelled by $0;(N-1)_1$, $1;(1,N-2)_{(0,1)}$, $1;(1,N-2)_{(-1,0)}$, $0;(N-1,1)_{(0,1)}$, $2;(N-1)_0$, and $1;(N-1,1)_{(0,1)}$. When $\varepsilon_{\rm J} \ll 1$ the truncated Hamiltonian consisting of these $4N$ (10 for $N=3$) charge states yields a reasonably accurate ground-state wave function. The inclusion of additional charge states does not change amplitudes or eigenenergies significantly. Nevertheless, even the leading order supercurrent is not reproduced, except for the shortest arrays, $N=3$ and $N=4$.

As previously explained, an $a$ basis is the smallest basis that reproduces the leading order inaccuracy. The charge states actively participating during each leg correspond to labels $1;(N-1-s,s)_{(0,1)}$, where $s = 1,\ldots,N-2$. The dominant charge states $0;(N-1)_0$ and $1;(N-1)_0$, bring the total up to $2^{N-1}$ out of $N \cdot 2^{N-2}$ charge states in the $a$ basis. Another, but more limited, way to express these states was given by classes $\vec{1} + (s)$ in Sec. II.10. Because one leg suffices when evaluating the pumped charge for homogeneous arrays, the truncation of the Hamiltonian matrix should be performed in accordance to labels $z_0; \bar{m}_{\bar{z}}$.

The Hamiltonian matrix (104) is invariant under transformation $\phi \to \phi + 2N\pi$. Consequently, the instantaneous eigenstates $|m\rangle$ and corresponding eigenenergies share this periodicity. Further simplification can be obtained by a change of basis $U\{|\vec{n}\rangle\} = \{e^{i\phi Y_{\vec{n}}/N}|\vec{n}\rangle\}$. The resulting representation matrix $\tilde{H} := UHU^\dagger$ has properties

$$\tilde{H}(\vec{q},\phi+2\pi) = \tilde{H}(\vec{q},\phi) \quad \text{and} \quad \tilde{H}(\vec{q},-\phi) = (\tilde{H}(\vec{q},\phi))^*. \qquad (112)$$

Because the eigenvalues of Hermitian matrices $H$ and $H^*$ are identical, the eigenenergies are symmetric $\phi$. Additionally, the eigenstates and eigenvalues of $\tilde{H}$ are periodic under $2\pi$,

or the state labels and the ordering of the states change cyclically. If the former happens, the eigenenergy can be written as a Fourier cosine series in integer multiples of $\phi$, and the supercurrent respectively as a Fourier sine series

$$\langle I_{\mathrm{S}} \rangle_{(N,\varepsilon_{\mathrm{J}},\phi,\vec{c},\vec{q})} := \sum_{l=1}^{\infty} \alpha_l \sin(l\phi). \tag{113}$$

Obviously, the supercurrent for these states vanishes when $\phi$ is a multiple of $\pi$.

The ground state supercurrent behaves differently only at the resonance points, where $N$ charge states are degenerate. For a homogeneous array they are located at $\vec{q}_{\vec{n},\pm} := \vec{n} \pm (1/N, \ldots, 1/N)$. In case of inhomogeneous arrays the resonance points are usually quite close to $\vec{q}_{\vec{n},\pm}$. The identification of the ground state changes when $\phi = \pi + 2\pi l$, $l \in \mathbb{Z}$. This degeneracy corresponds to a pole with respect to the Berry's phase. Adiabatic charge transfer is characterised by these poles in the limit of vanishing $\varepsilon_{\mathrm{J}}$. Because of the degeneracy, the adiabatic approximation fails spectacularly for circular gating paths with small radii $\rho$, although the result (53) is valid for $\phi = 0$. Thus the present theory fails in the neighbourhood of resonance points under any significant phase fluctuations. In case of sharp level crossings, the phase fluctuations should only smear the charge transfer as explained in Ref. [75].

The existence and uniqueness of the resonance points is easily proven. Near a resonance point one of the $N$ charge states $|\vec{n}_r\rangle = |\sum_{k=1}^{r-1} \vec{\delta}_k\rangle$ is certainly the charge state with the lowest charging energy. By Eqs. (99) and (100) the charging energies $E_{\mathrm{ch},\vec{n}_r}$ and $E_{\mathrm{ch},\vec{n}_{r+1}}$ are identical on an $(N-2)$-dimensional hyperplane. As the section of $N-1$ hyperplanes with linearly independent normals is exactly one point, each resonance point is uniquely defined in the region $[0, \frac{1}{2}]^{N-1}$. In short, all components of $\vec{q}_{\vec{n}_0,+}$ lie between 0 and $\frac{1}{2}$, regardless of the inhomogeneity of the array. The reflection and translation symmetries of the charging energy imply that all resonance points are of the form $\vec{q}_{\vec{n},+}$.

The local single-valuedness and continuity of the instantaneous eigenstates is obtained by fixing the phase of a single amplitude $a_{\vec{n}'}^{\vec{q},\phi}$ in the eigenstate $|m\rangle_{\vec{q},\phi} = \sum_{\vec{n}} a_{\vec{n}}^{\vec{q},\phi} |\vec{n}\rangle$ according to

$$a_{\vec{n}'}^{\vec{q},\phi} := |a_{\vec{n}'}^{\vec{q},\phi}| e^{i\phi Y_{\vec{n}'}/N}, \tag{114}$$

and requiring that $|a_{\vec{n}'}^{\vec{q},\phi}| > 0$ for all values of $\vec{q}$ and $\phi$ in the examined region of the configuration space. Due to the symmetry of the representation $\tilde{H}$, an arbitrary amplitude is given by a Fourier series

$$a_{\vec{n}}^{\vec{q},\phi} = \sum_{l=-\infty}^{\infty} a_{\vec{n},l}^{\vec{q}} e^{i\phi(l+Y_{\vec{n}}/N)}, \quad a_{\vec{n},l}^{\vec{q}} \in \mathbb{R}, \tag{115}$$

where specifically $a_{\vec{n}',l}^{\vec{q}} = a_{\vec{n}',-l}^{\vec{q}}$. The normalisation of the eigenstate implies orthonormality of the coefficients in the sense $\sum_{\vec{n},l} a_{\vec{n},l}^{\vec{q}'} a_{\vec{n},l+l'}^{\vec{q}'} = \delta_{l'0}$.

The condition (114), fixing the phase of the eigenstate, is a gauge condition and thus each charge state $|\vec{n}'\rangle$ defines a gauge for calculations. No universal gauge exists in the present case, even for the ground state because of the singularities related to the degeneracy in eigenenergy at the resonance points. Nevertheless, all gauges are identical at $\phi = 0$, because all of the ground-state amplitudes are positive definite, i.e. $a_{\vec{n}}^{\vec{q},\phi=0} = \sum_l a_{\vec{n},l}^{\vec{q}} > 0$ for any $\vec{n}$ and $\vec{q}$.

The averaged number of tunnelled Cooper pairs

$$\mathcal{M} := \int_0^{2\pi} \frac{\langle m|\hat{M}|m\rangle_\phi \, d\phi}{2\pi} = \sum_{\vec{n},l} (l + Y_{\vec{n}}/N)(a_{\vec{n},l}^{\vec{q}})^2, \tag{116}$$

is unique up to a gauge-dependent integer. The value of $\mathcal{M}$ is a continuous function of the gate charges $\vec{q}$, except across hyperplanes connecting certain resonance points, where the discontinuity is $+1$ or $-1$, depending on the direction. A gauge is unstable near a discontinuity, but everywhere away from the resonance points a multitude of valid gauges exist. The apparent contradiction between sharp phase difference combined with sharp value of $\mathcal{M}$ is an artifact due to gauge-fixing.

Numerical evaluation of the pumped charge can be done using the gauge-invariant differential expression

$$dQ_{\rm p}(\phi) = \sum_{l'=0}^{\infty} \sum_{\vec{n},l=-\infty}^{\infty} \left[ \frac{2(l + Y_{\vec{n}}/N) + l'}{1 + \delta_{l'0}} d(a_{\vec{n},l} a_{\vec{n},l+l'}) + l'(a_{\vec{n},l} da_{\vec{n},l+l'} - a_{\vec{n},l+l'} da_{\vec{n},l}) \right] \cos(l'\phi), \tag{117}$$

where the $\phi$-independent average ($l' = 0$) is simply $d\mathcal{M}$. The orthonormality of the coefficients $a_{\vec{n},l}^{\vec{q}}$ means that the terms multiplying the full differential by $l'$ can be removed. Complete gauge indepedence is obtained only for infinitesimally small steps when the orthonormality in the order $da$ is regained.

In actual calculations, the basis must be large enough in terms of charge states, and the number of angles used in a fast Fourier transform, $2^j$, must be so large as not to allow misidentification of components $a_{\vec{n},l}$ and $a_{\vec{n},l+2^j}$ as a single component if both are non-negligible. Failure to satisfy these requirements causes systematical error due to incorrect charge-state amplitudes and spurious interference between Fourier components, respectively. The integration points should be chosen so that the magnitude of norms $\| \, |dm\rangle \|$ is neither too large nor varies too much. A more detailed analysis will be given when evaluating the ground-state pumped charge.

The specific structure of the ground-state wave function when $\phi = 0$ facilitates an alternative method for evaluating $Q_{\rm p}$: First the differential contribution from charge state $\vec{n}$ is rewritten as

$$2\mathrm{Re}[-i\hbar \cdot a_{\vec{n}} \partial(da_{\vec{n}})/\partial\phi] = d(a_{\vec{n}})^2 \lim_{d\phi \to 0} (\mathrm{Im}[a_{\vec{n},d\phi}]/d\phi), \tag{118}$$

where the change in $a_{\vec{n}}$ is taken with respect to the gate charges $\vec{q}$ for fixed $\phi$. The overall phases of the wave functions must be fixed consistently. The differential pumped charge for $\phi = 0$ can now be calculated from the simple expression

$$dQ_{\mathrm{p}} \approx \sum_{\vec{n}} d(a_{\vec{n}}^2)\mathrm{Im}[a_{\vec{n},\Delta\phi}]/\Delta\phi, \tag{119}$$

where $\Delta\phi \ll 1$ is a small change in phase difference. The results from Eq. (119) agree with those obtained in [2]. Because the expression (119) is related to a specific value $\phi = 0$, it can be regarded as an interesting curiosity.

## 3. Symmetries of the ground-state wave function and the block-diagonalisation scheme

For $\phi = 0$ the tunnelling Hamiltonian $H_{\mathrm{J}}$ corresponds to a purely attractive coupling between charge eigenstates. Consequently, all amplitudes in the ground state wave function are positive definite. Continuity of the eigenenergy and the non-degeneracy of the ground state ensure that the ground state is obtained for all values of $\vec{q}$ and $\phi$. Thus the pumped charge $Q_{\mathrm{p}}$ can be generally evaluated after enforcing the symmetries explained in this section.

As the first step one shows that the identity $\langle\vec{n}\rangle = \vec{q}$ holds on the gating path at $x = 0$ and $x = \frac{1}{2}$, i.e. the expectation value matches the gate voltages. The reflection symmetry of the charging energies holds and all charge states, except $\vec{n}_0 = \vec{q}$ if necessary, are arranged in pairs satisfying $\vec{n}_{j,1} + \vec{n}_{j,2} = 2\vec{q}$, where $j \in \mathbb{N}$. The corresponding rows in the Schrödinger equation are given by

$$\begin{aligned}
(E_{\mathrm{ch},j} - E)a_{\vec{n}_{j,1}} &= \frac{E_{\mathrm{J}}}{2}\sum_{k=1}^{N} c_k \left(e^{i\phi/N} a_{\vec{n}_{j,1}-\vec{\delta}_k} + e^{-i\phi/N} a_{\vec{n}_{j,1}+\vec{\delta}_k}\right), \\
(E_{\mathrm{ch},j} - E)a_{\vec{n}_2} &= \frac{E_{\mathrm{J}}}{2}\sum_{k=1}^{N} c_k \left(e^{i\phi/N} a_{\vec{n}_{j,2}-\vec{\delta}_k} + e^{-i\phi/N} a_{\vec{n}_{j,2}+\vec{\delta}_k}\right).
\end{aligned}$$

Inserting the ansatz $a_{\vec{n}_{j,2}} = a^*_{\vec{n}_{j,1}}$ into the lower equation yields the complex conjugate of the upper equation. Consequently, $|a_{\vec{n}_{j,1}}|^2 = |a_{\vec{n}_{j,2}}|^2$ and no deviation from $\langle\vec{n}\rangle = \vec{q}$ occurs regardless of the phase difference, coupling strength or inhomogeneity of the array.

The averaged number of Cooper pairs, $\mathcal{M}$, in the gauge defined by the reference state $|\vec{n}_0\rangle$ also vanishes at $\vec{q} = \vec{n}_0$. Similar symmetry holds at $\vec{q} = \vec{n}_0 + \vec{\delta}_1$ with respect to the charge state $|\vec{n}_0 + \delta_1\rangle$, whence $\mathcal{M} = 1/N$ in accordance with the representation $\tilde{H}$. Consequently, the averaged charge transfer for ideal gating sequences, i.e. average value of the pumped charge $\langle Q_{\mathrm{p}}\rangle$ with respect to $\phi$, is $\Delta\mathcal{M} - 1/N$ for each leg. For any full cycle, not too far deformed from the ideal case, one always has $\langle Q_{\mathrm{p}}\rangle = \Delta\mathcal{M} = 1$ due to the discontinuity in the gauges.

A special case occurs at $\phi = 0$ and $\phi = N\pi$, where all amplitudes are real. Then $a_{\vec{n}_{j,2}} = a_{\vec{n}_{j,1}}$ and both equations in each pair become identical, in short, one of them is *redundant*. The symmetry assigns an additional label to the eigenstates of the system. Due to the Hermiticity of the Hamiltonian and subsequent orthogonality of eigenstates, the other label is antisymmetric, i.e $a_{\vec{n}_{j,1}} + a_{\vec{n}_{j,2}} = 0$. In the present model, the ground state always corresponds to the symmetric label.

The basic principles of quantum mechanics indicate that if the Hamiltonian is invariant under a certain transformation, the eigenstates can be classified according to different symmetry representations of the transformation [29, 30]. In other words, the Hamiltonian matrix is block diagonalised by the operator corresponding to the transformation. Because parity is the symmetry related to invariance under reflection, the symmetric and antisymmetric labels, as defined in the previous paragraph, are related to states of definite "positive" and "negative" parity, respectively.

More generally, group theoretical considerations guarantee that *irreducible representations* can be found. The Hamiltonian can be expressed as a direct sum $H = H_1 \oplus H_2 \oplus H_3 \oplus \cdots$, where the blocks $H_j$ are decoupled from each other and none of the blocks can be block diagonalised further, i.e. they are irreducible [30]. In the present case, the full irreducibility is not sought after, rather any simplifying block diagonalisation reducing the dimension of the problem will be accepted.

The elimination of redundant equations in the symmetric representation facilitates a direct block-diagonalisation scheme, since also the matrix elements in the symmetric block can be obtained. Because the ground state corresponds to this representation, the other blocks are usually discarded. For uniform arrays the multiple degeneracy of charging energies in Eqs. (110) and (111) hints that labels $\bar{m}_{\bar{z}}$ and $z_0; \bar{m}_{\bar{z}}$ could be the correct labels for the symmetric representation. A general "symmetric" block-diagonalisation scheme is constructed below. It can be understood as purging redundant, identical equations from the Schrödinger equation in a reversible manner. This is equivalent to a projection onto a subspace of the eigenstates of the Hamiltonian satisfying the symmetry requirement. Finally, the eigenstates can be obtained by diagonalising a "smaller" matrix.

Let the orthonormal basis $\{|s\rangle\}$ span the Hilbert space $\mathcal{H}$ and the matrix elements of a Hamiltonian $H$ be $h_{ss'} := \langle s|H|s'\rangle$. Choose orthogonal projection operators $\{P_i\}$ by

$$P_i = \sum_{k=1}^{d_i(<\infty)} |i_k\rangle\langle i_k|, \tag{120}$$

so that they also span the Hilbert space: in short $\sum_{ij} P_i P_j = \sum_i P_i = \hat{1}$. Then one defines

the row sums of each block $P_iHP_j$ as

$$W_{ij,k} := \sum_{k'=1}^{d_j} h_{i_k j_{k'}}, \quad k = 1, \ldots, d_i. \tag{121}$$

If the row sums depend only on $i$ and $j$, but not on $k$, the $d_i$ equations in the Schrödinger equation corresponding to $P_iH|\psi\rangle = EP_i|\psi\rangle$ are solved by the ansatz $c_{j,k} := c_j$, where $i$ and $j$ are arbitrary. Thus the Hamiltonian commutes with a projection operator

$$P := \sum_i |\chi_i\rangle\langle\chi_i|, \quad |\chi_i\rangle := d_i^{-1/2} \sum_{k=1}^{d_i} |i_k\rangle, \tag{122}$$

and $H$ can be written as a direct sum $H = PHP \oplus (\hat{1} - P)H(\hat{1} - P)$. The eigenstates corresponding to the part $PHP$ can be calculated using matrix elements

$$h_{ij} := \langle\chi_i|H|\chi_j\rangle = W_{ij}(d_i/d_j)^{1/2} = W_{ji}^*(d_j/d_i)^{1/2}. \tag{123}$$

The symmetry operation, i.e. projection onto the "symmetric" subspace $P$, has decoupled some of the eigenstates from others. The original amplitudes are of the form $c_{i,k} := \tilde{c}_i/\sqrt{d_i}$, where $|\psi\rangle = \sum_i \tilde{c}_i|\chi_i\rangle$. Unless all eigenstates of the Hamiltonian are needed for some reason, the part $(\hat{1} - P)H(\hat{1} - P)$ is usually discarded. These eigenstates are traceless with respect to each of the subspaces $P_i$, i.e. $\sum_k c_{i,k} = 0$ for all $i$, and $d_i = 1$ immediately implies $c_{i,1} = 0$.

This block-diagonalisation scheme is simple and probably dates back to the originators of finite-dimensional linear algebra. It can be applied whenever the Hamiltonian operator is sufficiently symmetric, so that one can choose at least some of the $d_i$ to be larger than one. The efficiency can be measured in terms of dimensions, i.e. $\dim(PHP)$ as compared to $\dim(H)$, or some suitable truncations in case of an infinite-dimensional Hamiltonian.

In the present case one chooses labels $\bar{m}_{\bar{z}}$ or $z_0; \bar{m}_{\bar{z}}$ whenever possible as they correspond to a considerable reduction of the dimension, especially when the array is longer ($N \geq 5$). The diagonal matrix elements are naturally given by the charging energies of Eqs. (110) and (111). A short reasoning shows that the block diagonalisation scheme is valid and that the off-diagonal matrix elements are of the form

$$h_{(z_0;)\bar{m}_{\bar{z}},(z_0';)\bar{m}'_{\bar{z}'}} = -(\varepsilon_J m_j/2)e^{\pm i\phi/N} \left[ d_{(z_0;)\bar{m}_{\bar{z}}}/d_{(z_0';)\bar{m}'_{\bar{z}'}} \right]^{1/2}, \tag{124}$$

if the classes $(z_0); \bar{m}_{\bar{z}}$ and $(z_0'; )\bar{m}'_{\bar{z}'}$ are nearest neighbours. In other words, nearest neighbours charge states $\vec{n}$ and $\vec{n}'$ can be found from the classes $(z_0); \bar{m}_{\bar{z}}$ and $(z_0'); \bar{m}'_{\bar{z}'}$, respectively. Here $m_0 = 1$, if applicable, and the multiplicity $m_j$ appears because the existence of $\vec{n}$ and $\vec{n}'$ implies that any of the $m_j$ occurences of $z_j$ can be changed by $\pm 1$. Considerable care is required when creating the neighbouring labels for $(z_0; )\bar{m}_{\bar{z}}$, as the labelling system is somewhat complicated.

TABLE VI: The efficiency of the block-diagonalisation scheme for bases $B_0^{(l)}$. For each $N$ the upper row gives the number of labels, while the lower row tabulates the corresponding number of charge states. $B_0^{(8)}$ bases have not been created for $N = 9$ and $N = 10$.

| $N$ | $l=1$ | $l=2$ | $l=3$ | $l=4$ | $l=6$ | $l=8$ |
|---|---|---|---|---|---|---|
| 4 | 26 | 52 | 90 | 142 | 296 | 530 |
| 4 | 78 | 182 | 346 | 582 | 1318 | 2486 |
| 5 | 37 | 82 | 154 | 264 | 636 | 1295 |
| 5 | 220 | 626 | 1396 | 2692 | 7660 | 17426 |
| 6 | 48 | 114 | 226 | 410 | 1092 | 2436 |
| 6 | 566 | 1918 | 4950 | 10822 | 37886 | $1.02 \cdot 10^5$ |
| 7 | 59 | 146 | 302 | 570 | 1641 | 3941 |
| 7 | 1372 | 5428 | 15978 | 39142 | $1.66 \cdot 10^5$ | $5.22 \cdot 10^5$ |
| 8 | 70 | 178 | 380 | 738 | 2250 | 5710 |
| 8 | 3198 | 14498 | 48030 | $1.31 \cdot 10^5$ | $6.61 \cdot 10^5$ | $2.41 \cdot 10^6$ |
| 9 | 81 | 210 | 458 | 910 | 2899 | – |
| 9 | 7260 | 37082 | $1.37 \cdot 10^5$ | $4.09 \cdot 10^5$ | $2.44 \cdot 10^6$ | – |
| 10 | 92 | 242 | 536 | 1084 | 3572 | – |
| 10 | 16182 | 91778 | $3.72 \cdot 10^5$ | $1.22 \cdot 10^6$ | $8.48 \cdot 10^6$ | – |

As a concrete example, take subspace labels $N_0$, $(N-1,1)_{(0,1)}$ and $(1,N-1)_{(0,1)}$, standing for $2N+1$ charge eigenstates at $\vec{q} = \vec{n}_0$. The block-diagonalised Hamiltonian then reads

$$H_{\mathrm{bd}} = \begin{pmatrix} 0 & K_N^* & K_N \\ K_N & (N-1)/N & 2\delta_{N3}K_N^*/\sqrt{N} \\ K_N^* & 2\delta_{N3}K_N/\sqrt{N} & (N-1)/N \end{pmatrix} \tag{125}$$

where $K_N := -(\varepsilon_J/2)e^{i\phi/N}\sqrt{N}$. For $N = 3$ the leading order supercurrent for $\varepsilon_J \ll 1$ is already reproduced. If $\phi$ is a multiple of $\pi$, the labels $(N-1,1)_{(0,1)}$ and $(1,N-1)_{(0,1)}$ can be joined in the representation $\tilde{H}$.

A truncation picks the charge states required for reliable evaluation of eigenstates and observables. First an initial truncation, a set of states $B_i = \{|\vec{n}_j\rangle\}$, is chosen. Its extensions, bases $B_i^{(l)}$, contain all neighbours up to and including $l$th nearest neighbours of each and

TABLE VII: The efficiency of the block-diagonalisation scheme for bases $B_1^{(l)}$ and $B_2^{(l)}$. For each $N$ the upper row gives the number of labels, while the lower row tabulates the corresponding number of charge states. Subscript 1 or 2 indicates the type of basis. Some of the largest bases have not been created at all.

| $N_{1/2}$ | $l=3$ | $l=5$ | $l=8$ | $l=11$ | $l=15$ | $l=19$ | $l=24$ |
|---|---|---|---|---|---|---|---|
| $5_1$ | 16 | 50 | 175 | 448 | 1200 | 2640 | 5915 |
| $5_1$ | 211 | 1201 | 6661 | 22111 | 72601 | $1.81\cdot10^5$ | $4.52\cdot10^5$ |
| $5_2$ | 51 | 176 | 670 | 1813 | 5076 | 11495 | – |
| $5_2$ | 302 | 1542 | 7902 | 25170 | 80072 | $1.96\cdot10^5$ | – |
| $8_1$ | 18 | 69 | 336 | 1187 | 4704 | 14727 | – |
| $8_1$ | 833 | 12331 | $2.09\cdot10^5$ | $1.62\cdot10^6$ | $1.26\cdot10^7$ | $6.15\cdot10^7$ | – |
| $8_2$ | 60 | 264 | 1470 | 5700 | – | – | – |
| $8_2$ | 1408 | 18912 | $1.30\cdot10^5$ | $2.09\cdot10^6$ | – | – | – |

every charge state in $B_i$. For non-ideal cycles and/or inhomogeneous arrays the initial truncation is the $b$ basis which reproduces leading order supercurrent and inaccuracy. A $c$ basis is just the first order extension of a $b$ basis, i.e. a $b^{(1)}$ basis.

For ideal cycles and homogeneous arrays the optimal $B_0$ truncation corresponds to $3N-2$ labels, that is $0;(N-1-j,j)_{(0,1)}$, "$1;(j,N-1-j)_{(-1,0)}$", $j=0,\ldots,N-1$, and $1;(N-1-j,j)_{(0,1)}$, $j=1,\ldots,N-2$. These $3\cdot2^{N-1}-2$ charge states actively contribute to the leading order supercurrent and inaccuracy. More restricted, few-state truncations $B_1=\{|\vec{n}_0\rangle\}$ and $B_2=\{|\vec{n}_0\rangle,|\vec{n}_1\rangle\}$ are of use especially when the ground state energy is sought.

The efficiency of the block diagonalisation for bases $B_0^{(l)}$ is shown in Table VI, where the number of labels is compared against the number of the included charge eigenstates. For each length of the array $N$, the upper row corresponds to number of labels $z_0;\bar{m}_{\bar{z}}$, while the lower tabulates the number of included charge states. The ratio between the number of labels and of charge states approaches $1/(N-1)!$ as $l\to\infty$.

This conclusion holds also for bases $B_2^{(l)}$, while for bases $B_1^{(l)}$ the ratio approaches $1/N!$. These bases obviously satisfy inclusion relations $B_1^{(l)}\subset B_2^{(l)}\subset B_1^{(l+1)}$. For $N=4$ there are $(l+1)(l+2)(l+3)/6$ labels and $2(l+1)^3$ charge states in a basis $B_2^{(l)}$. For $N\geq6$ the basis $B_2^{(2)}$ corresponds to 24 labels and $4N^2+2$ charge states. In comparison, for $N\geq5$ the basis $B_1^{(2)}$ corresponds to 8 labels and $2N^2+2N+1$ charge states. The number of charge states

TABLE VIII: The ground-state energy in units $E_C$ as a function of $\varepsilon_J$ for $N = 8$ and $N = 10$ at $\vec{q} = 0$ and $\phi = 0$ for bases $B_1^{(l)}$. Column $\Delta E$ gives the energy drop from basis $B_1^{(l-1)}$ to $B_1^{(l)}$. The order of the basis, $l$, is given as a subscript of the ground state energy.

| | $N = 8$ | | $N = 10$ | |
|---|---|---|---|---|
| $\varepsilon_J$ | $E_{g.s.}$ | $\Delta E$ | $E_{g.s.}$ | $\Delta E$ |
| 0 | 0 | – | 0 | – |
| 0.1 | $-0.0454990_7$ | $4.1 \cdot 10^{-14}$ | $-0.0552966_7$ | $6.3 \cdot 10^{-13}$ |
| 0.2 | $-0.1795552_9$ | $2.2 \cdot 10^{-12}$ | $-0.2181992_9$ | $4.0 \cdot 10^{-13}$ |
| 0.5 | $-1.047340_{11}$ | $1.3 \cdot 10^{-12}$ | $-1.261843_{12}$ | $3.1 \cdot 10^{-12}$ |
| 1.0 | $-3.478471_{14}$ | $1.2 \cdot 10^{-13}$ | $-4.209491_{15}$ | $2.2 \cdot 10^{-12}$ |
| 2.0 | $-9.407035_{16}$ | $2.7 \cdot 10^{-12}$ | $-11.53986_{14}$ | $4.7 \cdot 10^{-8}$ |
| 5.0 | $-29.32898_{19}$ | $1.4 \cdot 10^{-10}$ | $-36.295_{15}$ | $3.6 \cdot 10^{-4}$ |
| 10.0 | $-64.74000_{19}$ | $7.2 \cdot 10^{-7}$ | $-80.38_{15}$ | 0.024 |
| 20.0 | $-138.2535_{19}$ | $3.1 \cdot 10^{-4}$ | $-171.8_{15}$ | 0.32 |

can also be calculated by going through all charge states, no more than two tunnellings away from the initial charge states $\vec{n}_0$ and $\vec{n}_0 + \vec{\delta}_1$. Some examples of larger bases $B_1^{(l)}$ and $B_2^{(l)}$ are given in Table VII. As an example, array lengths $N = 5$ and $N = 8$ have been chosen.

The block diagonalisation scheme is most effective at $\vec{q} = \vec{n}_0$ and $\phi = 0$ as the dimension of the Hamiltonian can be approximated halved by a further block diagonalisation. The convergence of the ground state energy for $N = 8$ and $N = 10$ is examined in Table VIII. The convergence of the ground-state energy with respect to the size of the truncation is rather fast even for large values of the coupling strengh $\varepsilon_J$. In case of small enough bases the results can be crosschecked against diagonalisation of the single charge-state representation. Finally, it can be noted that for $N = 10$ the basis $B_1^{(15)}$ contains 7121 labels, or equivalently $2.00 \cdot 10^8$ charge states. Unfortunately, the pumped charge, $Q_p$, is non-integrable, so it can not be calculated from the ground state properties at the end points of a single leg. The deviations, stemming from the latter part of Eq. (117), become smaller and smaller in the limit $\varepsilon_J \dashrightarrow 0$, though.

## 4. Evaluation of the pumped charge for weak couplings

The pumped charge, $Q_{\rm p}$, for ideal gating sequences and homogeneous arrays should be evaluated using bases $B_0^{(l)}$ and corresponding labels, but bases $B_2^{(l)}$ can be used, also. The advantages of the block diagonalisation are highlighted by evaluating $Q_{\rm p}$ for an arbitrary $a$ basis, or more exactly the $2^{N-1}$ states contributing to the leading order of quantum inaccuracy. Choosing the labels in the order $\{0; (N-1)_0, 1; (N-1)_0, 1; (N-2,1)_{(0,1)}, 1; (N-3,2)_{(0,1)}, \cdots, 1; (1,N-2)_{(0,1)}\}$ produces a nearest neighbour Hamiltonian closely reminiscent of the Hamiltonian corresponding to original $N$-state truncation used in Sec. II.9. Actually, it is the same Hamiltonian matrix, apart from modified off-diagonal elements. In short, the couplings between the classes of charge states are no longer identical. For brevity, shorter labels 0 and $1s$, where $s = 0, 1, \ldots, N-2$, corresponding to the same ordering, are used in this section.

Evaluating the charging energies relative to 0, the diagonal matrix elements in units of $E_{\rm C}$ are given by

$$H_{0,0} = 0 \quad \text{and} \quad H_{1s,1s} = (N-s-1)(s+1-2x)/N, \tag{126}$$

where $s = 0, 1, \ldots, N-2$ and $x \in [0,1]$ is defined in Eq. (39). The off-diagonal matrix elements, scaled by $-\varepsilon_{\rm J} e^{i\phi/N}/2$, are given by

$$H_{10,0} = 1 \quad \text{and} \quad H_{1s+1,1s} = \sqrt{(N-s-1)(s+1)}, \tag{127}$$

where $s = 0, 1, \ldots, N-2$ and the label $1N-1$ corresponds to 0. The obtained eigenstates and $Q_{\rm p}$ are exact for the truncation of $2^{N-1}$ charge states. Due to symmetry, half a leg, i.e. the interval $x \in [0, \frac{1}{2}]$ suffices when evaluating $Q_{\rm p}$. As an example, the Hamiltonian matrix for $N = 5$ reads

$$\begin{pmatrix} 0 & K^* & 0 & 0 & 2K \\ K & (1-1/N)(1-2x) & 2K^* & 0 & 0 \\ 0 & 2K & (1-2/N)(2-2x) & \sqrt{6}K^* & 0 \\ 0 & 0 & \sqrt{6}K & (1-3/N)(3-2x) & \sqrt{6}K^* \\ 2K^* & 0 & 0 & \sqrt{6}K & (1-4/N)(4-2x) \end{pmatrix}, \tag{128}$$

where $K := -\varepsilon_{\rm J} e^{i\phi/5}/2$. Here a $5\times5$-matrix with nearest-neighbour coupling only is obtained instead of a $16 \times 16$-matrix.

For homogeneous arrays and ideal gating sequences, the general Fourier expansion of the geometric charge per cycle, or equivalently $N$ legs, reads

$$Q_{\rm p}(N, \varepsilon_{\rm J}, \phi) := 1 + \textstyle\sum_{l=1}^{\infty} b_l \cos(l\phi), \tag{129}$$

TABLE IX: The ratios $\beta_l$ and the limiting value $\tilde{\beta}$ for some short arrays with $N = 3-5$ and $\varepsilon_J \sim 0.002-0.04$. The last column $l$ indicates the coefficient $b_l$ used for the estimate. The results for the $N$-label ($B_0$) truncation are indicated by the subscript $N$ (0) in the first column.

| $N_{N/0}$ | $\varepsilon_J$ | $1000 \times \beta_1$ | $1000 \times \beta_2$ | $1000 \times \beta_3$ | $1000 \times \beta_4$ | $1000 \times \tilde{\beta}$ | $l$ |
|---|---|---|---|---|---|---|---|
| $3_N$ | 0.002 | 8.999 | 6.000 | 6.000 | 6.000 | 6.000 | 4 |
| $3_N$ | 0.005 | 22.49 | 15.00 | 15.00 | 15.00 | 15.00 | 6 |
| $3_N$ | 0.01 | 44.93 | 30.00 | 29.99 | 29.99 | 29.98 | 6 |
| $4_0$ | 0.01 | 1.198 | 0.600 | 0.600 | 0.600 | 0.600 | 4 |
| $4_0$ | 0.02 | 4.771 | 2.401 | 2.395 | 2.395 | 2.39 | 4 |
| $4_0$ | 0.03 | 10.66 | 5.402 | 5.374 | 5.372 | 5.37 | 5 |
| $5_N$ | 0.01 | 0.0260 | 0.0104 | – | – | 0.0104 | 2 |
| $5_0$ | 0.02 | 0.207 | 0.0834 | – | – | 0.083 | 2 |
| $5_0$ | 0.04 | 1.627 | 0.666 | 0.660 | – | 0.66 | 3 |

where $\Delta\mathcal{M} = 1$ is the averaged pumped charge with respect to $\phi$. Direct diagonalisation or renormalisation treatment for the $N$-dimensional Hamiltonian quickly yields the expected result $b_1 \sim -(N\varepsilon_J/2)^{N-2}N(N-1)/(N-2)!$, when $\varepsilon_J \to 0$. Numerical diagonalisation can be performed quickly and reliably in order to obtain the contribution of coefficients $b_l$, especially for short arrays, $N \leq 5$. First one evaluates the Fourier coefficients $a^{\vec{q}}_{\vec{n},l}$ in Eq. (115) using fast Fourier transform (FFT) of the wave functions for sufficiently small steps with respect to $\vec{q}$.

Numerical precision limits evaluation of coefficients $b_{l\geq 2}$, because they decay more rapidly than $b_1$. Additionally, other charge states become increasingly more important for longer arrays. Resorting to the optimal truncation $B_0$ with $3N-2$ labels improves the convergence considerably and some properties of the coefficients $\{b_l\}$ are immediately apparent. The ratio between successive coefficients is seen to be negative and decreasing.

After setting $b_0 := 2$, the ratios $\beta_l = -b_l/b_{l-1}$, where $l = 1, 2, \ldots$, form a decreasing sequence bounded from below by $|b_1/N| = 2\beta_1/N$. This is clearly seen from Table IX in cases $N = 3-5$, where the limiting value of the ratios is defined by $\tilde{\beta} := \lim_{l\to\infty} b_l$. Its actual value can not be obtained in numerical calculations using double precision numbers, but reliable estimates can be given by looking at the region, where the ratios $\beta_l$ no longer decrease significantly. In general, the determination of coefficients $b_l$ with magnitude greater

TABLE X: The first six ratios $\beta_l$ for $N = 3$ and extremely small values of $\varepsilon_J$. The results for the three-label ($B_0$) truncation are indicated by the subscript 3 (0) in the first column. In most cases 16 FFT angles were used, the exception being 32 angles at $\varepsilon_J = 10^{-4}$.

| $(\varepsilon_J)_{N/0}$ | $100000 \times \beta_1$ | $100000 \times \beta_2$ | $100000 \times \beta_3$ | $100000 \times \beta_4$ | $100000 \times \beta_5$ | $100000 \times \beta_6$ |
|---|---|---|---|---|---|---|
| $(10^{-5})_3$ | 4.500016 | 3.000004 | 3.000000 | 3.000000 | 3.000000 | 3.000000 |
| $(10^{-5})_0$ | 4.499981 | 3.000000 | 2.999999 | 2.999999 | 2.999999 | 2.999999 |
| $(2 \cdot 10^{-5})_3$ | 9.000041 | 6.000029 | 6.000015 | 6.000009 | 6.000006 | 6.000004 |
| $(10^{-4})_0$ | 44.99826 | 29.99990 | 29.99983 | 29.99984 | 29.99986 | 29.99987 |

than $10^{-9}$ should be reasonably accurate. Systematical errors are neglected at this stage of the analysis.

In the limit of vanishing $\varepsilon_J$ the pumped charge is expected to behave as

$$Q_p \approx 1 + \frac{N}{2}\sum_{l=1}^{\infty}[(b_1 e^{i\phi}/N)^l + (b_1 e^{-i\phi}/N)^l] = 1 + \frac{b_1(1 + e^{2i\phi} - (2b_1/N)e^{i\phi})}{2[1 - (b_1/N)e^{i\phi}][e^{i\phi} - (b_1/N)]}, \quad (130)$$

with lower limit $1 + b_1/(1 - b_1/N)$ and upper limit $1 - b_1/(1 + b_1/N)$ as $b_1 < 0$.

The case $N = 3$ with extremely small coupling coefficient $\varepsilon_J$ has been studied in detail. The numerical evaluation was done using high-precision floating point arithmetic of MAPLE with an accuracy of at least 40 decimal digits in all operations. For the three-label truncation the deviation from $\Delta\mathcal{M} = 1/N$ behaves approximately as $(15/40)\varepsilon_J^2$. For the $B_0$ truncation this symmetry holds even better.

Explicitly, at $\varepsilon_J = 10^{-5}$ the deviations $(3\Delta\mathcal{M} - 1)$ are given by $1.12500 \cdot 10^{-10}$ and $-3.9551 \cdot 10^{-21}$, for the three-label and $B_0$ truncation, respectively. The resulting ratios $\beta_l$ are shown in Table X, where the limit $\beta_{l>1} \to 2\beta_1/3$ is nicely satisfied. The smaller basis violates the condition $\beta_{l>1} > 2\beta_1/3$, but this violation is cured for the $B_0$ truncation. At $\varepsilon_J = 10^{-5}$ the decreasing nature of the sequence $\{\beta_l\}$ is very weakly violated, the relative increase in the size of the coefficients being less than $10^{-7}$. At $\varepsilon_J = 10^{-4}$ the violation is larger but still insignificant. Nevertheless, the violation is obviously due to the choice of integration points, rounding errors, and other systematical errors, so it is not an actual violation after all. It can be corrected by redoing the analysis using more accurate wave functions and a denser mesh of integration points.

Several symmetries related to the pumped charge have been identified and confirmed. Unfortunately, the full scope of the symmetries and their connection to the Hamiltonian and other observables are still uncertain. Once the nature of the symmetries is conclusively

established, the present results will be rigorously confirmed, but on the other hand the present analysis immediately becomes obsolete. The systematics of the pumped charge will follow directly from symmetry principles.

The symmetries of the charge state representation have been discussed above. Some initial ideas to the symmetry treatment are given by Celeghini et al [26], who have derived the dynamical algebra of single and coupled Josephson junctions. Because general, symmetry-based results are not available, the systematics must be obtained along the lines already described in this thesis.

### 5. The systematics of the pumped charge

Next, the general systematics of the pumped charge are obtained and proven whenever possible. Systematical errors caused by the truncation and the Fourier expansion are discussed. The convergence of $Q_\mathrm{p}$ with respect to the choice of integration points and used expressions are examined. Finally, the effects due to inhomogeneity of the array and non-ideal gating sequences are briefly discussed.

Due to symmetry, one has $\Delta\mathcal{M} = 1/N$ for each leg of an ideal gating sequence. The inhomogeneneous arrays can be considered simultaneously by generalising the pumped charge to

$$Q_\mathrm{p}(N, \varepsilon_\mathrm{J}, \phi, \vec{c}, \mathrm{leg}) := 1/N + \sum_{l=1}^{\infty} b_{l,\mathrm{leg}} \cos(l\phi), \tag{131}$$

where all parameters can be considered and varied separately. In case of non-ideal cycles $1/N$ should be replaced by the actual value, $\Delta\mathcal{M}$. There are four obvious sources of systematical error in the evaluation of $Q_\mathrm{p}$, or directly the coefficients $\{b_{l,\mathrm{leg}}\}_{l=0}^{\infty}$, where for convenience one sets $b_0 := 2/N$.

If the used truncation is too small as compared to the coupling strength $\varepsilon_\mathrm{J}$, the obtained wave functions are incorrect. This happens because important or at least significant correlations due to the omitted charge states are not included. The problem can be solved by increasing the size of the truncation until the amplitudes do not significantly change when further charge states are added. The convergence of the ground state energy and wave function is rigorously proven in [68].

A closely related problem is the misidentification of Fourier coefficients in the FFT of the wave function if the number of angles is not large enough. Fixing the gauge peaks the distribution of the coefficients by fixing the value of $\mathcal{M}$. Nevertheless, if the distribution is wide enough the ends may meet and two coefficients will spuriously interact. In other words, the distinction between the amplitudes $a_{\vec{n},l}$ and $a_{\vec{n},l+\#\mathrm{angles}}$ in Eq. (115) becomes blurred for some values of $l$ if both are non-negligible. Here #angles denotes the total number of angles

TABLE XI: The first five ratios $\beta_l$ and the limiting value $\tilde{\beta}$ for $N = 5$ as functions of $\varepsilon_J$. The ratios related to coefficients smaller than $10^{-10}$ and those otherwise subject to large uncertainty have been omitted. The last column indicates the coefficient $\beta_l$ used when estimating the limiting value.

| $\varepsilon_J$ | $\beta_1$ | $\beta_2$ | $\beta_3$ | $\beta_4$ | $\beta_5$ | $\tilde{\beta}$ | $l$ |
|---|---|---|---|---|---|---|---|
| 0.05 | 0.032 | 0.0013 | 0.0013 | – | – | 0.0013 | 3 |
| 0.1 | 0.0236 | 0.0103 | 0.0100 | 0.0100 | 0.0100 | 0.0100 | 5 |
| 0.2 | 0.1475 | 0.0764 | 0.0717 | 0.0708 | 0.0705 | 0.070 | 8 |
| 0.3 | 0.3501 | 0.2137 | 0.1977 | 0.1933 | 0.1917 | 0.190 | 12 |
| 0.4 | 0.5494 | 0.3842 | 0.3551 | 0.3451 | 0.3408 | 0.335 | 18 |
| 0.5 | 0.7007 | 0.5422 | 0.5048 | 0.4899 | 0.4825 | 0.471 | 18 |
| 0.6 | 0.8030 | 0.6682 | 0.6285 | 0.6107 | 0.6011 | 0.582 | 35 |
| 0.7 | 0.8694 | 0.7615 | 0.7238 | 0.7053 | 0.6947 | 0.669 | 45 |
| 0.8 | 0.912 | 0.8285 | 0.7950 | 0.7773 | 0.7666 | 0.736 | 50 |

used in the FFT. This problem is occasionally seen in the wave functions and even in some of the coefficients $b_l$. In general, the problem can be solved by increasing the number of angles. A suitable indicator for the quality of the truncation and FFT is given by the violation of the symmetry $\Delta\mathcal{M} = 1/N$, which measures both the spurious interaction in the Fourier expansion and the truncation-enhanced correlations.

The integration points should be chosen so that the magnitude of norms $\| |dm\rangle \|$ is neither too large nor varies too much. The hyperbolical sine, sinh, is suitable for parametrisation of the cycle as the mesh becomes denser near the halfway point of the leg. This limits $\| |dm\rangle \|$ and orthogonality of the wave functions is obeyed more strictly. The rate of convergence for each $\cos(l'\phi)$-dependent term in Eq. (129) behaves as $1/(\#\text{steps})^2$. The expression $2l' a_{\vec{n},l} da_{\vec{n},l+l'}$ has been used as the latter part of Eq. (117) for many of the earlier calculations. The corresponding rate of convergence behaves as $1/\#\text{steps}$.

For a reasonable choice of integration points, $300-500$ steps per leg, or about 200 per half a leg, the former expression usually gives a relative precision of the order of $10^{-5}$ for coefficients with magnitude greater than $10^{-8}$. Here the systematical errors due to truncation and Fourier expansion are not included. By using fewer steps one avoids many of the convergence problems due to the smallness of $da_{\vec{n},l}$ for large bases and large number

TABLE XII: The first five ratios $\beta_l$ and the limiting value $\tilde{\beta}$ for $N = 8$ as functions of $\varepsilon_J$. The ratios related to coefficients smaller than $10^{-10}$ and those otherwise subject to large uncertainty have been omitted. The last column indicates the coefficient $\beta_l$ used when estimating the limiting value.

| $\varepsilon_J$ | $\beta_1$ | $\beta_2$ | $\beta_3$ | $\beta_4$ | $\beta_5$ | $\tilde{\beta}$ | $l$ |
|---|---|---|---|---|---|---|---|
| 0.1 | 0.00014 | $3.9 \cdot 10^{-5}$ | – | – | – | – | – |
| 0.2 | 0.00666 | 0.00222 | 0.00207 | 0.00204 | 0.0020 | – | 4 |
| 0.3 | 0.0485 | 0.0200 | 0.0181 | 0.0177 | 0.0175 | 0.017 | 5 |
| 0.4 | 0.1563 | 0.0785 | 0.0708 | 0.0685 | 0.0675 | 0.067 | 9 |
| 0.5 | 0.3185 | 0.1892 | 0.1714 | 0.1650 | 0.1621 | 0.158 | 11 |
| 0.8 | 0.7491 | 0.6073 | 0.5682 | 0.5499 | 0.5395 | 0.514 | 20 |

of angles. Consequently, the calculations were extended to much stronger couplings in [3] as compared to the earlier cases in [1] and [2].

The fourth kind of systematical error is related to the floating point arithmetic. The sheer number of floating point operations required from diagonalisation of the Hamiltonian matrix to the evaluation of the coefficients $b_l$ limits the obtainable accuracy as rounding errors may accumulate. Quite good an accuracy is obtained by using double-precision digits and effective routines. Further improvement by using more precise floating point numbers is not worth the huge increase in the required CPU-time, except at some special cases as the limit of vanishing $\varepsilon_J$, already discussed above.

A large number of calculations using bases $B_2^{(l)}$ and $B_0^{(l)}$ for arrays of different values of $N$ and $\varepsilon_J$ have been performed in order to obtain numerical values of the coefficients $\{b_{l,\mathrm{leg}}\}_{l=0}^{\infty}$. The coefficients form an alternating and diminishing sequence. Furthermore, the ratios $\beta_l := |b_l/b_{l-1}|$, $l = 1, 2, \ldots$ form a decreasing sequence with limiting value $\tilde{\beta} := \lim_{l\to\infty} \beta_l \geq b_0\beta_1$. General considerations based on the renormalisation approach indicate that $\partial Q_\mathrm{p}/\partial\phi > 0$ in the range $\phi \in (0, \pi)$. Thus $Q_\mathrm{p}$ is bounded from above by $[2(1-\beta_1)^{-1} - 1]/N$ and from below by $1/N - 2\beta_1/(N + 2\beta_1)$.

For finite values of $\varepsilon_J$ the ratios $\beta_l$ and $\tilde{\beta}/\beta_1$ are monotonously increasing functions of $\varepsilon_J$ with limiting value of unity. The positive-definiteness of $Q_\mathrm{p}(\phi = 0, \varepsilon_J)$ and the limit $Q_\mathrm{p}(\phi = 0, \varepsilon_J \to \infty) \searrow 0$ enforce a stricter limit for the first ratio $\tilde{\beta}/\beta_1$. This behaviour is explained by the increasing long-range (high-$l'$) correlations in Eq. (117) or actually in the ground state itself. On the other hand, the ratios are monotonously decreasing functions of

TABLE XIII: The first five ratios $\beta_l$ and the limiting value $\tilde{\beta}$ for $\varepsilon_J = 0.4$ as functions of $N$. The ratios related to too small coefficients have been omitted. The last column indicates the coefficient $\beta_l$ used when estimating the limiting value.

| $(\varepsilon_J)_N$ | $\beta_1$ | $\beta_2$ | $\beta_3$ | $\beta_4$ | $\beta_5$ | $\tilde{\beta}$ | $l$ |
|---|---|---|---|---|---|---|---|
| 3 | 0.8802 | 0.7782 | 0.7470 | 0.7347 | 0.7291 | 0.722 | 60 |
| 4 | 0.7250 | 0.5706 | 0.5354 | 0.5225 | 0.5168 | 0.509 | 25 |
| 5 | 0.5494 | 0.3842 | 0.3551 | 0.3451 | 0.3408 | 0.335 | 20 |
| 6 | 0.3844 | 0.2393 | 0.2188 | 0.2121 | 0.20933 | 0.206 | 15 |
| 7 | 0.2516 | 0.1401 | 0.1272 | 0.1231 | 0.1214 | 0.120 | 11 |
| 8 | 0.1563 | 0.0785 | 0.0708 | 0.0685 | 0.0675 | 0.067 | 9 |
| 9 | 0.0934 | 0.0427 | 0.0383 | 0.0370 | 0.0364 | 0.036 | 7 |
| 10 | 0.0542 | 0.0227 | 0.0203 | 0.0196 | 0.0192 | 0.019 | 7 |
| 11 | 0.0308 | 0.0119 | 0.0106 | 0.0102 | 0.0101 | 0.010 | 5 |
| 12 | 0.0172 | 0.0062 | 0.0055 | 0.0053 | 0.0053 | 0.0052 | 5 |

$N$ for a fixed value of $\varepsilon_J$ as the correlations grow weaker in longer arrays.

All of the above-mentioned features of $\beta_l$ are highlighted in Tables XI, XII and XIII. The first two tables show the ratios $\beta_l$ for $N = 5$ and $N = 8$ as functions of $\varepsilon_J$, while the third depicts $\beta_l$ as functions of $N$ at $\varepsilon_J = 0.4$. These properties of the pumped charge are rather robust against systematical errors. Until further notice, the full data set and some tools for reproducing the data are available at http://www.jyu.fi/~mimaau/Cooper/

It is worth noting that the matrix elements $\langle m|\hat{M}|dm\rangle$ themselves share some properties of the integrated Fourier coefficient $b_l$. Especially the behaviour of the ratios $\beta_{l,\mathrm{step}}$ defined from the stepwise contribution exhibit many of the properties of the $\beta_l$. Some violations are observed, especially if the corresponding $\Delta\mathcal{M}$ is small. The size of the leading ratio $\beta_{l,\mathrm{step}}$ varies, being largest at the level crossing, or at $x = 0.5$.

The effects due to inhomogeneity of the array have also been examined. The coefficients $b_{l,\mathrm{leg}}$ must be calculated separately for each leg, and on each leg the sequence $\{\beta_{l,\mathrm{leg}}\}_{l=1}^{\infty}$ is diminishing and bounded from below by $2\beta_{1,\mathrm{leg}}/N$. Because the leading ratio $\beta_1$ is different for each leg, this symmetry does hold for the ratios $\beta_l$ calculated from the total pumped charge $Q_\mathrm{p}(N, \varepsilon_J, \phi, \vec{c}) = \sum_{\mathrm{leg}=1}^{N} Q_p(\mathrm{leg})$. Thus one may have $\beta_l > \beta_{l+1}$, although always $b_{l+1}/b_l < 1$. In the limit $l \to \infty$, the coefficients $b_l$ will be dominated by the contribution

TABLE XIV: The first five ratios $\beta_{l,\mathrm{leg}}$ for all legs of two ideal cycles in case of an inhomogeneous array with $N = 4$. The upper set corresponds to $\varepsilon_{\mathrm{J}} = 0.12$ and $X_{\mathrm{inh}} = 0.081$, and the lower set to $\varepsilon_{\mathrm{J}} = 0.06$ and $X_{\mathrm{inh}} = 0.193$. The relative capacitances $c_r$ are given in the first column. In the last column the coefficient $b_{1,\mathrm{leg}}$ has been divided by the prediction (132). The results agree in both cases even though the ratios $\beta_l$ are rather large. At $\varepsilon_{\mathrm{J}} = 0.07$ the ratios for $X_{\mathrm{inh}} = 0.081$ are given by 0.953, 0.945, 0.948, 0.947.

| $c_r$ | $\beta_1$ | $\beta_2$ | $\beta_3$ | $\beta_4$ | $\beta_5$ | $b_1$/prediction |
|---|---|---|---|---|---|---|
| 1.140 | 0.1016 | 0.0580 | 0.0558 | 0.0555 | 0.0554 | 0.882 |
| 0.907 | 0.2115 | 0.1174 | 0.1138 | 0.1133 | 0.1132 | 0.859 |
| 1.005 | 0.1513 | 0.0850 | 0.0821 | 0.0817 | 0.0816 | 0.869 |
| 0.975 | 0.1668 | 0.09332 | 0.0903 | 0.0898 | 0.0897 | 0.866 |
| 1.205 | 0.0256 | 0.135 | 0.0132 | 0.0132 | 0.0132 | 0.960 |
| 1.143 | 0.0304 | 0.0159 | 0.0157 | 0.0156 | 0.0156 | 0.959 |
| 1.028 | 0.0429 | 0.0224 | 0.0221 | 0.0220 | 0.0220 | 0.956 |
| 0.756 | 0.1216 | 0.0627 | 0.0621 | 0.0620 | 0.0620 | 0.947 |

from the leg on which the relative capacitance $c_r$ is smallest, i.e $b_{l,\mathrm{leg}\neq r} \ll b_{l,r}$

A quantitative analysis is based on the leading order inaccuracy prediction (90). By fixing the leg index $r$ in the summation one predicts the relative sizes of the leading coefficients $b_{1,\mathrm{leg}}$. This is the proper interpretation, more accurate than the one used in Sec. II.15, where total inaccuracies on each leg were compared at $\phi = 0$. The total contribution includes all orders, while the prediction is based purely on the leading order contribution, i.e. on $b_{1,\mathrm{leg}}$.

The prediction of the model when the array is inhomogeneous reads

$$b_{1,\mathrm{leg}} \approx -\tilde{W}_{\mathrm{inh,leg}} \left(\frac{N\varepsilon_{\mathrm{J}}}{2}\right)^{N-2} \frac{N-1}{(N-2)!}. \tag{132}$$

Here $\tilde{W}_{\mathrm{inh,leg}}$ is obtained from Eq. (90) by fixing the summation index. This prediction clearly overestimates the size of the coefficients $b_1$, because the suppressive effects described in Sec. II.14 have not been included. A slight overestimation of the ratio between largest and smallest of the coefficients $b_{1,\mathrm{leg}}$ is also observed. The results for two different sets of relative capacitances $\vec{c}$ and $\varepsilon_{\mathrm{J}}$ when $N = 4$ are shown in Table XIV. The numerical results agree with the simple prediction nicely. Although the deviation from $\Delta\mathcal{M} = 1/4$ is very small ($\sim 10^{-10}$), the total averaged pumped charge is 1 almost to the numerical precision

($\sim 10^{-15}$).

The inhomogeneity of the array only changes the size of the ratios $\beta_l$ for different legs, which can be predicted as shown above. On each leg the ratios behave almost as if the array was ideal. Although the amplitudes in the ground-state wave function are no longer identical in each class $z_0; \bar{m}_{\bar{z}}$, their collective behaviour seems to be uniform. Explicit evaluation is much more difficult, since each leg has to be treated separately and the block-diagonalisation is not applicable, so that larger matrices must be diagonalised. If the effective suppression can be evaluated, explicit predictions could be given. In any case, when $\varepsilon_{\mathrm{J}} \ll 1$ the ratio $W_{\mathrm{inh}}$ should be accurate enough.

Similar behaviour of the coefficients $b_{l,\mathrm{leg}}$ is observed for non-ideal gating sequences. Still, the symmetry $\beta_{l+1} < \beta_l$ is often mildly violated on each leg. This may indicate breakdown of the collective behaviour of amplitudes in classes $z_0; \bar{m}_{\bar{z}}$, as gate charge deviate from the symmetry axis. Because several parameters vary simultaneously, parametrisation is difficult. The resulting conclusion is that the ratio $W_{\mathrm{non}}$ is the most viable way to estimate effects due to non-ideal gating.

## IV. CONCLUSIONS

A model describing both the direct supercurrent and the induced charge transfer in gated arrays of Josephson junctions has been developed. The model is based on the canonical formalism of Josephson junctions with a fixed phase difference across the array, $\phi$. Additionally, it neglects the effects due to the coupling to the electromagnetic environment and other degrees of freedom, e.g. quasiparticle tunnelling. Further studies are especially required with respect to the dephasing, i.e. the fluctuations of $\phi$.

It was already known that the direct supercurrent in the present model can be evaluated from the phase dependence of the eigenvalues. The induced charge transfer or Cooper pair pumping for the ground state and suitable gating sequences is found deviate from the fundamental relation $I = (-2e)f$, where $f$ is the gating frequency. This occurs because the charge state amplitudes in the ground state behave in a coherent manner.

In the weak-coupling limit the model yields quantitative, analytical expressions for the Cooper pair pumping and the direct supercurrent as functions of $\phi$, the length of the array and the coupling strength. The leading order corrections due to the inhomogeneity of the array have been evaluated and their accuracy has confirmed numerically. By combining these effects and the precision of the gating sequence one obtains an expected range for the induced current which can be compared against experiments. Unfortunately, the observation and especially the separation of different contributions may prove extremely difficult due to their small size.

The calculations have been extended to stronger couplings by a renormalisation method which also gives the next-to-leading order corrections in the weak-coupling limit. An important result is that the pumped charge per cycle is linked to the geometrical Berry's phase by the canonical conjugate operator of $\phi$, measuring the average number of tunnelled Cooper pairs. The analytical properties of the pumped charge per cycle have been examined by explicitly enforcing the symmetries of the model Hamiltonian. In short, an effective block-diagonalisation scheme and a compatible Fourier expansion of the eigenstates have been constructed.

The Fourier expansion of the pumped charge shows many general characteristics which have not been rigorously proven. Regardless of the strong systematics, it is not possible to predict the results starting directly from the model parameters. Further analysis of the symmetry properties of the system are required, but this is clearly a problem in mathematical physics and should be tackled accordingly. Experimental confirmation of the systematics is quite unlikely, although the underlying properties could affect the properties of a real Cooper pair pump in a measurable way.

## REFERENCES


[1] J. P. Pekola, J. J. Toppari, M. Aunola, M. T. Savolainen and D. V. Averin, Phys. Rev. B **60**, R9931 (1999), publication 1 of the thesis.

[2] M. Aunola, J. J. Toppari and J. P. Pekola, Phys. Rev. B **62**, 1296 (2000), publication 2 of the thesis.

[3] M. Aunola, Phys. Rev. B **63**, 132508 (2001), publication 3 of the thesis.

[4] H. Kamerlingh Onnes, Leiden Comm. **120b**, **122b**, **124c** (1911).

[5] G. Bednorz and K. A. Müller, Z. Phys. B **64**, 189 (1986).

[6] W. Meissner and R. Ochsenfeld, Naturwissenschaften **21**, 787 (1933).

[7] F. and H. London, Proc. R. Soc. London **149**, 71 (1935).

[8] A. B. Pippard, Proc. R. Soc. London, A **216**, 547 (1950).

[9] J. Bardeen, L. N. Cooper, and J. R. Schrieffer, Phys. Rev. **107**, 1175 (1957).

[10] A. A. Abrikosov, Sov. Phys. JETP **5**, 1174 (1957).

[11] U. Essman and H. Träuble, Phys Lett. A **24**, 526 (1967).

[12] V. L. Ginzburg and L. D. Landau, Zh. Eksp. Teor. Fiz. **20**, 1064 (1950).

[13] B. S. Deaver and W. M. Fairbank, Phys. Rev. Lett. **7**, 43 (1961); R. Doll and M. Näbauer, Phys. Rev. Lett. **7**, 51 (1961).

[14] N. E. Phillips, Phys. Rev. **114**, 676 (1959).

[15] A. M. Lane, *Nuclear Theory*, (Benjamin, 1964).

[16] D. J. Rowe, *Nuclear Collective Motion*, (Metheuen, 1970).

[17] P. Ring and P. Schuck, *The Nuclear Many-Body Problem*, (Springer, 1980).

[18] D. Vollhardt and P. Wölfle, *The Superfluid Phases of* $^3$*He*, (Taylor and Francis, 1990).

[19] V. P. Mineev and K. V. Samokhin, *Introduction to Unconventional Superconductors*, (Gordon and Breach, 1999).

[20] B. D. Josephson, Phys. Lett. **1**, 251 (1962).

[21] D. Rogovin and J. Nagel, Phys. Rev. B **26**, 3698 (1982).

[22] W. H. Parker, D. N. Langenberg, A. Denenstein, and B. N. Taylor, Phys. Rev. **177**, 639 (1969).

[23] S. T. Ruggiero and D. A. Rudman (eds.), *Superconducting Devices*, (Academic Press, 1990).

[24] M. Tinkham, *Introduction to Superconductivity*, 2nd ed., (McGraw-Hill, 1996).

[25] M. Büttiker, Phys. Rev. B **36**, 3548 (1987).

[26] E. Celeghini, L. Faoro, and M. Rasetti, Phys. Rev. B **62**, 3054 (2000).

[27] H. Grabert and M. L. Devoret (eds.), *Single Charge Tunneling, Coulomb Blockade Phenomena in Nanostructures*, (Plenum Press, New York, 1992).

[28] Ph. Joyez, *Le Transistor a une Paire de Cooper: Un Systeme Quantique Macroscopique*,

Academic Dissertation for the Degree of Doctor of Philosophy, (University of Paris 6, 1995).

[29] F. Mandl, *Quantum Mechanics*, (John Wiley & Sons, 1992), pp. 71-109.

[30] M. Tinkham, *Group Theory and Quantum Mechanics*, (McGraw-Hill, 1964).

[31] I. Talmi, *Simple Models of Complex Nuclei: The Shell Model and Interacting Boson Model*, (Harwood Academic Publishers, 1993).

[32] V. Icke, *The Force of Symmetry*, (Cambridge University Press, 1995).

[33] E. Hille and R. S. Phillips, *Functional analysis and semi-groups*, Amer. Soc. Math. Colloq. Publ. **31** (1957).

[34] W. Rudin, *Functional Analysis*, (McGraw Hill, 1973).

[35] J. R. Anglin, P. Drummond, and A. Smerzi, cond-mat/0011440.

[36] G. Schön and A. D. Zaikin, Phys. Rep. **198**, 237 (1990).

[37] C. J. Milburn, J. Corney, E. M. Wright, and D. F. Walls, Phys. Rev. A **55**, 4318 (1997).

[38] S. Raghavan, A. Smerzi, and V. M. Kenkre, Phys. Rev. A **60**, R1787 (1999).

[39] W. H. Louisell, Phys. Lett. **7**, 60 (1963).

[40] R. Lynch, Phys. Rep. **256**, 367 (1995).

[41] M. Born and J. Oppenheimer, Ann. Phys. **84**, 457 (1927).

[42] A. Shnirman, G. Schön, and Y. Makhlin, Phys. Rev. Lett. **79**, 2371 (1997)

[43] G.-L. Ingold and Yu. V. Nazarov, in *Single Charge Tunneling, Coulomb Blockade Phenomena in Nanostructures*, eds. H. Grabert and M. L. Devoret, (Plenum Press, New York, 1992).

[44] L. J. Geerligs, S. M. Verbrugh, P. Hadley, J. E. Mooij, H. Pothier, P. Lafarge, C. Urbina, D. Esteve and M. H. Devoret, Z. Phys. B: Cond. Matter **85**, 349 (1991).

[45] H. Pothier, P. Lafarge, C. Urbina, D. Esteve and M. H. Devoret, Europhys. Lett **17**, 249 (1992).

[46] J. P. Pekola, A. B. Zorin, and M. A. Paalanen, Phys. Rev. B **50**, 11255 (1994).

[47] M. W. Keller, J. M. Martinis, N. M. Zimmermann and A. H. Steinbach, Appl. Phys. Lett. **69**, 1804 (1996); M. W. Keller, J. M. Martinis and R. L. Kautz, Phys. Rev. Lett. **80**, 4530 (1998).

[48] L. P. Kouwenhoven, A. T. Johnson, N. C. van der Vaart, C. J. P. M. Harmans, and C. T. Foxon, Phys. Rev. Lett. **67**, 1626 (1991).

[49] V. I. Talyanskii, J. M. Shilton, M. Pepper, C. G. Smith, C. J. B. Ford, E. H. Linfield, D. A. Ritchie, and G. A. C. Jones, Phys. Rev. B **56** 15180 (1997).

[50] H. D. Jensen and J. M. Martinis, Phys. Rev. B **46**, 13407 (1992).

[51] L. R. C. Fonseca, A. N. Korotkov, and K. K. Likharev, Appl. Phys. Lett. **69**, 1858 (1996).

[52] D. V. Averin, Solid State Commun. **105**, 659 (1998).

[53] A. Shnirman and G. Schön, Phys. Rev. B **57**, 15400 (1998).
[54] G. Falci, R. Fazio, G. M. Palma, J. Siewert, and V. Vedral, Nature **407**, 355 (2000).
[55] M. V. Berry, Proc. R. Soc. London A **392**, 45 (1984).
[56] H. Feshbach, Ann. Phys. (NY) **19**, 287 (1962).
[57] F. Bloch, and C. Horowitz, Nucl. Phys. **8**, 51 (1958).
[58] B. H. Brandow, Rev. Mod. Phys. **39**, 771 (1967).
[59] B. R. Barrett and M. Kirson, Adv. Nucl. Phys. **6**, 219 (1973).
[60] T. T. S. Kuo, Ann. Rev. Nucl. Science **24**, 101 (1974).
[61] P. J. Ellis and E. Osnes, Rev. Mod. Phys. **49**, 777 (1977).
[62] M. Hjorth-Jensen, T. T. S. Kuo, and E. Osnes, Phys. Rep. **261**, 125 (1995).
[63] C. P. Viazminsky and J. P. Vary, math-ph/9906022 (unpublished).
[64] S. Y. Lee and K. Suzuki, Phys. Lett. B **91**, 173 (1981).
[65] K. Suzuki and R. Okamoto, Prog. Theor. Phys. **71**, 1221 (1984).
[66] I. Lindgren and J. Morrison, J. Phys. B **24**, 1143 (1991).
[67] P. N. Shivakumar and R. Wong, Linear Alg. Appl. **7**, 53 (1973).
[68] P. N. Shivakumar, J. J. Williams, and N. Rudraiah, Linear Alg. Appl. **96**, 35 (1987).
[69] C. Wongtawatnugool, S. Y. Wu, and C. C. Shih, J. Math. Phys. **22**, 633 (1981).
[70] P. N. Shivakumar, and J. Xue, J. Comp. and Appl. Math. **107**, 111 (1999).
[71] H. Mei$\beta$ner and E. O. Steinborn, Phys. Rev. A **56**, 1189 (1999).
[72] M. Aunola, (unpublished, 2001).
[73] K. P. Hirvi, J. P. Kauppinen, A. N. Korotkov, M. A. Paalanen, and J. P. Pekola, Appl. Phys. Lett. **67**, 2096 (1995); Sh. Farhangfar, K. P. Hirvi, J. P. Kauppinen, J. P. Pekola, J. J. Toppari, D. V. Averin, and A. N. Korotkov, J. Low Temp. Phys. **108**, 191 (1997).
[74] J. P. Pekola, K. P. Hirvi, J. P. Kauppinen, and M. A. Paalanen, Phys. Rev. Lett. **73**, 2903 (1995).
[75] J. P. Pekola and J. J. Toppari, cond-mat/0102349 (unpublished).